

Multi-sectoral Impacts of H₂ and Synthetic Fuels Adoption for Heavy-duty Transportation Decarbonization

Youssef Shaker^a, Jun Wen Law^a, Audun Botterud^b and Dharik Mallapragada^{c,*}

^aMIT Energy Initiative, Massachusetts Institute of Technology, Cambridge, 02139, MA,

^bLaboratory for Information & Decision Systems, Massachusetts Institute of Technology, Cambridge, 02139, MA,

^cChemical and Biomolecular Engineering Department, Tandon School of Engineering, New York University, Brooklyn, 11201, NY,

ARTICLE INFO

Keywords:

Macro-energy systems
Power
Transportation
Hydrogen
Synthetic Fuels
Decarbonization

ABSTRACT

Policies focused on deep decarbonization of regional economies tend to emphasize electricity sector decarbonization alongside electrification of end-uses. There is also growing interest in utilizing hydrogen (H₂) produced via electricity to displace fossil fuels in difficult-to-electrify sectors. One such use case is heavy-duty vehicles (HDV), which represents a substantial and growing share of global transport emissions due to electrification of light duty vehicles. Here, we assess the bulk energy system impact of decarbonizing the HDV segment via the use of either H₂, or drop-in synthetic liquid fuels produced from H₂ and CO₂. Our analysis soft-links two modeling approaches: a) a bottom-up model of transportation energy demand that produces variety of final energy demand scenarios for the same service demand and b) a multi-sectoral capacity expansion model that co-optimizes power, H₂ and CO₂ supply chains subjected to technological and policy constraints to meet exogenous final energy demands. Through a case study of Western European countries under deep decarbonization constraints in 2040, we quantify the energy system implications of different levels of H₂ and synthetic fuels adoption in the HDV sector under scenarios with and without CO₂ sequestration. In the absence of CO₂ storage, substitution of liquid fossil fuels in HDVs is essential to meet the deep decarbonization constraint across the modeled power, H₂ and transport sectors. Additionally, utilizing H₂ HDVs reduces decarbonization costs and fossil liquids demand, but could increase natural gas consumption. While H₂ HDV adoption reduces the need for direct air capture (DAC), synthetic fuel adoption increases DAC investments and total system costs. The study highlights the trade-offs associated with different transportation decarbonization pathways, and underscores the importance of multi-sectoral consideration in decarbonization studies.

1. Introduction

Modeled pathways for energy system decarbonization are generally based on a two-pronged strategy of: a) decarbonizing the power sector by expanding variable renewable energy (VRE) supply, and b) increasing use of electricity to displace fossil fuel energy use. To date, only the first part of this two-pronged strategy has yielded meaningful progress in major-emitting regions like the European Union and U.S. – for example, power sector greenhouse gas (GHG) emissions in the European Union (EU) for 2021 were 40% lower than 2005, as VRE generation increased from 16% to 38% over the same period (European Environment Agency, 2023; Energy - Eurostat, 2023). In contrast, GHG emissions from the EU transportation sector have remained largely unchanged over the same period; electricity consumption as a share of total transportation energy consumption was less than 1% in 2021 (European Environment Agency, 2023; Energy - Eurostat, 2023).

The electrification of light duty vehicles (LDVs) is seemingly well underway, as indicated by the share of plug-in hybrid (PHEVs) and battery electric vehicles (EVs) as a percentage of new car sales (PHEV and EV car sales in the EU increased from 3% to 23 % of all new car sales between 2019 and 2023) (ACEA, 2023). However, the electrification of heavy-duty vehicles (HDV), which accounted for around 27% of the transportation sector's CO₂ emissions in EU in 2023, is uncertain due to several factors including concerns with payload reduction impacts, refueling time associated with state-of-art batteries, charging technologies, and grid impacts (Davis, Lewis, Shaner, Aggarwal, Arent, Azevedo, Benson, Bradley, Brouwer, Chiang, Clack, Cohen, Doig, Edmonds, Fennell, Field, Hanneagan, Hodge,

*Corresponding author

✉ shaker@mit.edu (Y. Shaker); junlaw@mit.edu (J.W. Law); audunb@mit.edu (A. Botterud); dharik.mallapragada@nyu.edu (D. Mallapragada)
ORCID(s):

Hoffert, Ingersoll, Jaramillo, Lackner, Mach, Mastrandrea, Ogden, Peterson, Sanchez, Sperling, Stagner, Trancik, Yang and Caldeira, 2018; Bethoux, 2020; Camacho, Jurburg and Tanco, 2022; European Environment Agency, 2023; Mowry and Mallapragada, 2021).

Besides electrification, other decarbonization strategies considered for HDVs include: a) direct use of hydrogen (H₂) produced from low-carbon sources, b) use of so-called synthetic liquid fuels (SFs) or e-fuels produced using electricity, H₂ and captured CO₂, and c) continued use of petroleum-based liquid fuels that are offset by atmospheric CO₂ capture using negative emissions technologies such as direct air capture (DAC). Each of these pathways could have a far-reaching impact on the electricity grid, as well as the H₂ and CO₂ supply chains. For instance, the production of SFs require substantial quantities of low-carbon H₂, which in turn relies on the coordinated development of H₂ infrastructure and the electricity grid (Eddy and Solomon, 2023; Drünert, Neuling, Zitscher and Kaltschmitt, 2020; Alsunousi and Kayabasi, 2024; Williams, Jones, Haley, Kwok, Hargreaves, Farbes and Torn, 2021). This is particularly important as electrolyzers are projected to supply a major share of H₂ under deep decarbonization scenarios, driving the need for additional investment in VRE resources (Law, Mignone and Mallapragada, 2025; Bødal, Mallapragada, Botterud and Korpås, 2020; Jensen, Larsen and Mogensen, 2007). Similarly, the CO₂ feedstock for SF production will require deployment of CO₂ capture and transport infrastructure to facilitate CO₂ utilization and could also facilitate CO₂ sequestration where available (Nguyen and Blum, 2015; Ishaq and Crawford, 2023; Karjunen, Tynjälä and Hyppänen, 2017). Besides technological coupling, decarbonization efforts across sectors are also coupled through policy instruments like emissions trading schemes (e.g. EU ETS) that allow for emissions reduction strategies across sectors to directly compete with each other. Here, we systematically explore the multi-sector impacts of the above-mentioned strategies for HDV decarbonization, which as noted in the literature review, remains one of the lesser studied topics in the area of transportation decarbonization.

Previous literature on transportation decarbonization can be categorized into a few broad themes: 1) the technoeconomics and efficiency of EVs, H₂ vehicles, and SFs (Brynnolf, Taljegard, Grahn and Hansson, 2018; Hänggi, Elbert, Büttler, Cabalzar, Teske, Bach and Onder, 2019; Mohideen, Subramanian, Sun, Ge, Guo, Radhamani, Ramakrishna and Liu, 2023; Cremades and Oller, 2024; Gough, Dickerson, Rowley and Walsh, 2017) 2) fleet evolution and the impact of policy interventions (Harrison and Thiel, 2017; Martins, Henriques, Figueira, Silva and Costa, 2023; Pasaoglu, Harrison, Jones, Hill, Beaudet and Thiel, 2016; Kester, Noel, Zarazua De Rubens and Sovacool, 2018) 3) scenario-based characterization of the energy demand and emissions associated with transportation decarbonization under various technology scenarios (Krause, Thiel, Tsokolis, Samaras, Rota, Ward, Prenninger, Coosemans, Neugebauer and Verhoeve, 2020; Siskos, Zazias, Petropoulos, Evangelopoulou and Capros, 2018; Karkatsoulis, Siskos, Paroussos and Capros, 2017) 4) energy system impacts of transportation decarbonization (Li, Ma, Hidalgo-Gonzalez, Lathem, Fedorova, He, Zhong, Chen and Kammen, 2021b; Li, Chen, Ma, He, Dai, Liu, Zhang and Zhong, 2021a; Michalski, Poltrum and Bünger, 2019; Nakano, Sano and Akimoto, 2022; McCollum, Krey, Kolp, Nagai and Riahi, 2014; Van Vliet, Van Den Broek, Turkenburg and Faaij, 2011). This study combines the latter two categories, by leveraging transportation energy demand scenarios as inputs into a multi-vector energy system model.

Some studies have investigated the use of SFs and H₂ in transportation (Brynnolf et al., 2018; Ueckerdt, Bauer, Dirnhaichner, Everall, Sacchi and Luderer, 2021; Millinger, Tafarte, Jordan, Hahn, Meisel and Thrän, 2021; Zang, Sun, Elgowainy, Bafana and Wang, 2021), focusing on quantifying the process-level efficiency, levelized costs and life cycle emissions impacts, where the grid interactions are generally treated in a static manner (i.e. exogenously determined emissions intensity and cost of grid electricity per scenario). These studies generally do not consider what the adoption of SFs or H₂ would imply for the power, H₂, or CO₂ infrastructure in a given region.

Studies investigating the impacts of transportation decarbonization on wider energy systems are often focused on LDV (Heuberger, Bains and Mac Dowell, 2020; Li et al., 2021a; Harrison and Thiel, 2017; Powell, Cezar, Min, Azevedo and Rajagopal, 2022). Additionally, because electrification of LDVs appears to be imminent, many of these studies focus on the impacts on the power sector, and studies that consider the impacts on adjacent H₂ and CO₂ infrastructure are limited (Colbertaldo, Guandalini and Campanari, 2018; Li et al., 2021a; Powell et al., 2022). Given the interactions between the infrastructure for these vectors noted earlier, particularly in the case of SFs and H₂, it is important to consider relevant supply chains in an integrated manner. Multiple studies have emphasized that transport decarbonization strategies have system-wide impacts on electricity, fuel, and CO₂ infrastructure, highlighting the importance for integrated, cross-sectoral assessments (Millinger, Reichenberg, Hedenus, Berndes, Zeyen and Brown, 2022; Speizer, Fuhrman, Aldrete Lopez, George, Kyle, Monteith and McJeon, 2024; Wan, Fu, Li, Wu, Luo and Zhang, 2025).

Studies that focus on the wider energy system impacts of transportation decarbonization incorporate transportation demand using three methods. The first approach assumes a set amount of transportation energy demand, and subsequently investigates the necessary supply infrastructure to meet this demand (Heuberger et al., 2020). The second approach relies on specifying transportation service demand (e.g. vehicle km or tonne-km), and then endogeneously optimizing for both energy and drivetrain choice to meet this demand (Li et al., 2021b). The third uses a multi-model approach, which determines transportation demand exogenously using a transportation demand model, and then uses said model's results as an input in a macro-energy systems model (Powell et al., 2022). The latter approach, which is also considered in this study, enables the inclusion of non-economic factors influencing drivetrain adoption to meet transportation demand. It also allows for evaluating how such choices affect energy infrastructure investments and operations. Compared to modeling final energy demands alone (the first approach), the multi-model framework is able to capture differences in end-use efficiency across alternative fuels used to satisfy transportation energy demands.

In this study, we use a multi-model approach, consisting of a bottom-up transportation energy demand model and a multi-vector energy system model, to study the role for H₂ and SFs for HDV decarbonization and its bulk energy system impact (Figure 1). For the demand-side analysis, we develop a model to evaluate alternative energy demand scenarios for HDVs that accounts for vehicle-specific factors like vehicle efficiency and market share of each vehicle sub-type. We then use these resulting scenarios as inputs to our supply-side multi-vector energy infrastructure planning model, DOLPHYN, to investigate the bulk energy infrastructure impact of wide-scale heavy-duty transportation decarbonization for the identified transportation energy demand scenarios (He, Mallapragada, Macdonald, Law, Shaker, Zhang, Cybulsky, Chakraborty and Giovanniello, 2023). As part of this study, we update DOLPHYN to include a representation of the CO₂ infrastructure, including storage, transportation and utilization (as SFs), as well as a representation of competition between conventional fossil fuels and SFs. In this way, we are able to capture the interactions between H₂, CO₂, and liquid fuels supply chains and their impact on the power sector which includes: a) changes in electricity consumption, b) inducing competition for constrained resources like VRE capacity for renewable electricity generation and CO₂ storage sites and c) affecting the available emissions budget for power and H₂ production as part of multi-sectoral decarbonization efforts. The goal of our analysis is to highlight the key technology and policy drivers for H₂ and SFs adoption as part of cost-optimized deeply decarbonized power, H₂ and transportation sectors.

Our analysis focuses on a case study of Western Europe in 2040 under deep decarbonization scenarios, where policy deliberations have recently focused on a multi-sectoral decarbonization effort (e.g. via the EU ETS, The European Green Deal, the Fit for 55 Package, and the EU 2024 Climate Target), reducing fossil fuels reliance and advancing deployment of H₂ and SFs for transportation decarbonization (Fetting, Constanze, 2020; Seibert, Peter, Jakob and Nora, 2024; Haas and Sander, 2020; Bayer and Aklin, 2020; Vivanco-Martín and Iranzo, 2023; Ovaere and Proost, 2022). On the other hand, there is also considerable uncertainty on the potential role for CO₂ storage in deep decarbonization scenarios for this region, with considerable public opposition to projects, as well as political and legislative barriers (Holz, Scherwath, Crespo del Granado, Skar, Olmos, Ploussard, Ramos and Herbst, 2021; Koukouzas, Christopoulou, Giannakopoulou, Rogkala, Gianni, Karkalis, Pyrgaki, Krassakis, Koutsovitis, Panagiotaras and Petrounias, 2022).

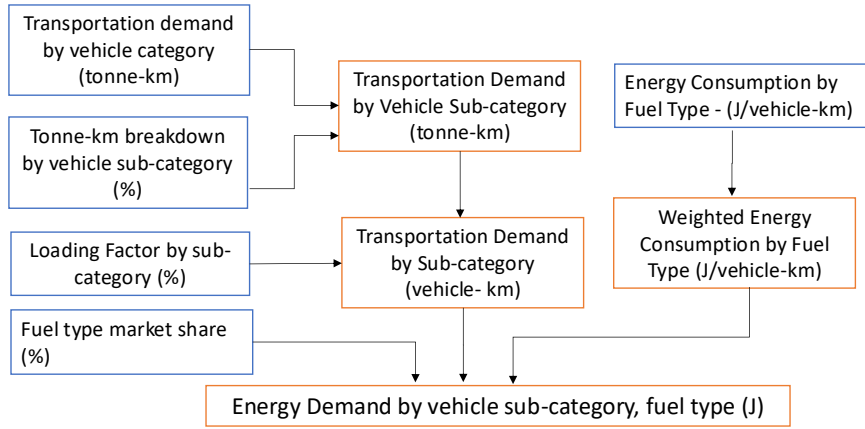
In this context, our analysis leads to a few key policy-relevant observations. First, we find that H₂ use for HDVs reduces bulk system (power-H₂ and transportation) cost of deep decarbonization and decreases demand for fossil liquids, but could increase overall natural gas (NG) consumption compared to equivalent decarbonization scenarios without H₂ use for HDVs. Part of the cost saving stems from the substitution of more expensive conventional fossil liquid fuels versus NG (on a per GJ of energy basis) for H₂ in end-use that also reduces need for atmospheric CO₂ removal via modeled DAC technologies. Second, limitations on CO₂ storage availability increase the bulk system cost savings (in absolute terms) of adopting H₂ use for HDVs. Third, the deployment of SFs results in substantial expansion of power and H₂ production capacity, with a preference for non-fossil fuel generation sources (electrolyzers for H₂ production and VRE for power generation) to maximize carbon abatement benefits of SF use. Fourth, while SF adoption generally increases bulk system costs, the cost increases vs. no SF adoption case are the lowest in case CO₂ storage availability is constrained and fossil fuels (NG and fossil liquids) are expensive. The use of H₂ for transport decarbonization reduces the upstream burden on the power and H₂ sectors, but comes with the additional downstream challenges of deploying extensive distribution, refueling, and vehicular infrastructure. Fifth, our analysis highlights that the optimal-level of sectoral decarbonization is dependent on the technology pathways adopted and reinforces the use of multi-sector emissions reduction strategies similar to the European emissions trading system, rather than sector-specific decarbonization approaches.

The rest of the paper is organized as follows. Section 2 outlines the methods and data used to answer key questions around heavy-duty transportation decarbonization, including an overview of the models, the case-study

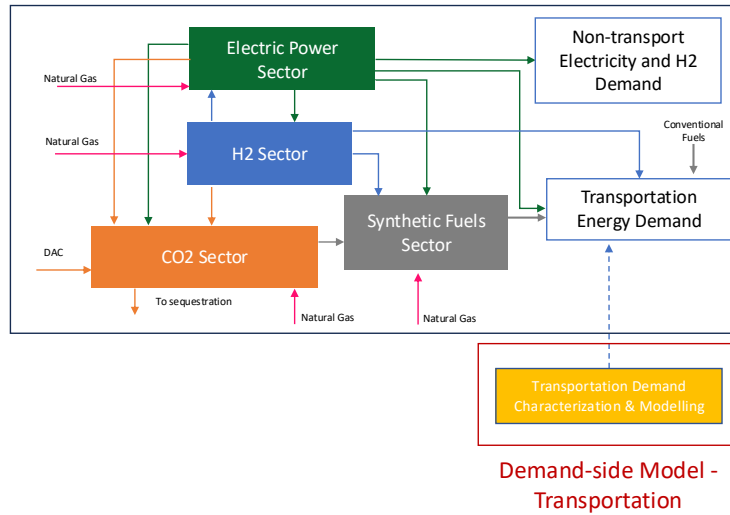
used, technology assumptions, and a summary of the scenarios analyzed. Further details are provided in the supporting information (SI). Section 3 describes the results on the impact of using H₂ for transportation decarbonization, while Section 4 explores the impact of using SFs in transportation decarbonization along with H₂. Section 5 discusses the results for key sensitivity scenarios. Finally, Section 6 delves into some key takeaways associated with power and transportation decarbonization and highlights areas for further research.

2. Data and Methods

2.1. Modeling Approach



(a)



(b)

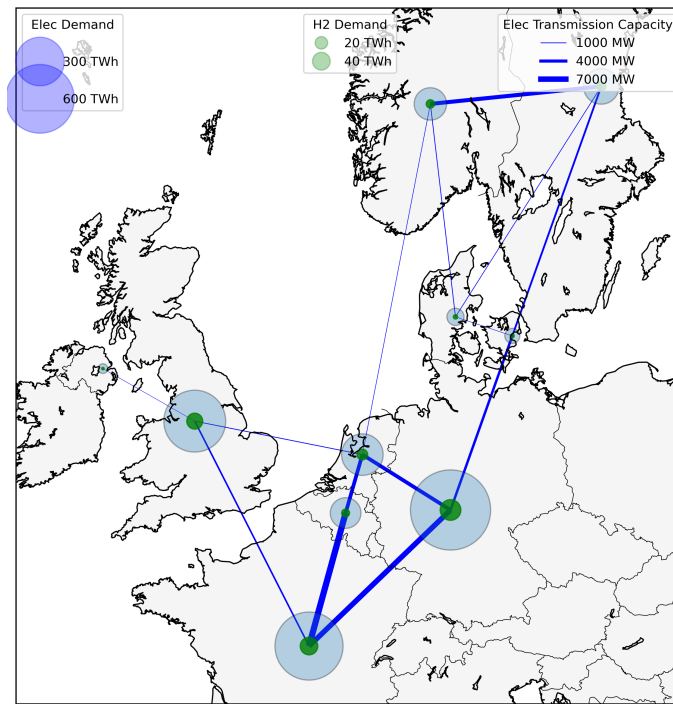
Figure 1: Overview of supply and demand-side modeling used for this study. a) Modeling approach to estimate transportation final energy demand by fuel type and vehicle sub-category, illustrated for the heavy-duty vehicle segment (HDV). Blue boxes are data inputs, while orange boxes are calculated values. Loading factor represents the fraction of vehicle loading capacity used on average. Input data is sourced from the 2020 Reference Scenario produced by the EU Commission (European Commission, 2020), Eurostat (Energy - Eurostat, 2023), a transportation survey of European countries (EMISIA, 2014), and (Krause et al., 2020). Modeling for LDV follows similar approach, but defines service demand in terms of passenger-km (pkm) instead of tonne-km (tkm) and occupancy rate instead of loading factor to convert pkm to vkm. b) Overview of DOLPHYN capacity expansion model used in this study and the link with the demand estimation model - available here: (He et al., 2023). The color of arrows highlight various vectors – green: electricity, blue: H₂, orange: CO₂, grey: fuels; magenta: natural gas.

We developed a data-driven model to estimate transportation energy demand in 2040 across various end-use technology scenarios. The model, summarized in Figure 1 (a) enables us to construct alternative fuel demand scenarios for the LDV and HDV transportation sector that are consistent in terms of delivering the same end-use service demand (e.g. vehicle-km (vkm) for LDVs or tonne-km (tkm) for HDVs). Through the demand-side model, we are able to modify the market share for different vehicle types, and by extension their energy consumption. Although the demand model allows for the creation of scenarios based on vehicle efficiency, modal shifts, and demand reduction, we focus on shifts in vehicle/fuel types for this study. To do so, we first disaggregate transportation energy demand into the following categories: 1) light-duty passenger vehicles, 2) buses and coaches, 3) 2-wheelers, and 4) heavy-duty and light commercial vehicles. This study focuses on decarbonization strategies for the HDV sub-category, defined as vehicles that have maximum gross weight greater than 7.5 tonnes, which is part of the heavy-duty vehicle and light commercial vehicles category. This category accounted for approximately 25% of transportation sector fuel consumption for the modeled region in 2015 (European Commission, 2020). Then, to construct the baseline energy demand for HDV transportation in 2040, we use the service demand (measured in tkm for HDVs) projections for 2040 as per the 2020 Reference Scenario produced by the EU Commission (European Commission, 2020). We decompose this projected service demand into service demand met by each vehicle sub-category using data from TRACCS, a transportation survey of European countries (EMISIA, 2014). To calculate service demand in vkm, we combine country-specific loading factors (i.e. vehicle load as a % of maximum-laden weight for each of the vehicle sub-categories as reported in Eurostat). Vehicle demand is then broken down by fuel type, the shares of which are determined using projected market shares. Baseline vehicles type market shares are based on projections by Krause et al. (Krause et al., 2020). Vehicle-level energy consumption per functional unit (vkm or tkm) is based on the EU Reference Scenarios Technology Assumptions (European Commission, 2020). Modeling for LDVs follows a similar form, but utilizes passenger-km (pkm) instead of vkm to characterize service demand. Additionally, to convert service demand from pkm to vkm, we utilize occupancy rate data from (EMISIA, 2014). Details on the demand model formulation and the demand model data can be found in sections B.1 and B.2 in the SI, respectively.

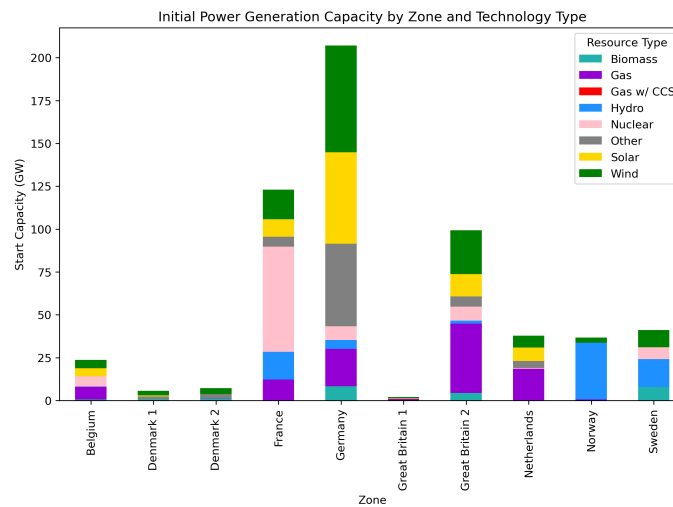
The supply-side modeling approach, summarized in Figure 1 (b), is based on the DOLPHYN capacity expansion model (CEM), which evaluates the cost-optimal investments in electricity, H₂, carbon-capture utilization and sequestration (CCUS), and SF infrastructure, while adhering to a range of technology-specific and system-specific operational constraints, as well as imposed policy constraints (He et al., 2023; He, Mallapragada, Bose, Heuberger and Genç, 2021a). For this study, we expanded the DOLPHYN model in the following ways: 1) we added investment and operation of infrastructure for CO₂ sequestration, transmission and utilization (to produce SF), along with their energy and CO₂ interactions with the power and H₂ supply chains, and 2) allowed the possibility to meet exogenous liquid fuel demand through a combination of fossil-derived fuels and SF production. The resulting modeling framework allows us to, for example, identify the location and scale of fossil fuel power generation with CO₂ capture in the electricity sector, given inputs on the location and cost of CO₂ sequestration. Similarly, the liquid fuels supply chain allows for the production of SFs, which induces demand for H₂ and CO₂ that needs to be balanced in the model. Details on the formulation of the supply-side model can be found in Section C of the SI.

2.2. Case study: Western European decarbonization scenarios for 2040

The developed models are applied to the case study of Western Europe (Germany, France, the United Kingdom, Belgium, the Netherlands, Denmark, Sweden, and Norway) using a transportation energy demand model, and a 10-zone network representation for power, H₂, and CCUS supply chains (Figure 2a). This region is central to European decarbonization efforts due to the availability of high quality onshore and offshore wind resources, domestic NG supply, and CO₂ sequestration potential. Countries in the region have also shown a significant commitment towards decarbonization and a willingness to invest in a H₂ supply chain (European Commission, 2019). Starting with a brownfield power sector representation (i.e. existing power transfer capacity between zones and existing generation capacity), we explore the least-cost system outcomes for alternative technology, demand, and policy scenarios for 2040. Additionally, we use a time domain reduction method to reduce the number of days modeled from 365 days, to 100 representative days to reduce the computational intensity of the model. Since we are focused on transportation energy demand and its energy system impacts, we fix the annual non-transport electricity and H₂ demand for the region to be equal to the projections available from ENTSOE for their Distributed Energy Scenario at 2,081 TWh and 468 TWh, respectively (ENTSOE). Table 1 summarizes the major case study assumptions.



(a) Energy network representation



(b) Initial Power Generation by Zone and Technology

Figure 2: a) 10-node model representation of the Western European region for the supply-side modeling, highlighting the initial power transfer capacities between the regions (as of 2020, which is assumed to be the built capacity in 2040) and regional distribution of non-transport electricity and H₂ demand for modeled 2040 demand scenarios. The size of each bubble represents the non-transportation demand for power (blue) and hydrogen (green), while the thickness of the edges between the nodes represents existing power transmission capacity. b) The second figure shows the initial power generation capacity by zone and technology type, corresponding to installed capacity in 2021. The existing available generation is based on data from the ENTSOE transparency platform for the year 2021 (ENTSOE). The network is based on PYPSA-EUR CEM (Hörsch et al., 2019).

Table 1

Major case study assumptions. More details on demand-side input assumptions can be found in Section B.2. Details on supply-side assumptions can be found in Section C.2. Non-transportation demand is based on (ENTSOE, 2022). Transportation demand is an output of transportation demand estimation model highlighted in Figure 1. Fuel price details can be found in Section C.2.5.

Parameter	Value
2040 Non-transportation Electric Demand	2,081 TWh
2040 Non-transportation H ₂ Demand	468 TWh
Natural Gas Price	8.56 EUR/GJ
Fossil Gasoline Price	21.95 EUR/GJ
Fossil Diesel Price	26.63 EUR/GJ
Jet Fuel Price	15.18 EUR/GJ
Discount Rate	4.5%

2.3. Technology assumptions

We model the region in DOLPHYN using a 10-node spatial representation as shown in Figure 2a, with existing infrastructure including power generation capacity (Figure 2b) and electricity transmission interconnections between the regions. The power system representation of this study is based on a brownfield representation of the European Grid, adapted from the representation used in a prior European energy system analysis study by researchers at TU Berlin using the PYPSA-EUR CEM (Hörsch et al., 2019). The existing available generation is based on data from the ENTSOE transparency platform for the year 2021 (ENTSOE). Costs and operational assumptions for power generation technologies are based on the NREL Annual Technology Baseline 2022 (using data for the year 2040, medium case, with a 1.11 EUR/USD conversion) and Sepulveda et al. (NREL, 2022; Sepulveda, Jenkins, De Sisternes and Lester, 2018). The maximum available generation capacity and temporally resolved capacity factors associated with the VRE generation technologies is based on PYPSA-EUR data set (Hörsch et al., 2019). Additionally, we assume that existing power transfer capacities between regions can be expanded by up to 4 times. New power lines are assumed to have a maximum capacity of up to 5,000 MW. A greenfield representation of H₂ and CO₂ infrastructure is utilized for this study. The candidate set of pipelines for CO₂ and H₂ is made up of all the possible combinations of zones (i.e. it is assumed that a pipeline could be built between any two modeled zones). Costs and assumptions for the main H₂ production technologies of electrolyzers, steam methane reforming (SMR), SMR with CCS, and autothermal reforming (ATR) with CCS are obtained from various technological reports in the literature (IEA, 2019; Lewis, McNaul, Jamieson, Henriksen, Matthews, Walsh, Grove, Shultz, Skone and Stevens, 2022).

Since the focus of this study is road transportation, the supply-side model considers supply-demand balance for two liquid fuels; diesel and gasoline. We assume that liquid fuel demand can be met in one of two ways. The first is using conventional fossil hydrocarbons purchased at a specified price (see Table 1), and the second is through SFs based on syngas production from CO₂ and H₂ followed by Fischer-Tropsch synthesis. Three SF plant configurations are modeled, summarized in Table 2: A) baseline SF plant based on Zang et al. with 52% energy efficiency and 47% of the feed carbon recovered as liquid fuel, B) high CO₂ capture variant of the process described in Zang et al. where 90% of the vented CO₂ is captured for sequestration purposes and C) high fuel production variant of the process where 90% of the vented CO₂ is captured and recycled to the syngas generation unit to enhance liquid fuel production (Zang et al., 2021). Technology cost and performance assumptions for option A are sourced from Zang et al. (Zang et al., 2021). The cost and performance assumptions for option B are developed by combining those of the SF process in option A with the estimated cost and energy requirements of a CO₂ capture system to capture 90% of the vented CO₂, adapted from literature studies on industrial point source carbon capture (Schmitt, Leptinsky, Turner, Zoelle, White, Hughes, Homsy, Woods, Hoffman, Shultz and James III, 2022). The assumptions for option C are developed by assuming that the vented CO₂ is captured in a process similar to option B, but that the captured CO₂ is recycled to the syngas generation unit of the SF process directly instead of being stored. As such, this option also results in increased use of electricity and H₂ per tonne of external CO₂ feed input. The model is allowed to choose between these 3 options as part of the optimization. The SF production facility also produces jet fuel, for which we do not model an exogenous demand. Instead, we credit the market value of jet fuel in the objective function of the supply-side model, while including the emissions associated with its end-use in the emissions constraint.

Table 2

Cost and performance assumptions for synthetic fuel production with different levels of CO₂ utilization. Process information for option B and C were obtained by accounting for the estimated additional energy requirements and costs of capturing 90% of flue gas CO₂ produced by the baseline plant (option A), using data from industrial point source CO₂ capture (Zang et al., 2021; Schmitt et al., 2022). Some minor modifications from original sources were made to ensure facility carbon balance is satisfied for the specified fuel carbon intensities. The carbon intensities of the diesel, gasoline, and jet fuel are 69.3, 67.7, and 68.4 kg of CO₂/GJ, respectively.

Synfuel Production Technology	Option A: Baseline Synfuel Plant	Option B: Synfuel Plant w/ Capture	Option C: Synfuel Plant w/ Capture and Recycling
CAPEX (MEUR/MW of Fuel Out)	1.90	2.48	2.48
CO ₂ Emissions (Tonnes of CO ₂ / Tonne of CO ₂ Feed)	0.52	0.05	0.10
H ₂ Consumption (GJ of H ₂ / Tonne of CO ₂ Feed)	11.2	11.2	21.3
Electricity Consumption (GJ of Electricity / Tonne of CO ₂ Feed)	0.13	2.10	4.00
Diesel Out (GJ / Tonne of CO ₂ Feed)	1.889	1.889	3.596
Gasoline Out (GJ / Tonne of CO ₂ Feed)	1.784	1.784	3.396
Jet Fuel Out (GJ / Tonne of CO ₂ Feed)	3.225	3.225	6.138

Table 3

Summary of technologies considered in the supply-side analysis. **Bolded resources** have spatially-resolved capacity deployment limits. *Italicized resources* are not considered for expansion. CCGT w CCS, SMR w CCS, and ATR w CCS capture rates are 95.0%, 96.2%, and 94.5%, respectively. Detailed technology cost and performance assumptions are provided in Section C.2. VRE = Variable Renewable Energy, CCGT = Combined Cycle Gas Turbine, CCS = Carbon Capture and Storage, OCGT = Open Cycle Gas Turbine.

Sector	Technologies considered
Power	Utility-scale VRE , CCGT w & w/o CCS, OCGT, Nuclear, Coal, Lignite, <i>Hydro</i> , <i>Pumped Hydro</i> , <i>Biomass</i> , Li-ion storage, Transmission
H ₂	Steam Methane Reforming (SMR) w and w/o CCS, Autothermal Reforming (ATR) w CCS, Electrolyzer, Tank H ₂ storage, CCGT-H ₂ , H ₂ pipelines
CO ₂	Direct air capture (DAC), CO ₂ transport pipelines, and CO₂ geological storage
Liquid Fuels	Conventional Fuels, Synthetic Fuels

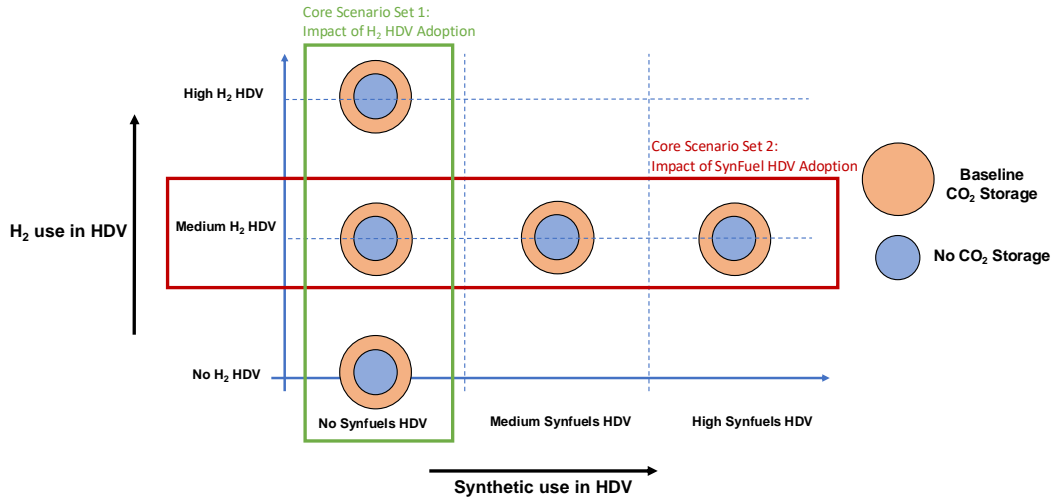
We model 3 DAC technologies based on solid-sorbent and solvent based schemes that use natural gas and electricity inputs as per the cost and performance assumptions from a recent study (Valentine, Zoelle, Homsy, Mantripragada, Woods, Roy, Kilstofte, Sturdivan, Steutermann and Fout, 2022b; Valentine, Zoelle, Homsy, Mantripragada, Kilstofte, Sturdivan, Steutermann and Fout, 2022a) (See Section C.2.3). We model CO₂ geological sequestration sites and capacities as per the data available for CO₂ storage in saline aquifers from the EU GeoCapacity project (Vangkilde-Pedersen, Thomas, 2009). The model is allowed to invest in CO₂ pipelines to connect CO₂ sources and sinks.

Table 3 summarizes the list of technologies considered across various sectors in the supply-side modeling efforts. Further details of demand-side input assumptions can be found in Section B.2.

2.4. Scenarios evaluated

We evaluated alternative scenarios spanning different assumptions for compressed H₂ use for HDV transportation, minimum levels of SF utilization, and CO₂ sequestration availability, as shown in Figure 3. Unless otherwise stated, the annual CO₂ emissions constraint for the modeled system shown in Figure 1b was set to be 103 MtCO₂/y. This emissions constraint corresponds to almost 90% reduction in electricity and heat production, and road transportation sector emissions relative to 2019 levels. Emission limits are enforced jointly across sectors, which allows for emissions trading across sectors in the model.

To test the impact of CO₂ sequestration availability on model outcomes, we consider a baseline CO₂ sequestration potential scenario, which allows for up to 650 MtCO₂/year of sequestration distributed across the region (as shown in Table C.24), and an alternative scenario where no CO₂ sequestration is available. Widespread availability of CO₂ sequestration is likely to incentivize adoption of carbon capture technologies, while their limited availability could motivate greater reliance on renewable energy adoption and CO₂ utilization via SF (Mignone, Clarke, Edmonds, Gurgel, Herzog, Johnson, Mallapragada, McJeon, Morris, O'Rourke, Paltsev, Rose, Steinberg and Venkatesh, 2024; Millinger et al., 2022).



(a) Core Scenario Sets

Scenario	Input Modified	Value(s) Tested
Sensitivity Set 1	Emissions Constraint	258 MtCO ₂ /y
Sensitivity Set 2	Natural Gas Price	+/- 30% of Base Scenario
Sensitivity Set 3	Uptake of Hydrogen Vehicles	0% Uptake of H ₂ HDVs
Sensitivity Set 4	Natural Gas Price	+/- 30% of Base Scenario

(b) Sensitivity Scenario Set Summary

Figure 3: a) Summary of core scenarios evaluated. The y-axis represents varying levels of H₂ HDV adoption (between 0 and 142 TWh of H₂ consumption), while the x-axis represents varying levels of synthetic fuel adoption (between 0 and 128 TWh of synthetic Diesel consumption). All scenarios are equivalent from an emissions capping perspective with a cap of 103 MtCO₂/y. The HDV fleet represents all vehicle types with gross weight greater than 7.5 tonnes. Each bubble in (a) represents a scenario. Baseline CO₂ storage corresponds to maximum annual CO₂ storage injections equal to 650 MtCO₂/year. More details on the transportation demand scenarios can be found in Figures 4, b) Shows sensitivity scenarios tested. Synfuel = SF.

To isolate the energy system impacts of H₂ and SF use for HDVs, we evaluated the model across different H₂ and SF adoption scenarios. We create a baseline case (no H₂ HDV, no SFs HDV, bottom left in Figure 3a where all the HDV demand is met through diesel either via internal combustion engine vehicles or PHEVs. For the purposes of this study, we assume that the percentage service demand of plug-in hybrid EV-diesel vehicles and other EVs is static. Scenario set 1 (green box in Figure 3a), evaluates impact of increasing H₂ use in HDVs, ranging from 0% (baseline scenario), 50% (medium), and 100% (high) of the service demand satisfied by the diesel ICE vehicles in the baseline scenario. SF adoption is not considered in this scenario set. Figure 4 shows the results of the demand-side model for the varying levels of H₂ HDV adoption. The scenario set 2 (red box in Figure 3a) evaluates impact of increasing SF use in HDVs and includes scenarios with 0%, 25% (medium), and 50% (high) of service demand met by diesel in the baseline scenario, while holding H₂ use in HDV at the medium level. This second scenario set is motivated by recent

policy discussions in the EU that utilize SF production as part of a set of transportation sector decarbonization policies (Wacket, 2023). Each scenario set is evaluated with and without CO₂ sequestration availability.

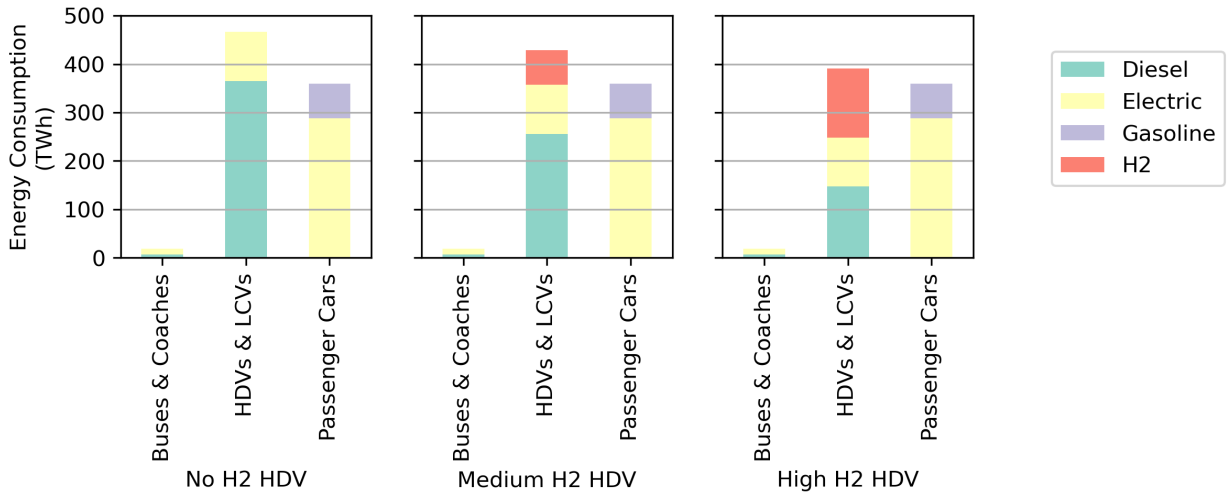


Figure 4: Transportation final energy consumption across different H₂ HDV adoption scenarios. HDV energy use, included in the category Heavy-duty Vehicles and Light Commercial Vehicles (HDVs & LCVs), represents 71-76% of the category's energy consumption and 36-42% of road transportation final energy consumption. Two-wheelers are excluded from the diagram as their demand is negligible compared to other vehicle categories.

For these transportation energy demand scenarios, a few key points are to be noted: a) all scenarios assume a fixed amount of electricity use for LDV and some segments of HDV with a high degree of electrification (illustrated in Figure 4). This also implies that gasoline consumption for road transportation also remains constant across the scenarios, b) scenarios with increasing H₂ adoption leads to reduced end-use diesel consumption, c) HDV energy consumption represents 36-42% of modeled road transportation energy consumption.

In addition to the core set of scenarios outlined above, we ran 4 additional sets of sensitivity scenarios as shown in Figure 3b. The first is based on Scenario Set 1, but with a less stringent emissions constraint (258 MtCO₂/y or corresponding to a 25% reduction compared to 2019 emissions from transport, power and heat production). The second is based on scenario set 1, but with sensitivities around NG price (+/- 30%) of the baseline NG price assumption. NG price is a key input as the relative price between NG and electricity determines the type of H₂ production, while the relative price between NG and liquid fuels determines the cost-effectiveness of H₂ and SF-based decarbonization solutions.

The third sensitivity set focuses on the impact of SF adoption with zero H₂ adoption in the transport sector. Here, we use the same assumptions as scenario set 2, but with a lower level of H₂ adoption. Because the gross demand for diesel is higher in the absence of any H₂ adoption, the percentage of synthetic diesel out of total diesel demand was adjusted to maintain the same gross amount of synthetic diesel demand across Scenario Set 2 and sensitivity set 3. The final set of sensitivities is the same as scenario set 2, but with sensitivities around NG price, +/- 30% of the baseline scenario NG price.

3. System impacts of H₂ adoption in HDVs

The power and H₂ generation impacts resulting from increasing H₂ adoption for HDVs under the two CO₂ storage scenarios and without any SF utilization are highlighted in Figure 5 (see Figure A.1 for capacity outcomes). In the absence of CO₂ storage, Figure 5 shows that the model produces an infeasible supply-side solution in the case of no H₂ use in HDVs. This infeasibility is a result of the emissions limit being lower than the CO₂ emissions associated with liquid fuel consumption in the transportation sector, where there are no abatement options available in this scenario. Use of H₂ for HDVs, however, resolves the model infeasibility and leads to incremental H₂ supply via electrolytic hydrogen production that consumes 110.1 - 206.2 TWh of electricity or approximately 5.3 - 9.9% of non-H₂ sector

electricity demand. Increasing the share of H₂ in HDVs from medium to high level results in CO₂ emissions reduction in the transportation sector at the expense of increased power sector emissions through utilization of NG generation without CCS that lowers the share of VRE generation. For example, wind and solar generation share with high H₂ HDV is 75% compared to 77% in the medium H₂ HDV case. Interestingly, increasing H₂ use in HDVs from medium to high levels reduces the marginal emissions abatement cost (see Table A.1). This result stems from the reduced investment in battery storage and transmission capacity (see Figures A.3 and A.4) and leveraging electrolyzer operational flexibility to support power system operations. In all cases, the maximum level of capacity deployment for VREs (including on-shore wind) is not reached for all regions. Finally, we see that battery storage is higher when CO₂ storage is not available (394 - 1006 GWh), compared to when it is available (12 - 22 GWh), as shown in Figure A.3. H₂ storage is not deployed across scenarios.

The availability of CO₂ storage results in deployment of CCS technologies for power and H₂ generation as shown in Figure 5 which reduces the power sector impacts of H₂ adoption in HDV and also leads to a feasible solution without H₂ use. This is achieved via the deployment of DAC and CCS technologies in conjunction with CO₂ storage, as indicated in the CO₂ inflows in Figure 6. CO₂ storage availability also leads to deployment of CO₂ infrastructure (Figure A.2), that is utilized by both DAC and CCS technologies in the power and H₂ sectors. Similar to the case without CO₂ storage, increasing H₂ use for HDVs leads to a greater role for gas-based power generation without CCS that comes at the expense of reduced consumption of liquid fuels in transport, gas power generation with CCS (Figure A.3) and DAC deployment (Figure 6). At the same time, we see an increase in CCS-based H₂ production (greater carbon inflows in Figure 6), which highlights relative cost-effectiveness of deploying CCS in H₂ vs. power generation.

Despite achieving the same emissions target, scenarios with CO₂ storage result in: a) greater overall CO₂ throughput as compared to scenarios without CO₂ storage, owing to greater total fossil fuel (i.e. NG) utilization (Figure 6 and 8) and b) lower marginal CO₂ abatement costs (Table A.1). Despite these substitution effects, it is important to note that NG consumption in the scenarios are 61 - 65% lower than the 2019 levels. Additionally, the percentage of electricity produced by fossil fuel sources is 9.8 - 10.1% in our scenarios compared to 26% in 2015, despite a significant expansion of the power sector (467 GW - 593 GW vs. 217 GW peak demand in 2019).

Comparing scenarios with and without CO₂ storage also reveals the complementary nature of VRE and electrolyzer deployment (Figure 5). This result, previously noted by other studies, is a result of the capability to operate electrolyzer in a flexible manner in conjunction with H₂ storage and H₂ pipelines, so as to maximize H₂ production during times and locations of low electricity prices, synonymous with abundant VRE electricity supply (Law et al., 2025; He, Mallapragada, Bose, Heuberger-Austin and Gençer, 2021b; Brown, Schlachtberger, Kies, Schramm and Greiner, 2018).

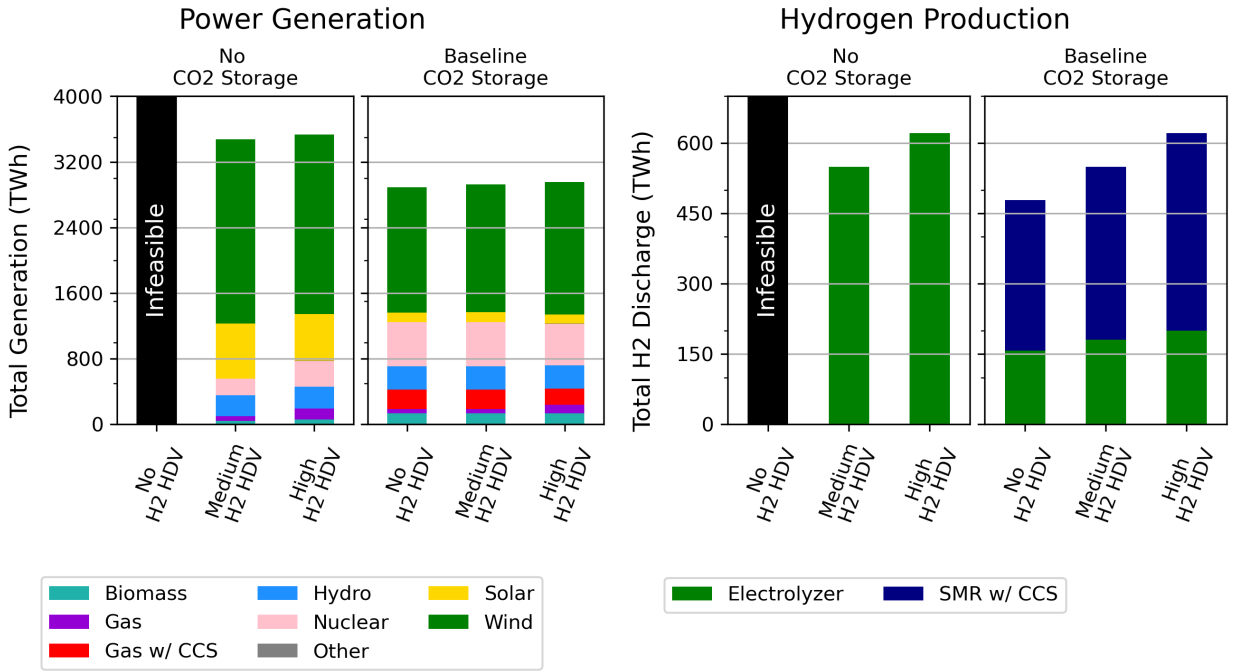


Figure 5: Power and H₂ generation for baseline and no CO₂ sequestration scenarios under no synthetic fuel adoption. The left set of charts shows power generation and the right set of charts shows H₂ generation. Within each panel, the amount of H₂ HDV adoption increases moving from left to right. Corresponding capacity charts are shown in Figure A.1.

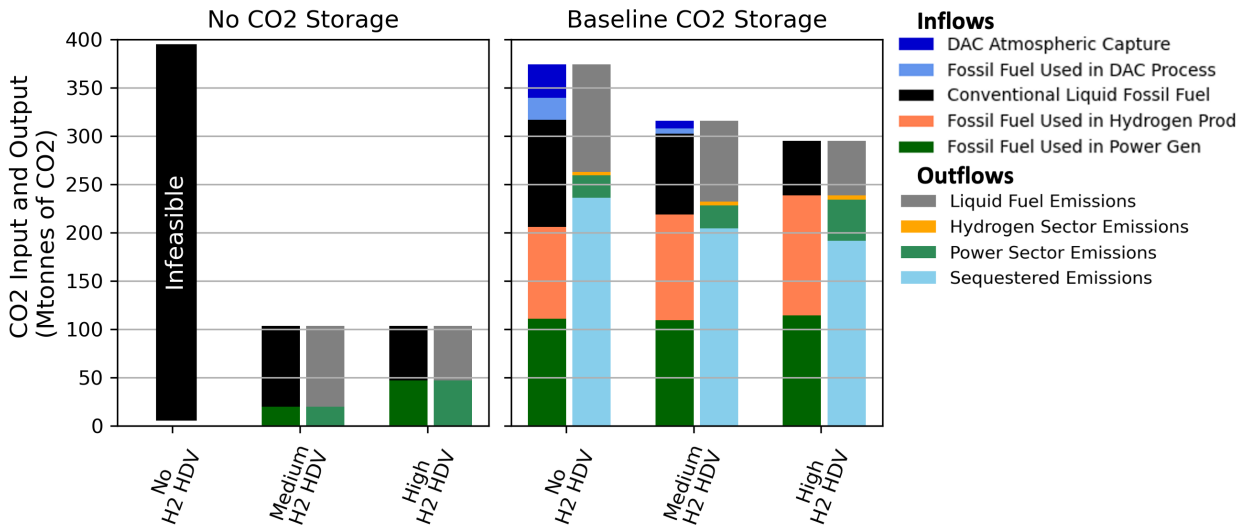


Figure 6: System CO₂ balance under varying levels of H₂ HDV adoption and no SF adoption (Scenario Set 1). The subfigure on the left shows the CO₂ balance under no CO₂ sequestration availability, while the one on the right shows the CO₂ balance under baseline CO₂ storage availability. Within each subplot the H₂ HDV adoption level increases left to right. The leftward column in each subfigure represents CO₂ input into the system, while the rightward column represents CO₂ outputted by the system. All scenarios adhere to the same emissions constraint of 103 MtCO₂/y. System net emissions can be calculated from the chart by subtracting sequestered emissions and DAC atmospheric capture from the emission outflows. It is worth noting that all CO₂ diagrams include all transportation emissions including non-HDV vehicle categories.

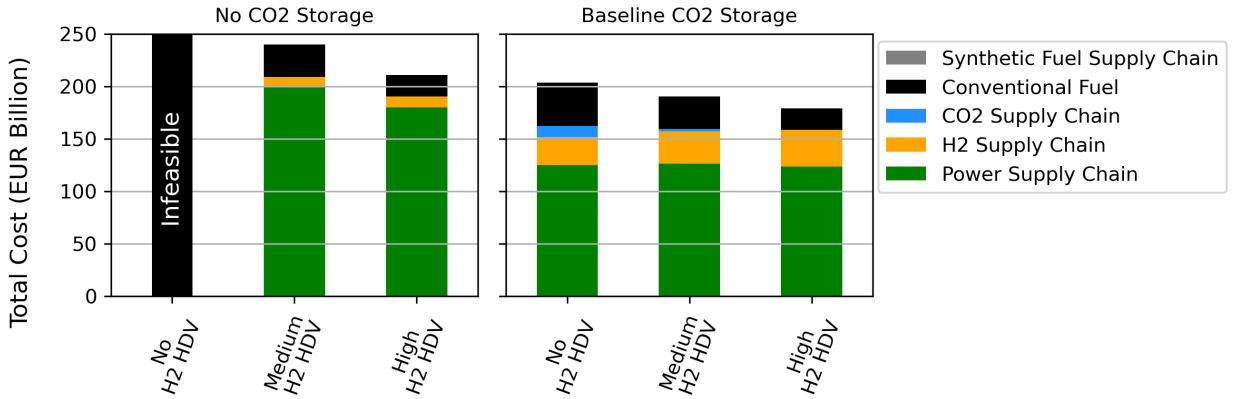


Figure 7: Annualized bulk-system costs under varying levels of H₂ HDV adoption and no SF adoption. The subfigure on the left shows the cost breakdown under no CO₂ sequestration availability, while the one on the right shows the cost breakdown under baseline CO₂ sequestration availability. Within each subplot the H₂ HDV adoption level increases left to right. The costs do not include vehicle replacement or H₂ distribution costs.

Irrespective of CO₂ storage availability, increasing H₂ use in the transportation sector reduces bulk energy system costs, with reductions of up to 6% observed when comparing the no H₂ HDV scenarios to the high H₂ HDV adoption scenarios (Annualized cost savings of 21 Billion EUR/year in the case with CO₂ storage). As seen in Figure 7, the cost savings primarily stem from reduced liquid fuel consumption, but also lower power system costs due to reduced decarbonization of this sector and lower carbon supply chain costs due to the reduced reliance on DAC. These savings fully counteract the net increase in H₂ system costs associated with meeting the added H₂ demand. There are two important caveats to these findings. First, these results only represent bulk system costs and do not include the cost of distribution, refueling and vehicular infrastructure associated with H₂ use for HDV. H₂ use in HDV transportation would only be cost-effective, if the additional end-use infrastructure and equipment upgrades do not outweigh the bulk energy system cost savings estimated here. Second, because H₂ use displaces liquid fuels in lieu of increases in NG utilization in some scenarios, these results are sensitive to the relative price of NG and diesel, in the case with CO₂ storage available. In Figure A.31, we show how decreasing spread between NG and liquid fuel costs reduces the incentive for H₂ use in HDVs and vice versa (see section 5.2).

The results uncover trade-offs between the utilization of liquid fossil fuels and NG, as shown in Figure 8. In scenarios without CO₂ storage, the adoption of H₂ HDVs results in an increase of NG consumption. This occurs due to the reallocation of the emissions budget from the transportation to the power sector, allowing for expanded NG-based generation. The relationship is not as straight-forward in the scenarios with CO₂ storage: while NG consumption increases due to the expansion of NG-based H₂ production, it decreases due to the contraction of DAC, specifically solvent-based DAC technologies that use NG as energy input (NETL, 2022). The net change in NG consumption depends on the relative size of these two effects.

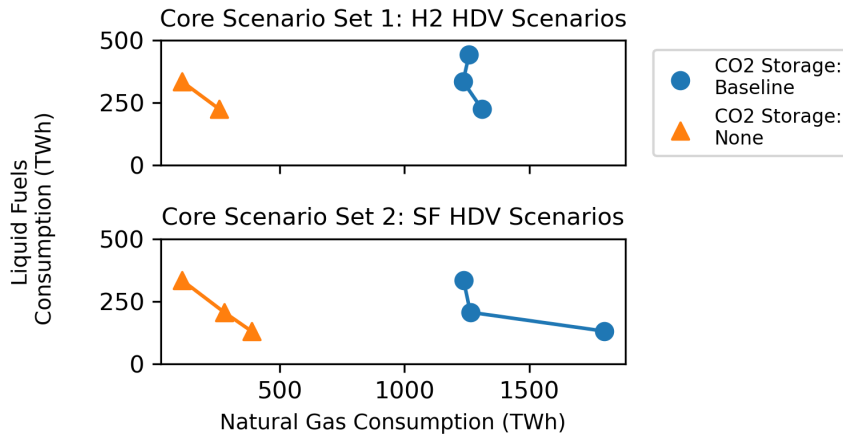


Figure 8: Trade-off between natural gas (NG) and liquid fossil fuel utilization. The subfigure on the top shows the relationship for the H₂ HDV scenarios (i.e. scenario set 1), while the one on the bottom shows the relationship for SF adoption scenarios (i.e. scenario set 2). Within each subplot the amount of natural gas consumption can be examined on the x-axis, while the amount of liquid fossil fuel consumption can be examined on the y-axis. The amount of H₂ and SF HDV adoption increases from top to bottom. The liquid fossil fuel consumption represents the final energy demand for diesel and gasoline in the transport sector, and excludes jet fuel as well as excess fuel supply produced in some of the scenarios.

4. System Impacts of Synthetic Fuel Adoption

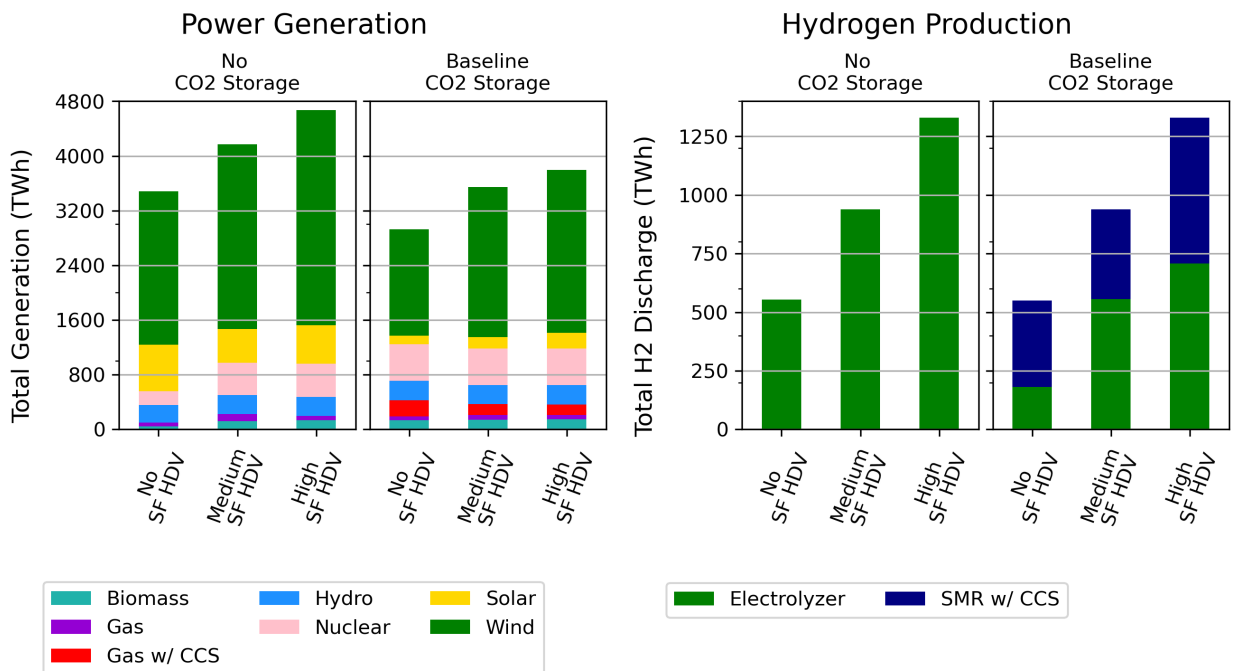


Figure 9: Power and hydrogen generation for baseline and no CO₂ sequestration scenarios under medium H₂ HDV adoption and varying scenarios of synthetic fuel adoption. The left set of charts shows power generation and the right set of charts shows H₂ generation. Within each panel, the amount of synthetic fuel adoption increases moving from left to right. Total system emissions constrained to 103 MtCO₂/y.

The power and H₂ generation impacts resulting from SF production under various CO₂ storage scenarios and with medium H₂ HDV utilization are highlighted in Figure 9 (capacity results are shown in Figure A.7). The production of SFs requires three inputs: H₂, CO₂ and small quantities of electricity inputs (Table 2). The maximum CO₂ abatement potential of SFs is realized when the H₂ and electricity supply are sourced from low-carbon sources while the CO₂ is sourced from the atmosphere. Consequently, we find that the hydrogen for medium levels of SFs production is sourced primarily via electrolysis (Figure 9). However, increasing electrolyzer deployment raises electricity demand and consequently, the average electricity price seen by the electrolyzer (Mallapragada, Junge, Wang, Pfeifenberger, Joskow and Schmalensee, 2023). For further increases in SF production, it is more cost-effective to produce H₂ via NG SMR with CCS rather than electrolysis when CO₂ storage is available, as shown in Figure 9. Overall, SF production is accompanied by a 142% increase in H₂ production vs. non-transport H₂ demand, as compared to 30% increase in the case of H₂ use in HDVs (Figure 5), reflecting the lower energy efficiency of SF based decarbonization strategies. By extension, and as a result of the expanded electrolyzer-based H₂ demand, a large incremental growth in the power sector is also required for SF production, with a growth in power generation of 44% and 33% vs. non-transport power demand in the no CO₂ and baseline CO₂ storage cases, respectively. As shown in Figure 9, the growth in power sector generation resulting from SF adoption is dominated by VRE, primarily wind, reinforcing the synergies between electrolyzers and VREs noted earlier.

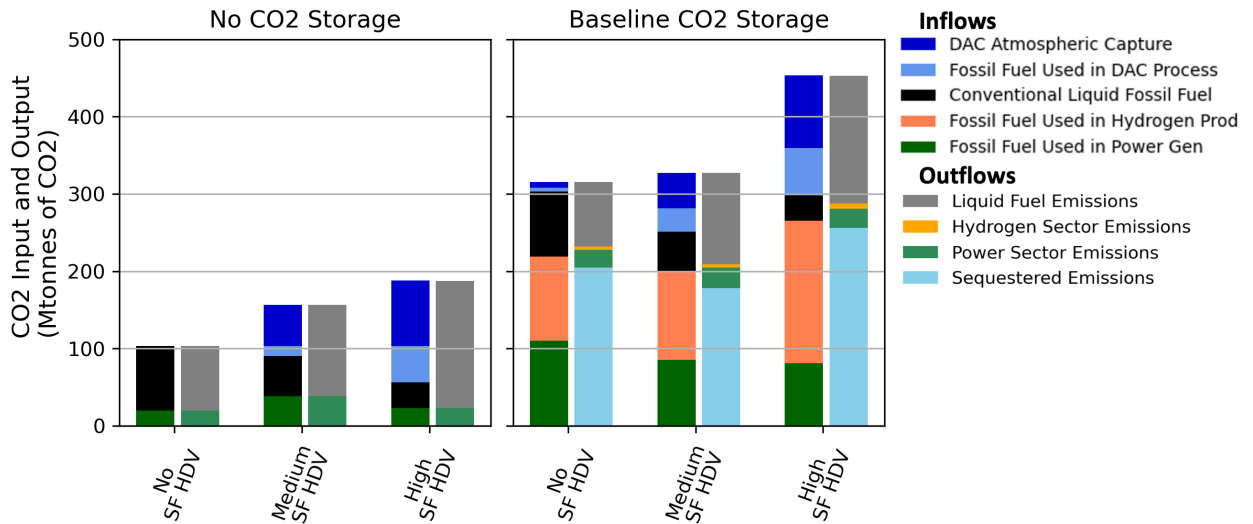


Figure 10: System CO₂ balance under varying levels of SF adoption and medium H₂ HDV adoption and varying scenarios of synthetic fuel adoption. The subfigure on the left shows the CO₂ balance under no CO₂ sequestration availability, while the one on the right shows the CO₂ balance under baseline CO₂ sequestration availability. Within each subplot the SF adoption level increases left to right. The leftward column represents CO₂ input into the system, while the rightward column represents CO₂ outputted by the system. System emissions can be calculated from the chart by subtracting sequestered emissions and DAC atmospheric capture from the emission outflows.

In both CO₂ storage scenarios, increasing SF production also leads to additional DAC deployment, as highlighted in Figures 10 and A.9. DAC deployment rises substantially with high SF adoption due to the need to meet increased diesel demand via synthetic fuels. However, the SF production facility has a fixed product distribution and this leads to excess gasoline production beyond system requirements. This excess gasoline represents lost carbon that reduces the facility's overall carbon efficiency for producing valuable fuels. Consequently, high SF adoption leads to increased carbon inflows for the DAC process. In the baseline CO₂ storage case, CO₂ sequestration requirements are reduced in the medium SF adoption case, but are subsequently increased in the high SF adoption case to account for the expansion of NG based H₂ production with CCS. Among SF production processes considered, we see a consistent preference for the pathway with the lowest overall emissions as noted in Table 2, option B. In other words, pathways that maximize feed carbon conversion into one of two co-products, either SF or captured CO₂, are preferred over pathways with lower carbon conversion.

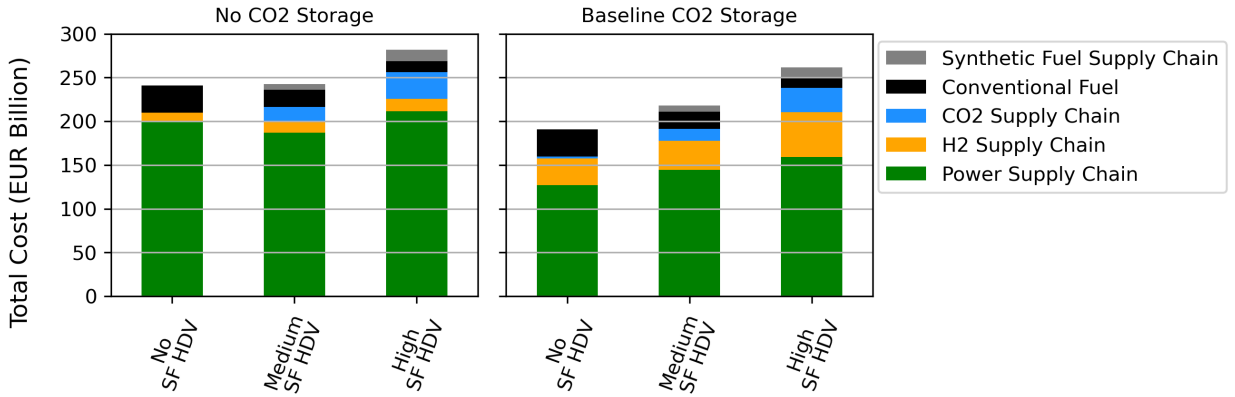


Figure 11: Annualized bulk-system costs under varying levels of SF adoption and medium H₂ HDV adoption and varying scenarios of synthetic fuel adoption. The subfigure on the left shows the cost breakdown under no CO₂ sequestration availability, while the one on the right shows the cost breakdown under baseline CO₂ sequestration availability. Within each subplot the SF adoption level increases left to right. The costs do not include vehicle replacement or H₂ distribution costs.

The cost impacts of SF adoption are shown in Figure 11, where we see that cost savings from reduced purchases of liquid fossil fuel are more than offset by cost increases resulting from expanding energy infrastructure of other vectors (H₂, CO₂, electricity) to produce SFs. Thus, per our modeled assumptions, SFs would not be cost-optimal to deploy across any of the scenarios evaluated here (note that we modeled SF adoption as a minimum requirement per Eqn. C.1.1). Interestingly, in both CO₂ storage cases, the adoption of SFs increases costs by differing magnitudes; in the no CO₂ storage scenario, system cost increase by 3% and 14% for the medium and high SF adoption cases, respectively. In the baseline case, the cost increase is more even; the costs increase by 14% from the No SF case to the Medium SF case, and then 18% from the Medium SF to the High SF case. As such, the system cost increase resulting from SF deployment is lower when no CO₂ storage is available due to the limited number of abatement options in the power generation and H₂ sectors. Similar to scenario set 1, we also observe trade-offs between the utilization of liquid fossil fuels and NG in scenarios with SF adoption, (Figure 8). In all scenarios, we see an increase in the amount of NG consumed as a result of SF deployment. The increase results from the increased adoption of DAC (that uses NG for energy input), expansion of NG-based H₂ production needed for SF production processes. This is particularly true in the high SF case, where there is a large expansion of DAC, in addition to an expansion of NG-based H₂ production.

5. Sensitivities of Emissions Constraints, Natural Gas Price, and Level of Fuel Substitution in HDV Sector

5.1. Sensitivity Scenario Set 1: Sensitivity to Stringency of Emissions Constraint

The first sensitivity scenario set is based on Scenario Set 1, but at a less stringent emissions constraint of 258 MtCO₂/y (detailed results can be found in Section A.3).

In this case, without CO₂ storage, the incremental H₂ demand is primarily met through grey H₂, while in baseline CO₂ storage scenario, the added H₂ demand from H₂ HDVs is met primarily via combination of H₂ production with and without CCS (Figure A.14). The substitution of fossil fuels in the transportation sector also reduces the need for fossil fuel substitution in the power sector (See Figure A.14), resulting in the expansion of fossil fuel power generation without CCS in the baseline scenario (i.e. zero H₂ use in HDV). In the baseline CO₂ sequestration scenario, we also see a substitution of less polluting fossil fuel power generation for more polluting fossil fuel generation (i.e. a substitution of NG with CCS to NG, and NG to coal, as seen in Figure A.14).

Relaxed CO₂ emissions constraints leads to no DAC deployment. In addition, the bulk system cost savings of H₂ use in HDV are lower compared to the stringent emissions cap case (See Figure A.20), which highlights the increased importance of transportation decarbonization under stringent emissions constraints.

5.2. Sensitivity Scenario Set 2: Impact of Natural Gas Prices on H₂ HDV Adoption Scenarios

The second sensitivity scenario set investigates impact of NG prices (See Section A.4 for detailed results) on results of Scenario Set 1. This sensitivity analysis is motivated by the recent volatility in European NG prices (IEA, 2022a). While our base case NG prices are based on the assumption that supply for NG in European context is based on liquefied NG (LNG), there is considerable uncertainty in the future evolution of the LNG market itself. For these reasons, our sensitivity focuses on testing how our model outcomes regarding H₂ and SF adoption change with changes in NG prices.

Changes in NG prices have little effect under the no CO₂ sequestration scenario due to low levels of NG consumption in these cases (See Figure A.21). The impacts in baseline CO₂ storage case are more substantial. For instance, the amount of H₂ produced using electrolyzers increases from 101.75 TWh to 217.7 TWh in medium H₂ HDV case between the low NG price and the high NG price sensitivities (See Figure A.23). Additionally, a shift away from NG power generation towards VREs also occurs; in the medium H₂ HDV case for instance, the percentage of wind and solar generation increases from 52% in the low NG price case to 61% in the high NG price case. Additionally, the amount of gas-based power generation also decreases (See Figure A.21). This combination of shifts in H₂ generation and power production, as well as a reduction in DAC deployment, results in a reduction of CO₂ sequestration requirements from 273 MtCO₂/y of CO₂ to 163 MtCO₂/y of CO₂ in the medium H₂ HDV adoption case (See Figure A.30). The cost savings arising from the increased adoption of H₂ HDVs from none to high with baseline CO₂, decreases from 13% in the low NG price case to 11% in high NG price case (See Figure A.31). While the cost savings margin decreases with higher price of NG, the limited change suggest that the results are somewhat robust to the price of NG. Finally, the cost of NG has a large impact on the total amount of NG consumption as seen in Figure A.32.

5.3. Sensitivity Scenario Set 3: Effect of zero H₂ use in HDVs on System Impacts of Synthetic Fuel Adoption

The third sensitivity scenario set is based on second Scenario Set 2, but with no H₂ HDVs as opposed to a medium level of H₂ HDV adoption (See Section A.5 for detailed results). The motivation behind this scenario is to explore the robustness of the results to the base level of H₂ HDVs. As in Scenario Set 1, without the adoption of transportation fuel substitution measures and with the lack of CO₂ storage availability, the supply-system is infeasible. However, we see that the adoption of SFs allow for sufficient system decarbonization to meet the necessary emission constraints (See Figure A.33). This highlights the key role SFs can play in highly decarbonized systems. In the no CO₂ storage case, the expansion of the power sector to meet electrolyzer demand in H₂ sector is notable, mostly occurring with the expansion of VREs. Additionally, we see that the existence of a CO₂ utilization pathway allows for the deployment of DAC, even in the absence of CO₂ storage (See Figure A.41). In the baseline CO₂ storage case, the H₂ demand is met with a mixture of fossil H₂ with CCS and electrolytic H₂ (See Figure A.33).

5.4. Sensitivity Scenario Set 4: Impact of Natural Gas Prices on SF HDV Adoption Scenarios

The final sensitivity is based on Scenario Set 2, but with varying NG prices (See Section A.6 for detailed results). The impact of the higher NG prices mirrors some of the findings from the Sensitivity Set 2 discussed earlier, including limited impact of NG prices on the power and H₂ supply mixes under the no CO₂ storage scenario. Further, as in the sensitivity set 2, higher NG prices result in a larger share of H₂ production from electrolyzers (See Figure A.44). Additionally, the cost increases from the increased adoption of SFs from none to high, increases from 35.9% in the low NG price case to 36.4% in high NG price case under baseline CO₂ storage, and increases from 16% in the low NG price case to 18% in high NG price case under the no CO₂ storage (See Figure A.54).

6. Discussion and Policy Takeaways

Our analysis reveals the inter-dependence between different sectoral decarbonization strategies, resulting from the modeled system carbon balance shown in Figure 12. These strategies include: 1) fossil fuel substitution in the transportation sector (e.g. use of H₂ or SFs) 2) fossil fuel emissions abatement via CO₂ sequestration, 3) fossil fuel substitution in power and H₂ production, and 4) atmospheric CO₂ removal. All these strategies change the inflows and outflows of CO₂ into the system as highlighted in Figures 6 and 10. We see how the emphasis on each decarbonization strategy changes depending on CO₂ storage availability and emissions constraint (see sensitivity results in SI). For example, as H₂ use in HDVs increases, the reliance on fossil fuel substitution in the power and H₂ sector, carbon

sequestration (when available), and atmospheric carbon removal decreases. In contrast, the adoption of SFs generally increases the reliance on atmospheric carbon removal and sequestration, when available, as well as increasing the role for fossil fuel substitution in the power and H₂ production mix. Below we discuss the policy implications of our findings, while considering the prevailing policy landscape in the European context that was the basis for our case study.

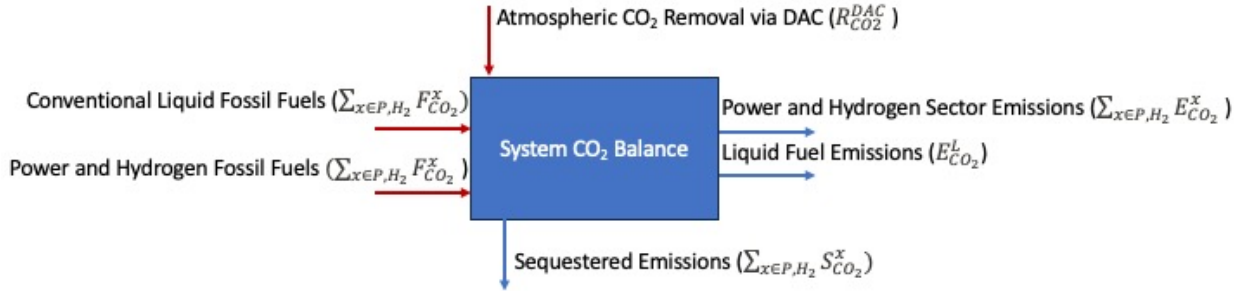


Figure 12: System emissions balance. All terms are assumed to be positive in value.

In the absence of CO₂ storage, deep decarbonization of power, H₂ and transportation sectors without liquid fossil fuel substitution (using H₂, SFs, or other methods not considered in this study) may not be viable, as illustrated by the infeasible outcomes from the modeled scenarios mimicking these conditions. This finding reinforces the importance for demand-side measures to enable transport decarbonization that reduce fossil fuel consumption, including HDV vehicle efficiency improvements, as well as regulations to phase out new ICE vehicle sales etc.. Such measures have been introduced by some of the countries in our case study, albeit to a limited extent so far (Shapps, 2021; Berge, 2023).

Our study notes the bulk system cost savings from adopting H₂ directly in HDVs, as opposed to system cost increases resulting from its use to first produce SFs that are then used in HDVs. While the bulk system cost savings are one measure of relevance, several other factors need to be considered when comparing the two different fuel options. In the case of H₂, substantial investment in distribution, refueling and vehicular infrastructure will be needed that is not accounted in our analysis. For SFs, these costs are expected to be small, because SFs can use the existing vehicular, distribution, and refueling infrastructure developed for fossil-based liquid fuels, thereby minimizing impact on vehicle owners and operators.

We find that SFs adoption tends to lead to lower system cost increases in the absence of CO₂ sequestration capacity and when deployed at a limited scale. The widespread adoption of SFs (high SF adoption scenario representing 50% of HDV demand) results in much larger cost impacts irrespective of the CO₂ storage assumption. These cost increases stem from the significant investment in H₂ and by extension electricity supply chains, but also CO₂ supply chains; in particular deployment and substantial scale up of emerging DAC technologies, as well as CO₂ transportation infrastructure. Further, the system carbon balance (Figure 10) with SFs has many more components than the system without SFs adoption. At an individual producer level, ascertaining the low-carbon nature of SFs will require establishing regulations and possibly new tracking mechanisms that account for the induced grid emissions associated with each new load. Recent discussions in the U.S. and European context on ascertaining the carbon intensity of low-carbon H₂ (Ricks, Xu and Jenkins, 2023; Giovanniello, Cybulsky, Schittekatte and Mallapragada, 2024) are a harbinger to the challenges facing carbon intensity assessment for SF producers, who also have to consider embodied emissions burdens of the CO₂ feedstock.

This study also reinforces findings from other studies regarding the impact of CO₂ sequestration availability on energy system decarbonization pathways (Mignone et al., 2024; Millinger et al., 2022). While spatially-resolved estimates of CO₂ storage capacity have been developed, other factors like social acceptance might constrain practically available CO₂ sequestration capacity (Huijts, Midden and Meijnders, 2007). At the same time, limiting sequestration capacity results in increased reliance on electrolyzer based H₂ production and consequently VRE generation for power supply, highlighting societal trade-offs implicit in the choice of decarbonization pathway (Mignone et al., 2024).

Another interesting trade-off revealed in our analysis is the increase in NG consumption in lieu of liquid fossil fuels displacement via H₂ or SFs adoption. This is particularly relevant for policy makers to consider given the precarious nature of European NG supply after the Russian invasion of Ukraine (IEA, 2022b). In our standard cases, our NG prices are synonymous with long-term projections for liquefied NG prices. That assumption, combined with the deep decarbonization emissions constraint ensure that overall NG consumption levels for power and H₂ production are well below 2019 levels in our cases. At the same time, we find that substitution of fossil liquids with NG is part of many of the cost-optimized decarbonization scenarios studied here and potentially provides a roadmap for reducing fossil liquid fuel imports in the European context, at the cost of increasing NG imports and reliance.

The integrated energy system modeling framework used here allows for co-optimizing supply chains for electricity, H₂, CO₂ and liquid fuels and thus evaluate potential cross-sectoral impacts of multi-sector deep decarbonization. Through the case of power-H₂-transportation interactions in the European context, we highlight key enabling opportunities for cost-beneficial sector coupling across sectors.

This study has several important limitations that present opportunities for future research. In particular, we did not explore the role of bioenergy pathways in meeting demands for liquid fuels, hydrogen, and electricity under emissions-constrained scenarios. Prior energy system modeling studies have shown that available biomass resources are typically fully utilized under deep decarbonization pathways, either for electricity generation or fuel production—depending on the relative costs of production technologies and competing alternatives. However, these studies generally do not account for the potential of hydrogen to displace liquid fuels in the transportation sector. A valuable extension of this work would be to assess the relative value of hydrogen for transportation decarbonization in the context of competing bioenergy uses (Mignone et al., 2024; Millinger et al., 2022). Another area of interest is exploring alternative synthetic fuel production pathways with varying fuel product slates, to assess how product flexibility influences the relative cost-effectiveness of these pathways. Finally, it would be interesting to undertake a distribution-level assessment to quantify the cost of switching from liquid fuels to H₂ to support HDV transportation. Such a study would complement the findings of this work that focused on the bulk energy system assessment and thus provide a holistic assessment of H₂-based transport decarbonization.

7. Conclusions

Here, we used a multi-model approach to study the energy system impacts of H₂ and synthetic fuel adoption for decarbonizing the HDV transportation sector in the context of a Western European decarbonization case study. Our analysis leads to a few key policy-relevant observations. First, we find that H₂ use for HDVs reduces bulk system (power-H₂ and transportation) cost of deep decarbonization and decreases demand for fossil liquids, but could increase overall NG consumption compared to equivalent decarbonization scenarios without H₂ use for HDVs. Part of the cost saving stems from the substitution of more expensive conventional fossil liquid fuels (vs. NG on a per GJ of energy basis) for H₂ in end-use that also reduces need for atmospheric CO₂ removal via modeled DAC technologies. Second, limitations on CO₂ storage availability increase the bulk system cost savings (in absolute terms) of adopting H₂ use for HDVs. Third, the deployment of SFs results in substantial expansion of power and H₂ production capacity, with a preference for low carbon fuel generation sources (electrolyzers and SMR w/ CCS for H₂ production and VRE for power generation) to maximize carbon abatement benefits of SF use. This suggests that the impacts of SF adoption on other sectors should be considered when creating policies that encourage SF adoption. Fourth, while SF adoption generally increases bulk system costs, the cost increases vs. no SF adoption case are the lowest in case CO₂ storage availability is constrained and fossil fuels (NG and fossil liquids) are expensive. The role for H₂ for transport decarbonization reduces the upstream burden on the power and H₂ sectors but comes with the additional downstream challenges of deploying extensive distribution, refueling and vehicular infrastructure. Finally, our analysis highlights that the optimal-level of sectoral decarbonization is dependent on the technology pathways adopted and reinforces the use of multi-sector emissions reduction strategies.

8. Acknowledgements

The authors acknowledge the MIT SuperCloud and Lincoln Laboratory Supercomputing Center for providing HPC resources that have contributed to the research results reported within this paper (Reuther, Kepner, Byun, Samsi, Arcand, Bestor, Bergeron, Gadepally, Houle, Hubbell, Jones, Klein, Milechin, Mullen, Prout, Rosa, Yee and Michaleas,

2018). Funding for this project was provided by the MIT Energy Initiative Future Energy Systems Center. The authors acknowledge Anna Cybulska's contribution in developing the European energy system data set and visualizations.

CRedit authorship contribution statement

Youssef Shaker: Research framing, modeling, data collection, data visualization, writing. **Jun Wen Law:** Modeling, data collection, manuscript writing, manuscript feedback. **Audun Botterud:** Conceptualization of this study, revision of results, manuscript feedback. **Dharik Mallapragada:** Conceptualization of this study, Data curation, manuscript writing, manuscript feedback.

References

- ACEA, 2023. Fuel types of new passenger cars in the EU. URL: <https://www.acea.auto/figure/fuel-types-of-new-passenger-cars-in-eu/>.
- Alsunousi, M., Kayabasi, E., 2024. The role of hydrogen in synthetic fuel production strategies. *International Journal of Hydrogen Energy* 54, 1169–1178. URL: <https://linkinghub.elsevier.com/retrieve/pii/S0360319923062237>, doi:10.1016/j.ijhydene.2023.11.359.
- Barchart, 2023. Dutch TTF Gas Prices and Dutch TTF Gas Futures Prices. URL: <https://www.barchart.com/futures/quotes/TGZ33/futures-prices>.
- Bayer, P., Aklin, M., 2020. The European Union Emissions Trading System reduced CO₂ emissions despite low prices. *Proceedings of the National Academy of Sciences* 117, 8804–8812. URL: <https://pnas.org/doi/full/10.1073/pnas.1918128117>, doi:10.1073/pnas.1918128117.
- Berge, U., 2023. Nå får Norge et eget nullutslipps-mål også for lastebiler. URL: <https://elbil.no/na-far-norge-et-nullutslipps-mal-ogsa-for-lastebiler/>. publication Title: Norsk elbilforening.
- Bethoux, O., 2020. Hydrogen Fuel Cell Road Vehicles: State of the Art and Perspectives. *Energies* 13, 5843. URL: <https://www.mdpi.com/1996-1073/13/21/5843>, doi:10.3390/en13215843.
- Brown, T., Schlachtberger, D., Kies, A., Schramm, S., Greiner, M., 2018. Synergies of sector coupling and transmission reinforcement in a cost-optimised, highly renewable European energy system. *Energy* 160, 720–739. URL: <https://linkinghub.elsevier.com/retrieve/pii/S036054421831288X>, doi:10.1016/j.energy.2018.06.222.
- Brynnolf, S., Taljegard, M., Grahm, M., Hansson, J., 2018. Electrofuels for the transport sector: A review of production costs. *Renewable and Sustainable Energy Reviews* 81, 1887–1905. URL: <https://www.sciencedirect.com/science/article/pii/S1364032117309358>, doi:10.1016/j.rser.2017.05.288.
- Bødal, E.F., Mallapragada, D., Botterud, A., Korpås, M., 2020. Decarbonization synergies from joint planning of electricity and hydrogen production: A Texas case study. *International Journal of Hydrogen Energy* 45, 32899–32915. URL: <https://linkinghub.elsevier.com/retrieve/pii/S0360319920335679>, doi:10.1016/j.ijhydene.2020.09.127.
- Camacho, M.d.l.N., Jurburg, D., Tanco, M., 2022. Hydrogen fuel cell heavy-duty trucks: Review of main research topics. *International Journal of Hydrogen Energy* 47, 29505–29525. URL: <https://www.sciencedirect.com/science/article/pii/S0360319922029068>, doi:10.1016/j.ijhydene.2022.06.271.
- Colbertaldo, P., Guandalini, G., Campanari, S., 2018. Modelling the integrated power and transport energy system: The role of power-to-gas and hydrogen in long-term scenarios for Italy. *Energy* 154, 592–601. URL: <https://www.sciencedirect.com/science/article/pii/S0360544218306960>, doi:10.1016/j.energy.2018.04.089.
- Commission, E.U., 2020. Technology Assumptions EU Reference Scenario 2020 - European Commission. URL: https://energy.ec.europa.eu/document/download/5959845e-435c-4780-9281-b64a709b273b_en?filename=ref2020_technology_assumptions.zip.
- Committee on Developing a Research Agenda for Carbon Dioxide Removal and Reliable Sequestration, Board on Atmospheric Sciences and Climate, Board on Energy and Environmental Systems, Board on Agriculture and Natural Resources, Board on Earth Sciences and Resources, Board on Chemical Sciences and Technology, Ocean Studies Board, Division on Earth and Life Studies, National Academies of Sciences, Engineering, and Medicine, 2019. Negative Emissions Technologies and Reliable Sequestration: A Research Agenda. National Academies Press, Washington, D.C. URL: <https://www.nap.edu/catalog/25259>, doi:10.17226/25259. pages: 25259.
- Cremades, L.V., Oller, L., 2024. Techno-environmental feasibility of synthetic fuels in ground transportation. Application to the Spanish automobile fleet in 2035. *Energy Reports* 11, 5466–5474. URL: <https://linkinghub.elsevier.com/retrieve/pii/S2352484724003135>, doi:10.1016/j.egyr.2024.05.032.
- Davis, S.J., Lewis, N.S., Shaner, M., Aggarwal, S., Arent, D., Azevedo, I.L., Benson, S.M., Bradley, T., Brouwer, J., Chiang, Y.M., Clack, C.T.M., Cohen, A., Doig, S., Edmonds, J., Fennell, P., Field, C.B., Hannegan, B., Hodge, B.M., Hoffert, M.I., Ingersoll, E., Jaramillo, P., Lackner, K.S., Mach, K.J., Mastrandrea, M., Ogdén, J., Peterson, P.F., Sanchez, D.L., Sperling, D., Stagner, J., Trancik, J.E., Yang, C.J., Caldeira, K., 2018. Net-zero emissions energy systems. *Science* 360, eaas9793. URL: <https://www.science.org/doi/10.1126/science.aas9793>, doi:10.1126/science.aas9793.
- Drünert, S., Neuling, U., Zitscher, T., Kaltschmitt, M., 2020. Power-to-Liquid fuels for aviation – Processes, resources and supply potential under German conditions. *Applied Energy* 277, 115578. URL: <https://linkinghub.elsevier.com/retrieve/pii/S0360261920310904>, doi:10.1016/j.apenergy.2020.115578.
- Eddy, M., Solomon, E., 2023. Germany Pushes for Exception in Law Banning Combustion Engines. *The New York Times* URL: <https://www.nytimes.com/2023/03/22/business/germany-eu-climate-combustion-engines.html>. section: Business.
- EMISIA, 2014. TRACCS. URL: <https://traccs.emisia.com/>.
- en2x, 2024. Verbraucherpreise. URL: <https://en2x.de/service/statistiken/verbraucherpreise/>. publication Title: en2x.

- Energy - Eurostat, 2023. SHARES - Energy Eurostat. URL: [https://ec.europa.eu/eurostat/web/energy/database/additional-data#Short%20assessment%20of%20renewable%20energy%20sources%20\(SHARES\)](https://ec.europa.eu/eurostat/web/energy/database/additional-data#Short%20assessment%20of%20renewable%20energy%20sources%20(SHARES)).
- ENTSOE, . ENTSO-E Transparency Platform. URL: <https://transparency.entsoe.eu/>.
- ENTSOE, 2022. TYNDP 2022 Scenario Building Guidelines. URL: https://2022.entsos-tyndp-scenarios.eu/wp-content/uploads/2022/04/TYNDP_2022_Scenario_Building_Guidelines_Version_April_2022.pdf.
- European Commission, 2019. The european green deal. URL: <https://eur-lex.europa.eu/legal-content/EN/TXT/?uri=COM%3A2019%3A640%3AFIN>.
- European Commission, 2020. EU Reference Scenario 2020. URL: https://energy.ec.europa.eu/data-and-analysis/energy-modelling/eu-reference-scenario-2020_en.
- European Environment Agency, 2023. EEA greenhouse gases Data Viewer. URL: [https://www.eea.europa.eu/data-and-maps/data/data-viewers/greenhouse-gases-viewer.type:Dashboard\(Tableau\)](https://www.eea.europa.eu/data-and-maps/data/data-viewers/greenhouse-gases-viewer.type:Dashboard(Tableau)).
- Fetting, Constanze, 2020. The European Green Deal. Technical Report. ESDN Office. Vienna.
- Giovanniello, M.A., Cybulsky, A.N., Schittekatte, T., Mallapragada, D.S., 2024. The influence of additionality and time-matching requirements on the emissions from grid-connected hydrogen production. *Nature Energy* 9, 197–207. URL: <https://www.nature.com/articles/s41560-023-01435-0>, doi:10.1038/s41560-023-01435-0.
- Gough, R., Dickerson, C., Rowley, P., Walsh, C., 2017. Vehicle-to-grid feasibility: A techno-economic analysis of EV-based energy storage. *Applied Energy* 192, 12–23. URL: <https://linkinghub.elsevier.com/retrieve/pii/S0306261917301149>, doi:10.1016/j.apenergy.2017.01.102.
- Haas, T., Sander, H., 2020. Decarbonizing Transport in the European Union: Emission Performance Standards and the Perspectives for a European Green Deal. *Sustainability* 12, 8381. URL: <https://www.mdpi.com/2071-1050/12/20/8381>, doi:10.3390/su12208381.
- Harrison, G., Thiel, C., 2017. Policy insights and modelling challenges: The case of passenger car powertrain technology transition in the European Union. *European Transport Research Review* 9, 1–14. URL: <https://etrr.springeropen.com/articles/10.1007/s12544-017-0252-x>, doi:10.1007/s12544-017-0252-x.
- He, G., Mallapragada, D., Macdonald, R., Law, J.W., Shaker, Y., Zhang, Y., Cybulsky, A., Chakraborty, S., Giovanniello, M., 2023. DOLPHYN: decision optimization for low-carbon power and hydrogen networks. URL: https://github.com/macroenergy/Dolphyn.jl/tree/Liquid_Fuels_Merge.
- He, G., Mallapragada, D.S., Bose, A., Heuberger, C.F., Gençer, E., 2021a. Hydrogen Supply Chain Planning With Flexible Transmission and Storage Scheduling. *IEEE Transactions on Sustainable Energy* 12, 1730–1740. doi:10.1109/TSTE.2021.3064015.
- He, G., Mallapragada, D.S., Bose, A., Heuberger-Austin, C.F., Gençer, E., 2021b. Sector coupling *via* hydrogen to lower the cost of energy system decarbonization. *Energy & Environmental Science* 14, 4635–4646. URL: <https://xlink.rsc.org/?DOI=D1EE00627D>, doi:10.1039/D1EE00627D.
- Heuberger, C.F., Bains, P.K., Mac Dowell, N., 2020. The EV-olution of the power system: A spatio-temporal optimisation model to investigate the impact of electric vehicle deployment. *Applied Energy* 257, 113715. URL: <https://www.sciencedirect.com/science/article/pii/S0306261919314023>, doi:10.1016/j.apenergy.2019.113715.
- Holz, F., Scherwath, T., Crespo del Granado, P., Skar, C., Olmos, L., Ploussard, Q., Ramos, A., Herbst, A., 2021. A 2050 perspective on the role for carbon capture and storage in the European power system and industry sector. *Energy Economics* 104, 105631. URL: <https://www.sciencedirect.com/science/article/pii/S0140988321004941>, doi:10.1016/j.eneco.2021.105631.
- Huijts, N.M.A., Midden, C.J.H., Meijnders, A.L., 2007. Social acceptance of carbon dioxide storage. *Energy Policy* 35, 2780–2789. URL: <https://www.sciencedirect.com/science/article/pii/S0301421506004915>, doi:10.1016/j.enpol.2006.12.007.
- Hänggi, S., Elbert, P., Büttler, T., Cabalzar, U., Teske, S., Bach, C., Onder, C., 2019. A review of synthetic fuels for passenger vehicles. *Energy Reports* 5, 555–569. URL: <https://www.sciencedirect.com/science/article/pii/S235248471830266X>, doi:10.1016/j.egyr.2019.04.007.
- Hörsch, J., Hofmann, F., Schlachtberger, D., Brown, T., Neumann, F., 2019. Complete Data Bundle for PyPSA-Eur: An Open Optimisation Model of the European Transmission System. URL: <https://zenodo.org/record/3517935>, doi:10.5281/zenodo.3517935.
- IEA, 2019. The Future of Hydrogen. Technical Report. IEA. Paris. URL: <https://www.iea.org/reports/the-future-of-hydrogen>.
- IEA, 2022a. A 10-Point Plan to Reduce the European Union's Reliance on Russian Natural Gas. URL: <https://www.iea.org/topics/russias-war-on-ukraine>. publication Title: IEA.
- IEA, 2022b. How to Avoid Gas Shortages in the European Union in 2023 – Analysis. URL: <https://www.iea.org/reports/how-to-avoid-gas-shortages-in-the-european-union-in-2023/the-need-for-action>. publication Title: IEA.
- Ishaq, H., Crawford, C., 2023. CO₂-based alternative fuel production to support development of CO₂ capture, utilization and storage. *Fuel* 331, 125684. URL: <https://linkinghub.elsevier.com/retrieve/pii/S0016236122025133>, doi:10.1016/j.fuel.2022.125684.
- Jensen, S.H., Larsen, P.H., Mogensen, M., 2007. Hydrogen and synthetic fuel production from renewable energy sources. *International Journal of Hydrogen Energy* 32, 3253–3257. URL: <https://linkinghub.elsevier.com/retrieve/pii/S0360319907002480>, doi:10.1016/j.ijhydene.2007.04.042.
- Karjunen, H., Tynjälä, T., Hyppänen, T., 2017. A method for assessing infrastructure for CO₂ utilization: A case study of Finland. *Applied Energy* 205, 33–43. URL: <https://linkinghub.elsevier.com/retrieve/pii/S0306261917309844>, doi:10.1016/j.apenergy.2017.07.111.
- Karkatsoulis, P., Siskos, P., Paroussos, L., Capros, P., 2017. Simulating deep CO₂ emission reduction in transport in a general equilibrium framework: The GEM-E3T model. *Transportation Research Part D: Transport and Environment* 55, 343–358. URL: <https://linkinghub.elsevier.com/retrieve/pii/S136192091630044X>, doi:10.1016/j.trd.2016.11.026.
- Kester, J., Noel, L., Zarazua De Rubens, G., Sovacool, B.K., 2018. Policy mechanisms to accelerate electric vehicle adoption: A qualitative review from the Nordic region. *Renewable and Sustainable Energy Reviews* 94, 719–731. URL: <https://linkinghub.elsevier.com/retrieve/pii/S136403211830426X>, doi:10.1016/j.rser.2018.05.067.

- Koukouzas, N., Christopoulou, M., Giannakopoulou, P.P., Rogkala, A., Gianni, E., Karkalis, C., Pyrgaki, K., Krassakis, P., Koutsovit, P., Panagiotaras, D., Petrounias, P., 2022. Current CO₂ Capture and Storage Trends in Europe in a View of Social Knowledge and Acceptance. A Short Review. *Energies* 15, 5716. URL: <https://www.mdpi.com/1996-1073/15/15/5716>, doi:10.3390/en15155716.
- Krause, J., Thiel, C., Tsokolis, D., Samaras, Z., Rota, C., Ward, A., Prenninger, P., Coosemans, T., Neugebauer, S., Verhoeve, W., 2020. EU road vehicle energy consumption and CO₂ emissions by 2050 – Expert-based scenarios. *Energy Policy* 138, 111224. URL: <https://linkinghub.elsevier.com/retrieve/pii/S0301421519308067>, doi:10.1016/j.enpol.2019.111224.
- Law, J.W., Mignone, B.K., Mallapragada, D.S., 2025. Role of Technology Flexibility and Grid Coupling on Hydrogen Deployment in Net-Zero Energy Systems. *Environmental Science & Technology* 59, 4974–4988. URL: <https://pubs.acs.org/doi/10.1021/acs.est.4c12166>, doi:10.1021/acs.est.4c12166.
- Lewis, E., McNaul, S., Jamieson, M., Henriksen, M., Matthews, H., Walsh, L., Grove, J., Shultz, T., Skone, T., Stevens, R., 2022. Comparison of Commercial, State-of-the-Art, Fossil-Based Hydrogen Production Technologies. Technical Report DOE/NETL-2022/3241, 1862910. URL: <https://www.osti.gov/servlets/purl/1862910/>, doi:10.2172/1862910.
- Li, B., Chen, M., Ma, Z., He, G., Dai, W., Liu, D., Zhang, C., Zhong, H., 2021a. Modelling integrated power and transportation sectors decarbonization with hydrogen energy storage. *IEEE Transactions on Industry Applications*, 1–1doi:10.1109/TIA.2021.3116916.
- Li, B., Ma, Z., Hidalgo-Gonzalez, P., Latham, A., Fedorova, N., He, G., Zhong, H., Chen, M., Kammen, D.M., 2021b. Modeling the impact of EVs in the Chinese power system: Pathways for implementing emissions reduction commitments in the power and transportation sectors. *Energy Policy* 149, 111962. URL: <https://www.sciencedirect.com/science/article/pii/S030142152030673X>, doi:10.1016/j.enpol.2020.111962.
- Lisazeyen, Euronion, Millinger, M., Neumann, F., Parzen, M., Brown, T., Franken, L., Martavp, Lukasnacken, 2023. PyPSA/technology-data: Technology Data v0.6.2. URL: <https://zenodo.org/record/3994163>, doi:10.5281/ZENODO.3994163.
- Mallapragada, D.S., Junge, C., Wang, C., Pfeifenberger, H., Joskow, P.L., Schmalensee, R., 2023. Electricity pricing challenges in future renewables-dominant power systems. *Energy Economics* 126, 106981. URL: <https://www.sciencedirect.com/science/article/pii/S0140988323004796>, doi:10.1016/j.eneco.2023.106981.
- Martins, H., Henriques, C., Figueira, J., Silva, C., Costa, A., 2023. Assessing policy interventions to stimulate the transition of electric vehicle technology in the European Union. *Socio-Economic Planning Sciences* 87, 101505. URL: <https://linkinghub.elsevier.com/retrieve/pii/S0038012122003123>, doi:10.1016/j.seps.2022.101505.
- McCollum, D., Krey, V., Kolp, P., Nagai, Y., Riahi, K., 2014. Transport electrification: A key element for energy system transformation and climate stabilization. *Climatic Change* 123, 651–664. URL: <http://link.springer.com/10.1007/s10584-013-0969-z>, doi:10.1007/s10584-013-0969-z.
- Michalski, J., Poltrum, M., Bünger, U., 2019. The role of renewable fuel supply in the transport sector in a future decarbonized energy system. *International Journal of Hydrogen Energy* 44, 12554–12565. URL: <https://linkinghub.elsevier.com/retrieve/pii/S0360319918333093>, doi:10.1016/j.ijhydene.2018.10.110.
- Mignone, B.K., Clarke, L., Edmonds, J.A., Gurgel, A., Herzog, H.J., Johnson, J.X., Mallapragada, D.S., McJeon, H., Morris, J., O'Rourke, P.R., Paltsev, S., Rose, S.K., Steinberg, D.C., Venkatesh, A., 2024. Drivers and implications of alternative routes to fuels decarbonization in net-zero energy systems. *Nature Communications* 15, 3938. URL: <https://www.nature.com/articles/s41467-024-47059-0>, doi:10.1038/s41467-024-47059-0.
- Millinger, M., Reichenberg, L., Hedenus, F., Berndes, G., Zeyen, E., Brown, T., 2022. Are biofuel mandates cost-effective? - An analysis of transport fuels and biomass usage to achieve emissions targets in the European energy system. *Applied Energy* 326, 120016. URL: <https://www.sciencedirect.com/science/article/pii/S0306261922012739>, doi:10.1016/j.apenergy.2022.120016.
- Millinger, M., Tafarte, P., Jordan, M., Hahn, A., Meisel, K., Thrän, D., 2021. Electrofuels from excess renewable electricity at high variable renewable shares: cost, greenhouse gas abatement, carbon use and competition. *Sustainable Energy & Fuels* 5, 828–843. URL: <https://pubs.rsc.org/en/content/articlelanding/2021/se/d0se01067g>, doi:10.1039/D0SE01067G.
- Mohideen, M.M., Subramanian, B., Sun, J., Ge, J., Guo, H., Radhamani, A.V., Ramakrishna, S., Liu, Y., 2023. Techno-economic analysis of different shades of renewable and non-renewable energy-based hydrogen for fuel cell electric vehicles. *Renewable and Sustainable Energy Reviews* 174, 113153. URL: <https://linkinghub.elsevier.com/retrieve/pii/S1364032123000096>, doi:10.1016/j.rser.2023.113153.
- Mortensen, G.M., 2014. CO₂ storage atlas for Sweden - a contribution to the Nordic Competence Centre for CCS, NORDICCS. Technical Report. Nordics CCS Competence Center. URL: https://www.sintef.no/globalassets/sintef-energi/nordiccs/d-6.1.7.1407-1-co2-storage-atlas-for-sweden-a-contribution-to-the-nordic-competence-centre-for-ccs-nordiccs_web.pdf.
- Mowry, A.M., Mallapragada, D.S., 2021. Grid impacts of highway electric vehicle charging and role for mitigation via energy storage. *Energy Policy* 157, 112508. URL: <https://www.sciencedirect.com/science/article/pii/S0301421521003785>, doi:10.1016/j.enpol.2021.112508.
- Mundi, I., 2024. Jet Fuel - Monthly Price (Euro per Gallon) - Commodity Prices. URL: <https://www.indexmundi.com/commodities/?commodity=jet-fuel&months=60¤cy=eur>.
- Nakano, Y., Sano, F., Akimoto, K., 2022. Impacts of decarbonization technologies in air transport on the global energy system. *Transportation Research Part D: Transport and Environment* 110, 103417. URL: <https://linkinghub.elsevier.com/retrieve/pii/S1361920922002437>, doi:10.1016/j.trd.2022.103417.
- NETL, 2022. COMPARISON OF COMMERCIAL, STATE-OF-THE-ART, FOSSIL-BASED HYDROGEN PRODUCTION TECHNOLOGIES. Technical Report DOE/NETL-2022/3241. NETL. URL: https://www.netl.doe.gov/projects/files/ComparisonofCommercialStateofArtFossilBasedHydrogenProductionTechnologies_041222.pdf.
- Nguyen, V.N., Blum, L., 2015. Syngas and Synfuels from H₂O and CO₂: Current Status. *Chemie Ingenieur Technik* 87, 354–375. URL: <https://onlinelibrary.wiley.com/doi/10.1002/cite.201400090>, doi:10.1002/cite.201400090.
- NREL, 2022. NREL ATB. URL: <https://atb.nrel.gov/electricity/2022/technologies>.

- OPEC, 2024. OPEC Basket Price. URL: https://www.opec.org/opec_web/en/data_graphs/40.htm. publication Title: OPEC.
- Ovaere, M., Proost, S., 2022. Cost-effective reduction of fossil energy use in the European transport sector: An assessment of the Fit for 55 Package. Energy Policy 168, 113085. URL: <https://linkinghub.elsevier.com/retrieve/pii/S030142152200310X>, doi:10.1016/j.enpol.2022.113085.
- Papadias, D., Ahluwalia, R., 2021. Bulk storage of hydrogen. International Journal of Hydrogen Energy 46, 34527–34541. URL: <https://linkinghub.elsevier.com/retrieve/pii/S0360319921030834>, doi:10.1016/j.ijhydene.2021.08.028.
- Pasaoglu, G., Harrison, G., Jones, L., Hill, A., Beaudet, A., Thiel, C., 2016. A system dynamics based market agent model simulating future powertrain technology transition: Scenarios in the EU light duty vehicle road transport sector. Technological Forecasting and Social Change 104, 133–146. URL: <https://linkinghub.elsevier.com/retrieve/pii/S0040162515003911>, doi:10.1016/j.techfore.2015.11.028.
- Powell, S., Cezar, G.V., Min, L., Azevedo, I.M.L., Rajagopal, R., 2022. Charging infrastructure access and operation to reduce the grid impacts of deep electric vehicle adoption. Nature Energy 7, 932–945. URL: <https://www.nature.com/articles/s41560-022-01105-7>, doi:10.1038/s41560-022-01105-7.
- Reuther, A., Kepner, J., Byun, C., Samsi, S., Arcand, W., Bestor, D., Bergeron, B., Gadepally, V., Houle, M., Hubbell, M., Jones, M., Klein, A., Milechin, L., Mullen, J., Prout, A., Rosa, A., Yee, C., Michaleas, P., 2018. Interactive Supercomputing on 40,000 Cores for Machine Learning and Data Analysis URL: <https://arxiv.org/abs/1807.07814>, doi:10.48550/ARXIV.1807.07814. publisher: arXiv Version Number: 1.
- Ricks, W., Xu, Q., Jenkins, J.D., 2023. Minimizing emissions from grid-based hydrogen production in the United States. Environmental Research Letters 18, 014025. URL: <https://iopscience.iop.org/article/10.1088/1748-9326/acacb5>, doi:10.1088/1748-9326/acacb5.
- Schmitt, T., Leptinsky, S., Turner, M., Zoelle, A., White, C.W., Hughes, S., Homsy, S., Woods, M., Hoffman, H., Shultz, T., James III, R.E., 2022. Cost and Performance Baseline for Fossil Energy Plants Volume 1: Bituminous Coal and Natural Gas to Electricity. Technical Report DOE/NETL-2023/4320. National Energy Technology Laboratory (NETL), Pittsburgh, PA, Morgantown, WV, and Albany, OR (United States). URL: <https://www.osti.gov/biblio/1893822>, doi:10.2172/1893822.
- Seibert, D., Peter, K., Jakob, G., Nora, W., 2024. EU 2040 Climate Target: Potential contributions of the transport sector. Technical Report. Oeko-Institut. Berlin.
- Sepulveda, N.A., Jenkins, J.D., De Sisternes, F.J., Lester, R.K., 2018. The Role of Firm Low-Carbon Electricity Resources in Deep Decarbonization of Power Generation. Joule 2, 2403–2420. URL: <https://linkinghub.elsevier.com/retrieve/pii/S2542435118303866>, doi:10.1016/j.joule.2018.08.006.
- Shapps, G., 2021. UK confirms pledge for zero-emission HGVs by 2040 and unveils new chargepoint design. URL: <https://www.gov.uk/government/news/uk-confirms-pledge-for-zero-emission-hgvs-by-2040-and-unveils-new-chargepoint-design>. publication Title: GOV.UK.
- Siskos, P., Zazias, G., Petropoulos, A., Evangelopoulou, S., Capros, P., 2018. Implications of delaying transport decarbonisation in the EU: A systems analysis using the PRIMES model. Energy Policy 121, 48–60. URL: <https://linkinghub.elsevier.com/retrieve/pii/S030142151830404X>, doi:10.1016/j.enpol.2018.06.016.
- Speizer, S., Fuhrman, J., Aldrete Lopez, L., George, M., Kyle, P., Monteith, S., McJeon, H., 2024. Integrated assessment modeling of a zero-emissions global transportation sector. Nature Communications 15, 4439. URL: <https://www.nature.com/articles/s41467-024-48424-9>, doi:10.1038/s41467-024-48424-9.
- Ueckerdt, F., Bauer, C., Dirnhaichner, A., Everall, J., Sacchi, R., Luderer, G., 2021. Potential and risks of hydrogen-based e-fuels in climate change mitigation. Nature Climate Change 11, 384–393. URL: <https://www.nature.com/articles/s41558-021-01032-7>, doi:10.1038/s41558-021-01032-7.
- Valentine, J., Zoelle, A., Homsy, S., Mantripragada, H., Kilstofte, A., Sturdivan, M., Steutermann, M., Fout, T., 2022a. Direct Air Capture Case Studies: Solvent System. Technical Report DOE/NETL-2021/2864, 1893369. URL: <https://www.osti.gov/servlets/purl/1893369/>, doi:10.2172/1893369.
- Valentine, J., Zoelle, A., Homsy, S., Mantripragada, H., Woods, M., Roy, N., Kilstofte, A., Sturdivan, M., Steutermann, M., Fout, T., 2022b. Direct Air Capture Case Studies: Sorbent System. Technical Report DOE/NETL-2021/2865, 1879535. URL: <https://www.osti.gov/servlets/purl/1879535/>, doi:10.2172/1879535.
- Van Vliet, O., Van Den Broek, M., Turkenburg, W., Faaij, A., 2011. Combining hybrid cars and synthetic fuels with electricity generation and carbon capture and storage. Energy Policy 39, 248–268. URL: <https://linkinghub.elsevier.com/retrieve/pii/S030142151000724X>, doi:10.1016/j.enpol.2010.09.038.
- Vangkilde-Pedersen, Thomas, 2009. EU GeoCapacity: Assessing European Capacity for Geological Storage of Carbon Dioxide. Technical Report. De Nationale Geologische Undersøgelser for Dan- mark og Grønland. URL: https://cordis.europa.eu/docs/results/518/518318/126625721-6_en.pdf.
- Vivanco-Martín, B., Iranzo, A., 2023. Analysis of the European Strategy for Hydrogen: A Comprehensive Review. Energies 16, 3866. URL: <https://www.mdpi.com/1996-1073/16/9/3866>, doi:10.3390/en16093866.
- Wacket, M., 2023. Exclusive: EU drafts plan to allow e-fuel combustion engine cars. Reuters URL: <https://www.reuters.com/business/autos-transportation/eu-proposes-exception-e-fuel-combustion-engines-2035-2023-03-21/>. section: Autos & Transportation.
- Wan, T., Fu, H., Li, X., Wu, F., Luo, C., Zhang, L., 2025. Assessment of decarbonization pathway for Chinese road transport sector based on transportation-energy integration systems framework. Energy 317, 134727. URL: <https://linkinghub.elsevier.com/retrieve/pii/S036054422500369X>, doi:10.1016/j.energy.2025.134727.
- Williams, J.H., Jones, R.A., Haley, B., Kwok, G., Hargreaves, J., Farbes, J., Torn, M.S., 2021. Carbon-Neutral Pathways for the United States. AGU Advances 2, e2020AV000284. URL: <https://agupubs.onlinelibrary.wiley.com/doi/10.1029/2020AV000284>, doi:10.1029/2020AV000284.

Zang, G., Sun, P., Elgowainy, A., Bafana, A., Wang, M., 2021. Life Cycle Analysis of Electrofuels: Fischer–Tropsch Fuel Production from Hydrogen and Corn Ethanol Byproduct CO₂. *Environmental Science & Technology* 55, 3888–3897. URL: <https://doi.org/10.1021/acs.est.0c05893>, doi:10.1021/acs.est.0c05893.

A. SI 1: Detailed Scenario Results

A.1. Core Scenario Set 1 Detailed Results

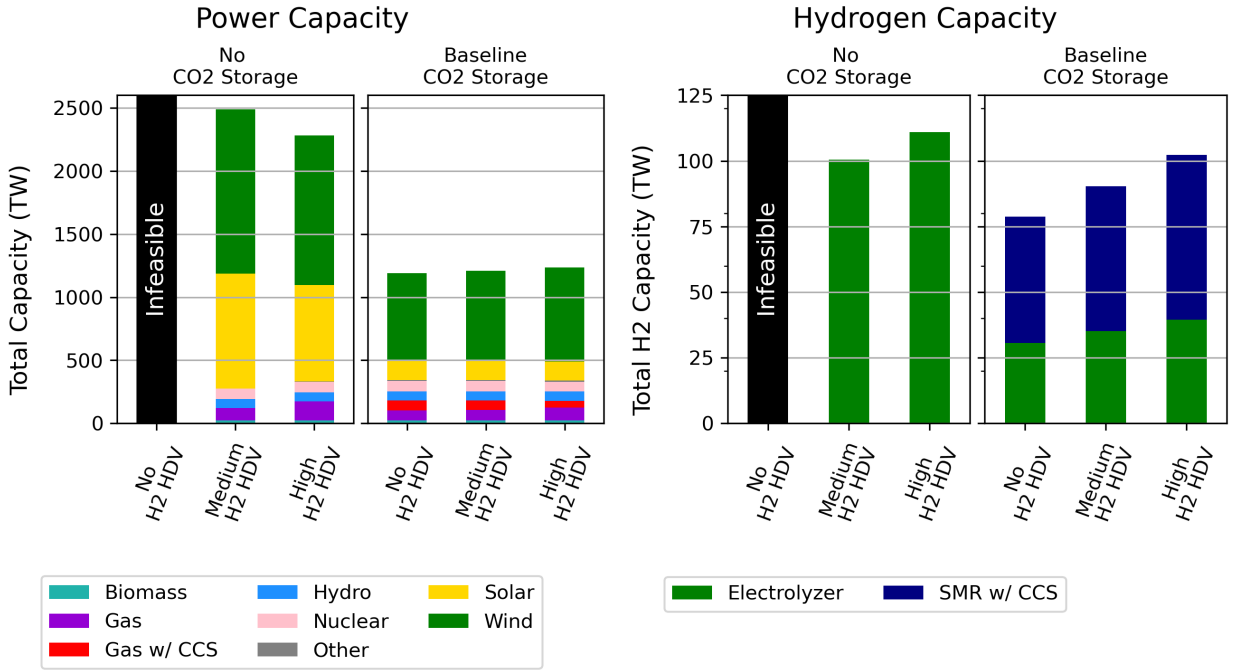


Figure A.1: Power and H₂ capacity for baseline and no CO₂ sequestration scenarios under no synthetic fuel adoption. The left set of charts shows power generation and the right set of charts shows H₂ generation. Within each panel, the amount of H₂ HDV adoption increases moving from left to right.

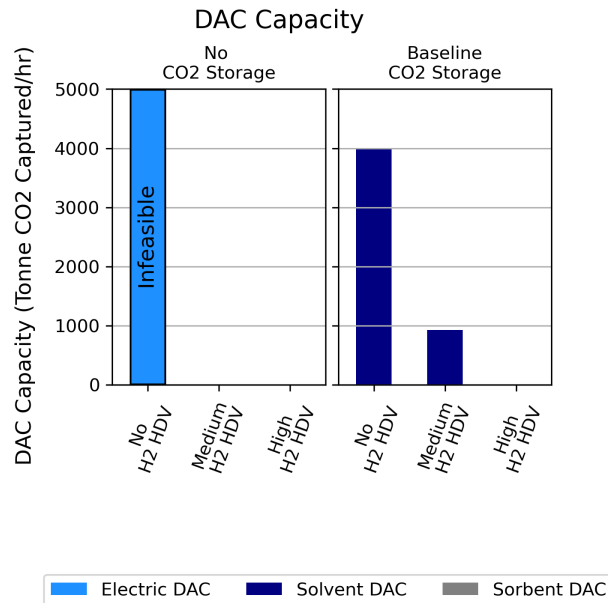


Figure A.2: Direct Air Capture capacity for baseline and no CO₂ sequestration scenarios under no synthetic fuel adoption. Within each panel, the amount of H₂ HDV adoption increases moving from left to right.

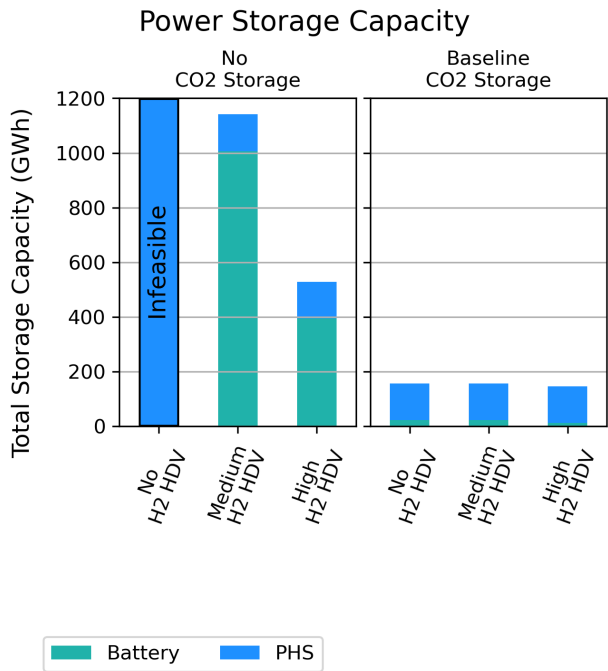


Figure A.3: Power storage capacity for baseline and no CO₂ sequestration scenarios under no synthetic fuel adoption. Within each panel, the amount of H₂ HDV adoption increases moving from left to right.

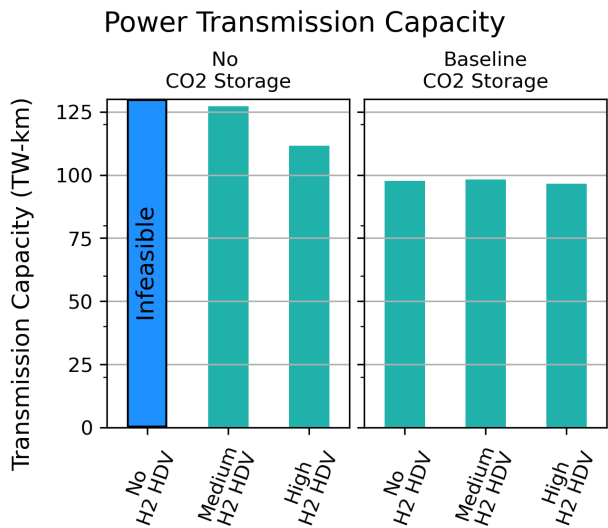


Figure A.4: Power transmission capacity for baseline and no CO₂ sequestration scenarios under no synthetic fuel adoption. Within each panel, the amount of H₂ HDV adoption increases moving from left to right.

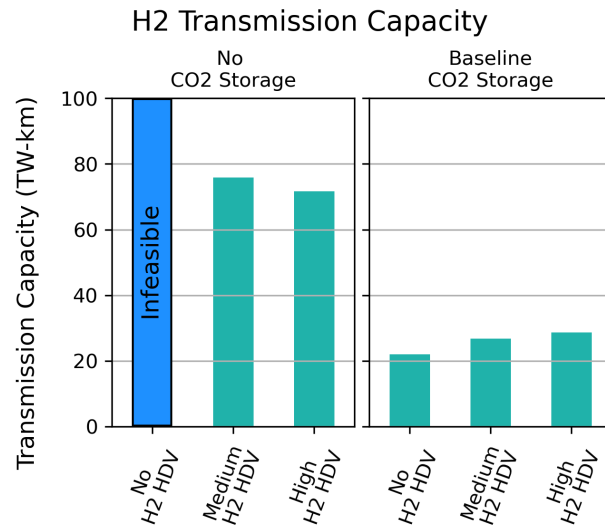


Figure A.5: H₂ transmission capacity for baseline and no CO₂ sequestration scenarios under no synthetic fuel adoption. Within each panel, the amount of H₂ HDV adoption increases moving from left to right.

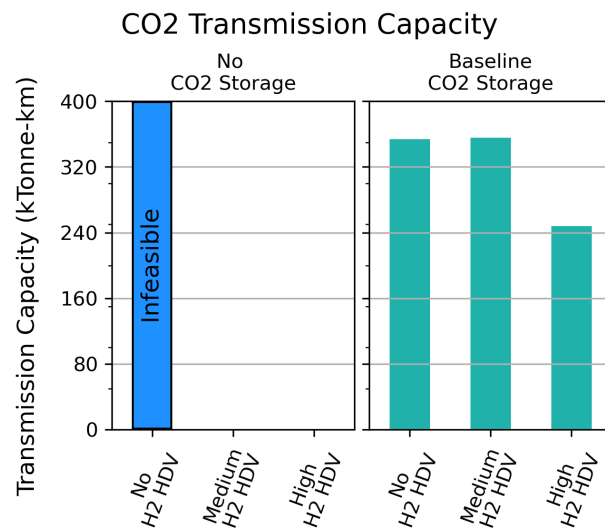


Figure A.6: CO₂ transmission capacity for baseline and no CO₂ sequestration scenarios under no synthetic fuel adoption. Within each panel, the amount of H₂ HDV adoption increases moving from left to right.

Table A.1

This table shows the marginal price of abatement of CO₂ for Core Scenario Set 1

CO ₂ Storage	H ₂ HDV Level	Synthetic Fuel HDV Level	CO ₂ Marginal Cost of Abatement
Baseline	None	None	293.92
Baseline	Medium	None	293.92
Baseline	High	None	149.79
None	Medium	None	1523.03
None	High	None	746.25

A.2. Core Scenario Set 2 Detailed Results

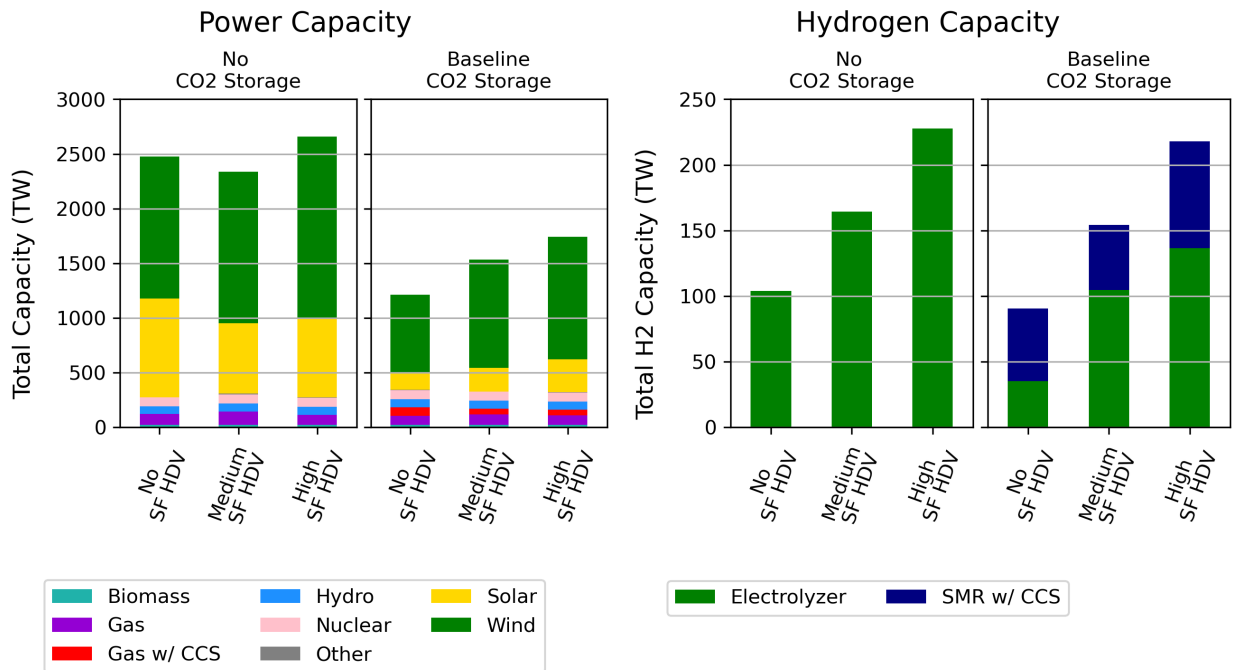


Figure A.7: Power and H₂ capacity for baseline and no CO₂ sequestration scenarios under medium H₂ HDV adoption and varying scenarios of synthetic fuel adoption. The left set of charts shows power generation and the right set of charts shows H₂ generation. Within each panel, the amount of synthetic fuel adoption increases moving from left to right.

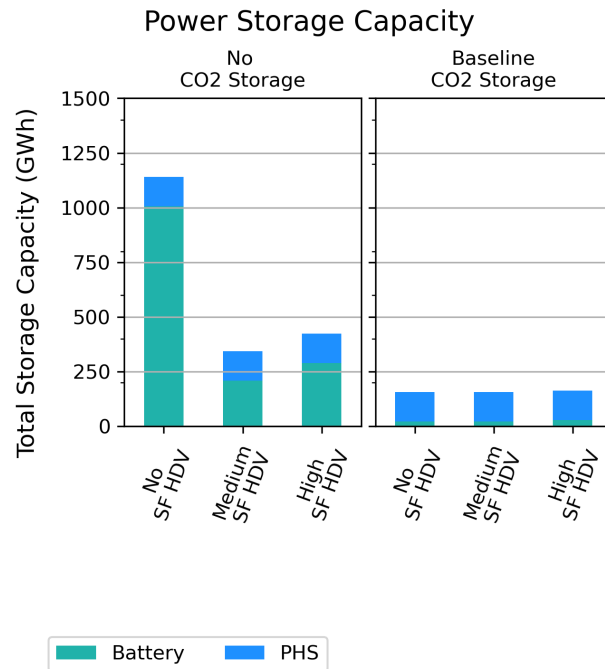


Figure A.8: Power storage capacity for baseline and no CO₂ sequestration scenarios under medium H₂ HDV adoption and varying scenarios of synthetic fuel adoption. Within each panel, the amount of synthetic fuel adoption increases moving from left to right.

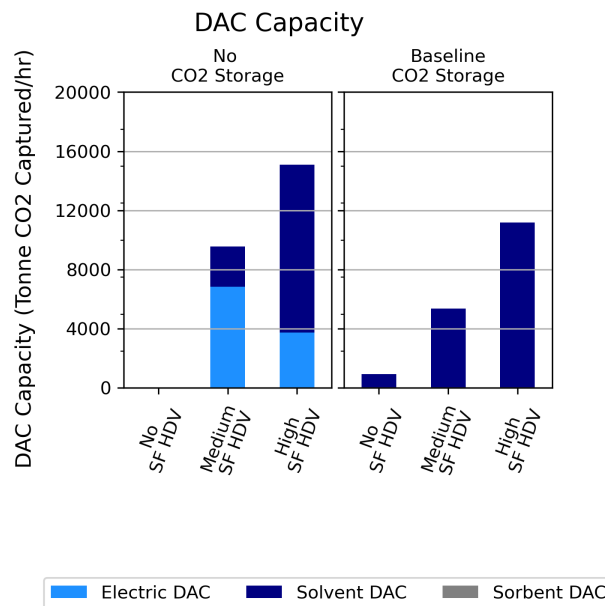


Figure A.9: Direct Air Capture capacity for baseline and no CO₂ sequestration scenarios under medium H₂ HDV adoption and varying scenarios of synthetic fuel adoption. Within each panel, the amount of synthetic fuel adoption increases moving from left to right.

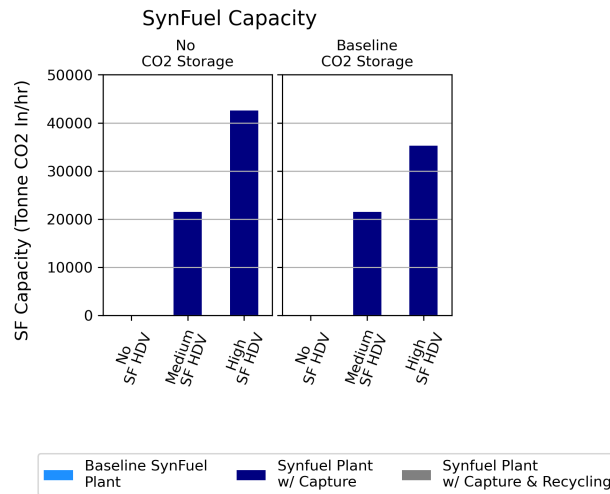


Figure A.10: synthetic fuel capacity for baseline and no CO₂ sequestration scenarios under medium H₂ HDV adoption and varying scenarios of synthetic fuel adoption. Within each panel, the amount of synthetic fuel adoption increases moving from left to right.

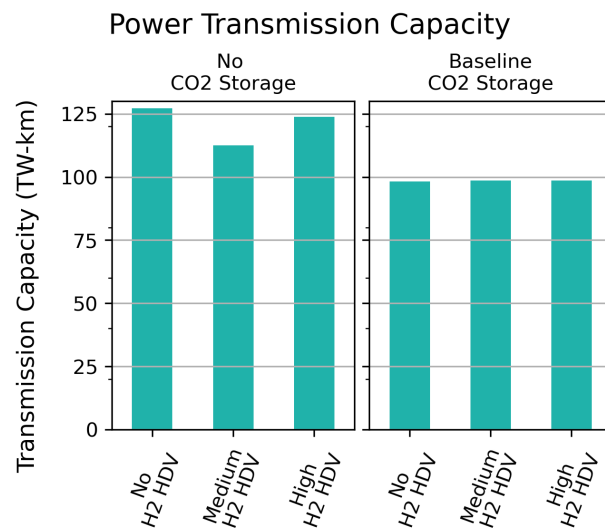


Figure A.11: Power transmission capacity for baseline and no CO₂ sequestration scenarios under medium H₂ HDV adoption and varying scenarios of synthetic fuel adoption. Within each panel, the amount of synthetic fuel adoption increases moving from left to right.

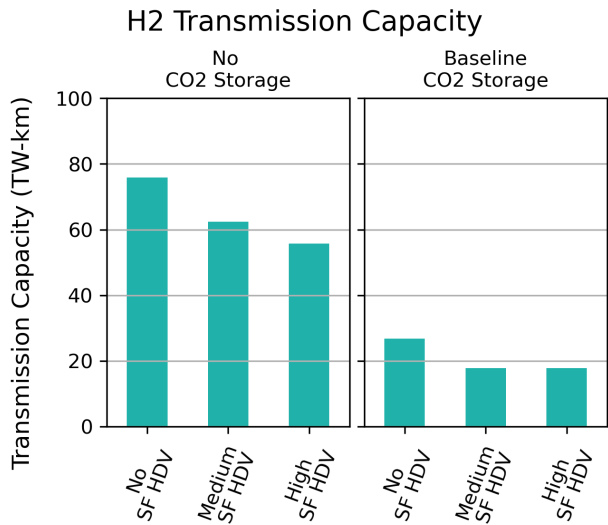


Figure A.12: H₂ transmission capacity for baseline and no CO₂ sequestration scenarios under medium H₂ HDV adoption and varying scenarios of synthetic fuel adoption. Within each panel, the amount of synthetic fuel adoption increases moving from left to right.

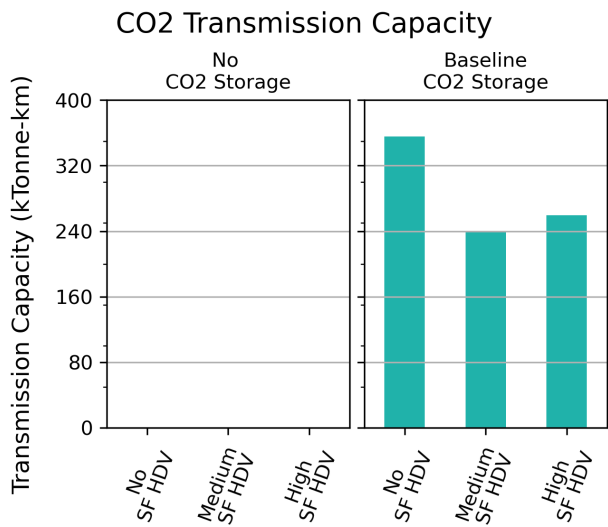


Figure A.13: CO₂ transmission capacity for baseline and no CO₂ sequestration scenarios under medium H₂ HDV adoption and varying scenarios of synthetic fuel adoption. Within each panel, the amount of synthetic fuel adoption increases moving from left to right.

Table A.2

This tables shows the marginal price of abatement of CO₂ for Core Scenario Set 2

CO ₂ Storage	H ₂ HDV Level	Synthetic Fuel HDV Level	CO ₂ Marginal Cost of Abatement
Baseline	Medium	None	293.92
Baseline	Medium	Medium	268.80
Baseline	Medium	High	293.91
None	Medium	None	1603.09
None	Medium	Medium	480.12
None	Medium	High	567.48

A.3. Sensitivity Set 1: Core Scenario Set 1 with Relaxed Emissions Constraint

The results in this section represent Sensitivity Set 1 as described in Figure 3b of the main text.

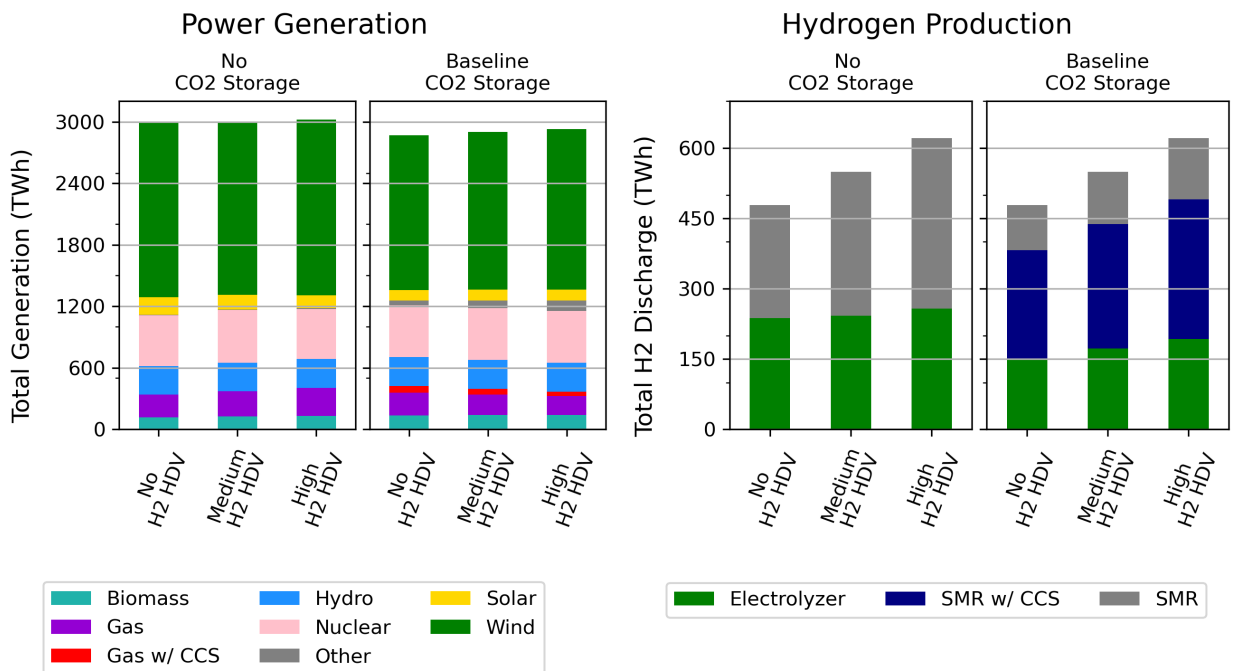


Figure A.14: Power and H₂ generation for baseline and no CO₂ sequestration scenarios under no synthetic fuel adoption. The left set of charts shows power generation and the right set of charts shows H₂ generation. Within each panel, the amount of H₂ HDV adoption increases moving from left to right. CO₂ constraint is relaxed compared to core scenario set 1.

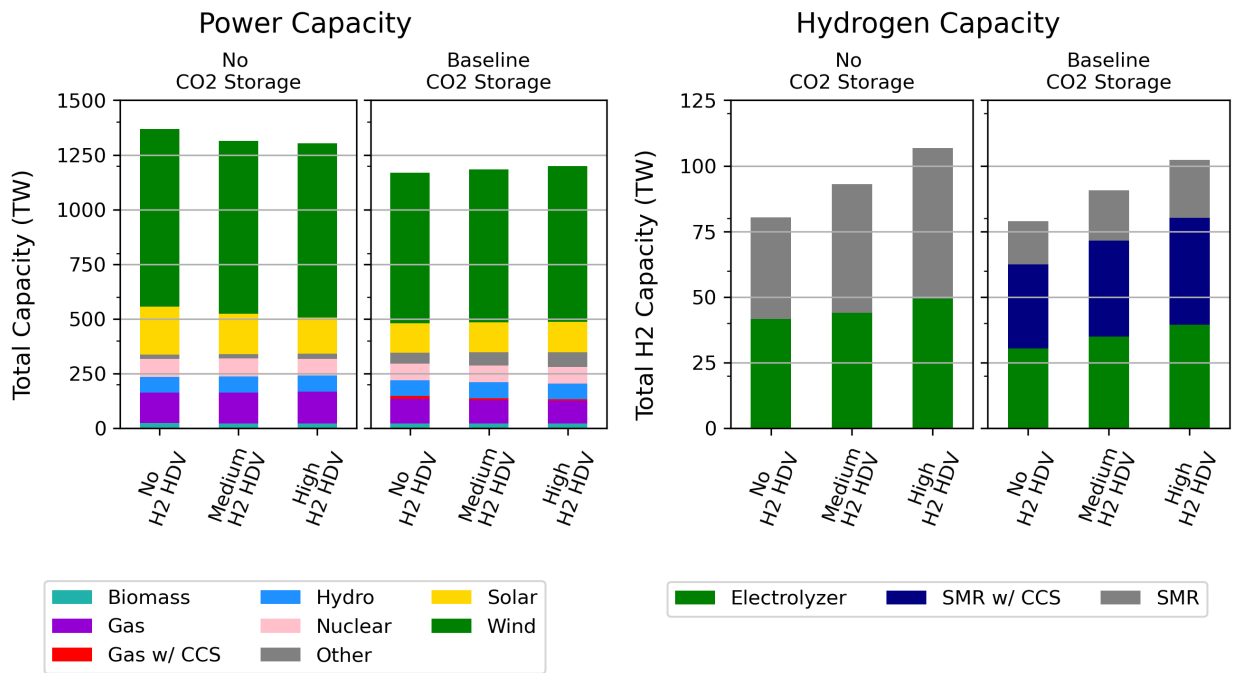


Figure A.15: Power and H₂ capacity for baseline and no CO₂ sequestration scenarios under no synthetic fuel adoption. The left set of charts shows power generation and the right set of charts shows H₂ generation. Within each panel, the amount of H₂ HDV adoption increases moving from left to right. CO₂ constraint is relaxed compared to core scenario set 1.

No DAC is deployed in this scenario set.

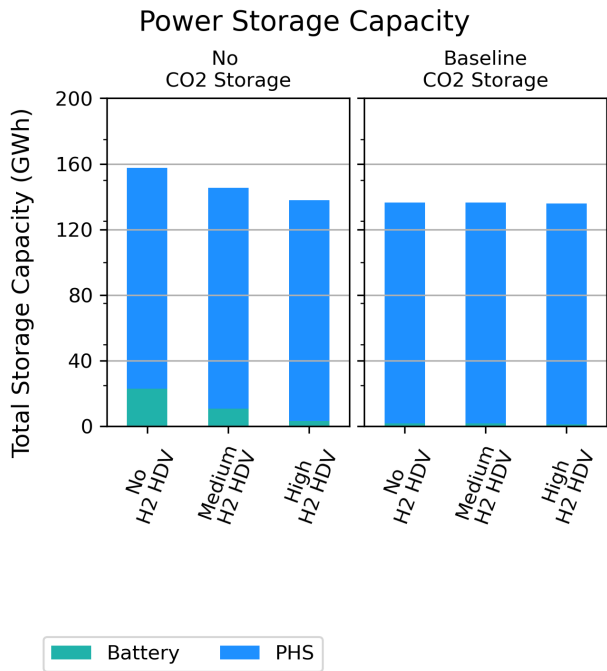


Figure A.16: Power storage capacity for baseline and no CO₂ sequestration scenarios under no synthetic fuel adoption. Within each panel, the amount of H₂ HDV adoption increases moving from left to right. CO₂ constraint is relaxed compared to core scenario set 1.

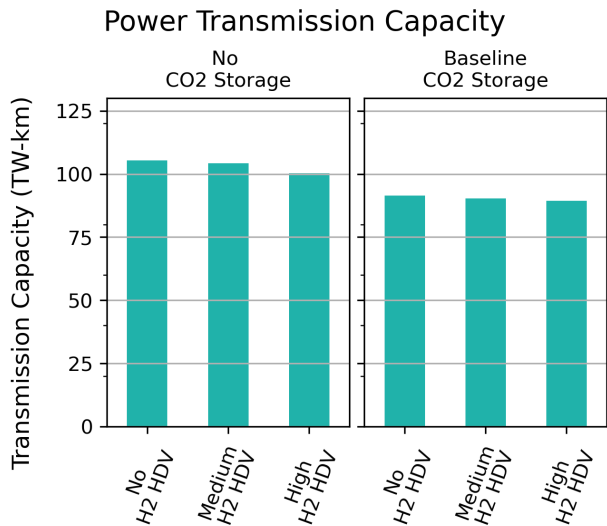


Figure A.17: Power transmission capacity for baseline and no CO₂ sequestration scenarios under no synthetic fuel adoption. Within each panel, the amount of H₂ HDV adoption increases moving from left to right. CO₂ constraint is relaxed compared to core scenario set 1.

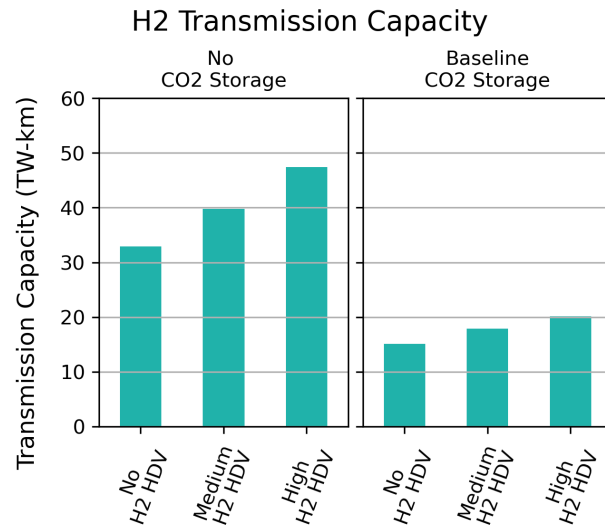


Figure A.18: H₂ transmission capacity for baseline and no CO₂ sequestration scenarios under no synthetic fuel adoption. Within each panel, the amount of H₂ HDV adoption increases moving from left to right. CO₂ constraint is relaxed compared to core scenario set 1.

No CO₂ transmission is build in this scenario set.

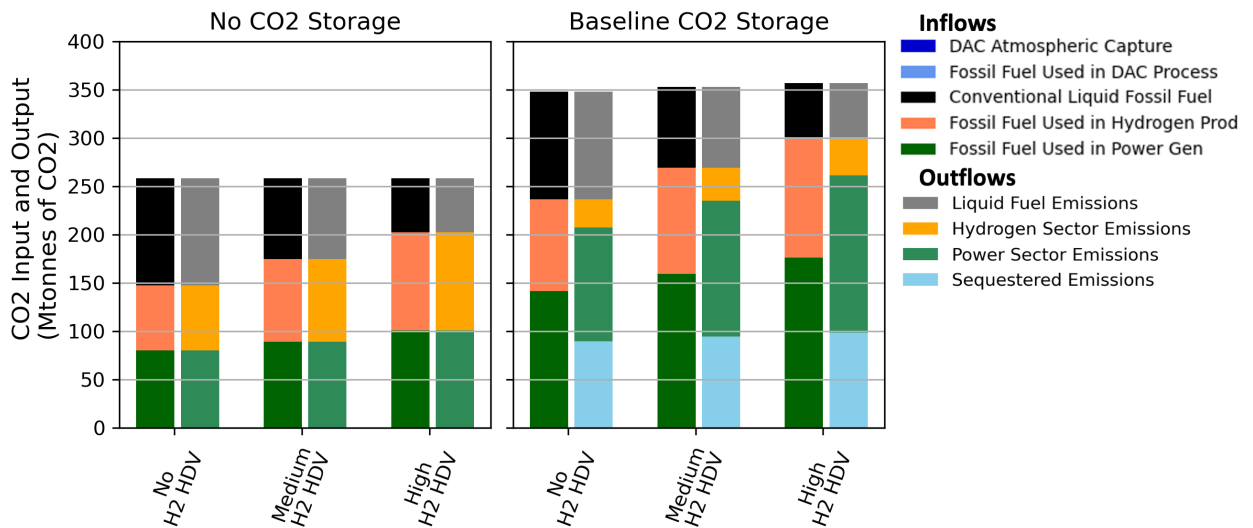


Figure A.19: System CO₂ balance under varying levels of H₂ HDV adoption and no SF adoption. The subfigure on the left shows the CO₂ balance under no CO₂ sequestration availability, while the one on the right shows the CO₂ balance under baseline CO₂ storage availability. Within each subplot the H₂ HDV adoption level increases left to right. The leftward column represents CO₂ input into the system, while the rightward column represents CO₂ outputted by the system. All scenarios adhere to the same emissions constraint of 258 Mtonnes. CO₂ constraint is relaxed compared to core scenario set 1. Emissions constraint can be calculated from the chart by subtracting sequestered emissions and DAC atmospheric capture from the emission outflows.

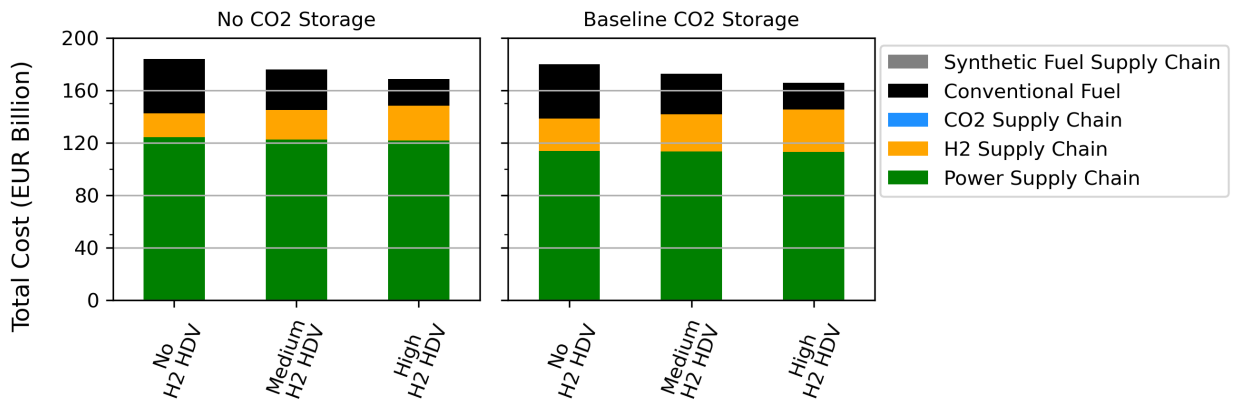


Figure A.20: Annualized bulk-system costs under varying levels of H₂ HDV adoption and no SF adoption. The subfigure on the left shows the cost breakdown under no CO₂ sequestration availability, while the one on the right shows the cost breakdown under baseline CO₂ sequestration availability. Within each subplot the H₂ HDV adoption level increases left to right. CO₂ constraint is relaxed compared to core scenario set 1. The costs do not include vehicle replacement or H₂ distribution costs.

Table A.3

This table shows the marginal price of abatement of CO₂ for Sensitivity Set 1

CO ₂ Storage	H ₂ HDV Level	Synthetic Fuel HDV Level	CO ₂ Marginal Cost of Abatement
Baseline	None	None	71.88
Baseline	Medium	None	69.72
Baseline	High	None	67.32
None	None	None	159.88
None	Medium	None	118.86
None	High	None	90.71

A.4. Sensitivity Set 2: Core Scenario Set 1 Natural Gas Price Sensitivity

The results in this section represent Sensitivity Set 2 as described in Figure 3b of the main text.

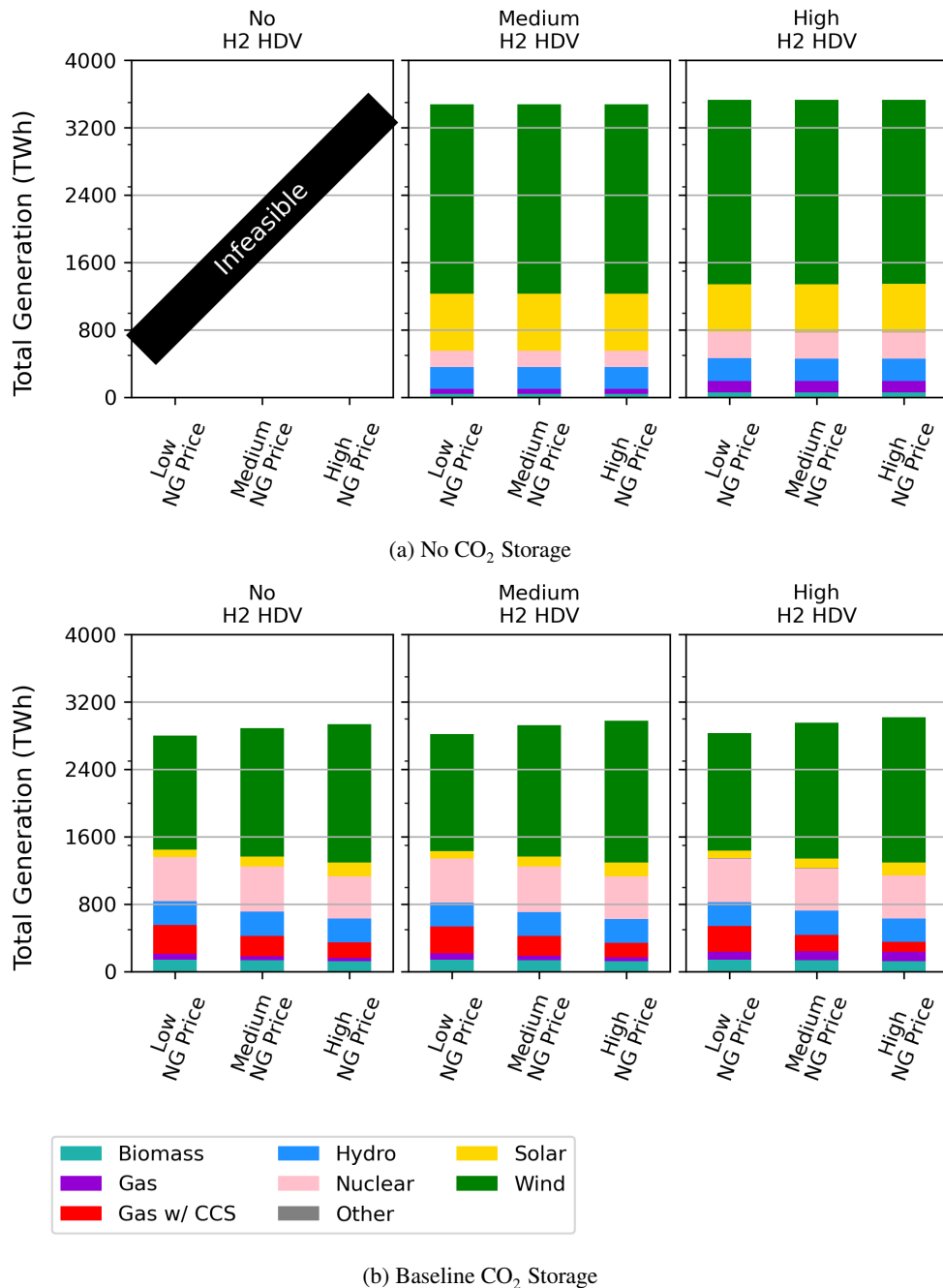


Figure A.21: Power generation for no (sub-figure a) and baseline (sub-figure b) CO₂ sequestration scenarios under no synthetic fuel adoption. Within each panel, the price of natural gas increases left to right. Across panels, the amount of H₂ HDV adoption increases moving from left to right. The middle panels correspond to the core set of scenarios.

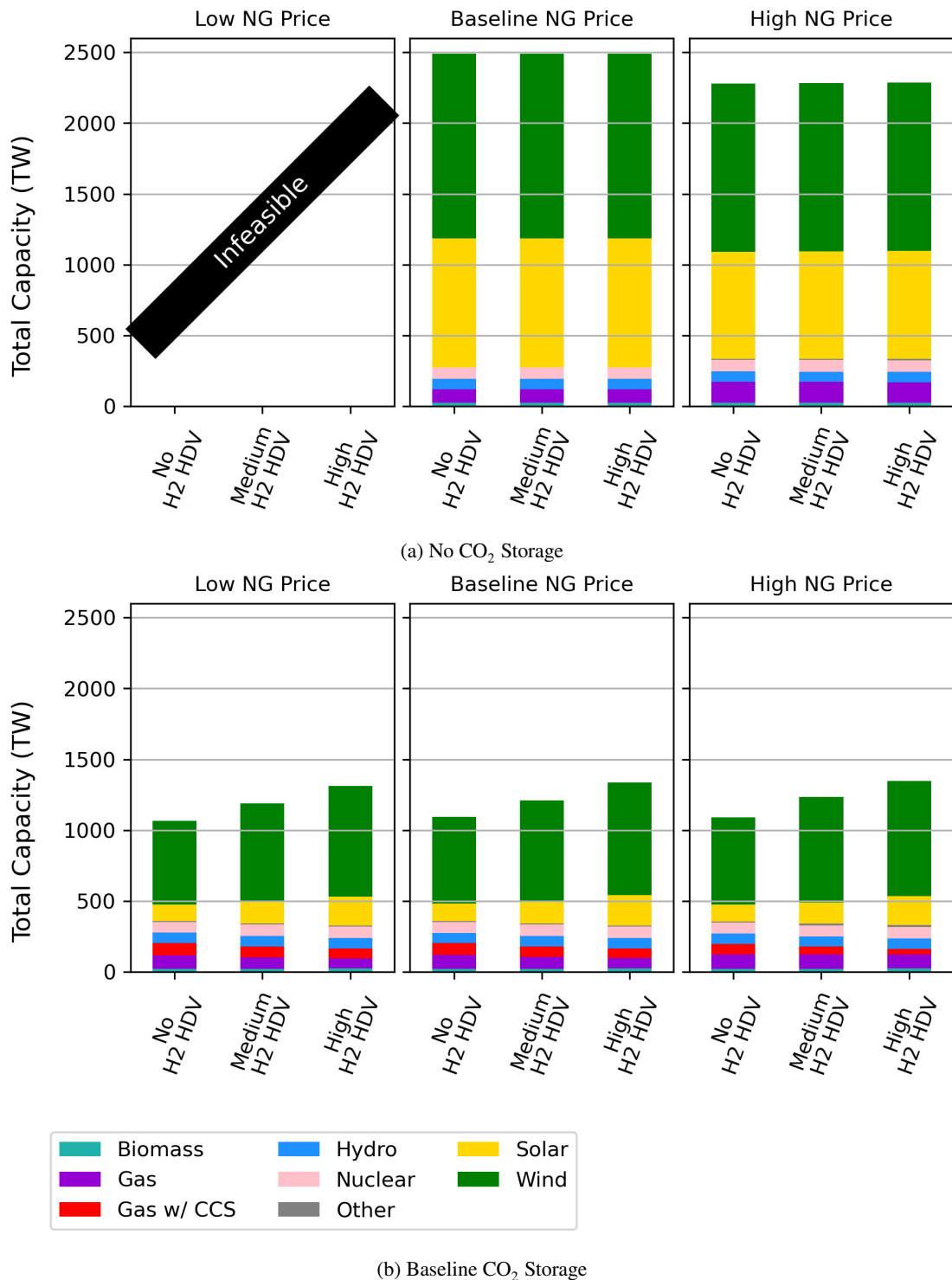


Figure A.22: Power capacity for no (sub-figure a) and baseline (sub-figure b) CO₂ sequestration scenarios under no synthetic fuel adoption. Within each panel, the price of natural gas increases left to right. Across panels, the amount of H₂ HDV adoption increases moving from left to right. The middle panels correspond to the core set of scenarios.

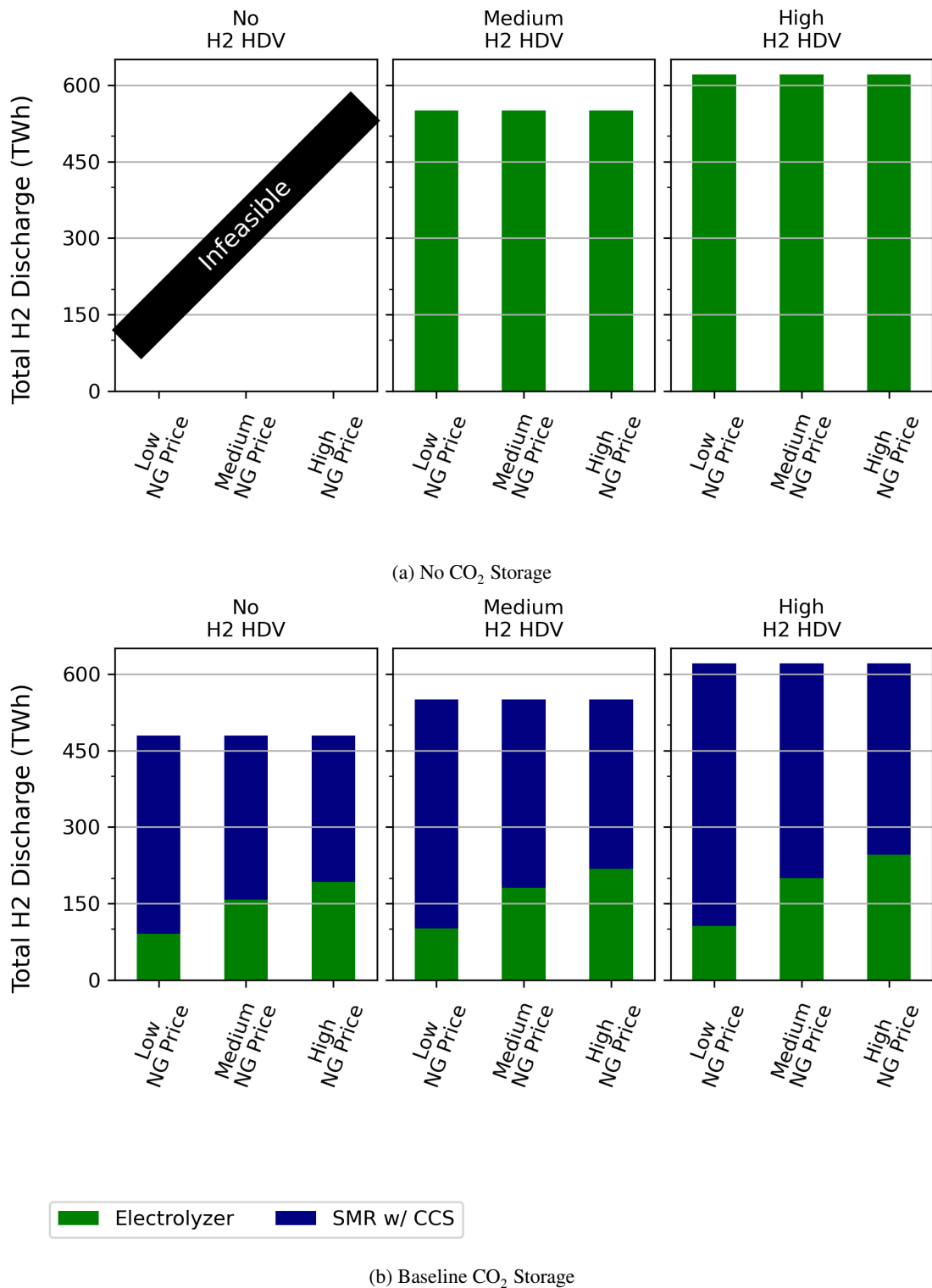


Figure A.23: H₂ generation for no (sub-figure a) and baseline (sub-figure b) CO₂ sequestration scenarios under no synthetic fuel adoption. Within each panel, the price of natural gas increases left to right. Across panels, the amount of H₂ HDV adoption increases moving from left to right. The middle panels correspond to the core set of scenarios.

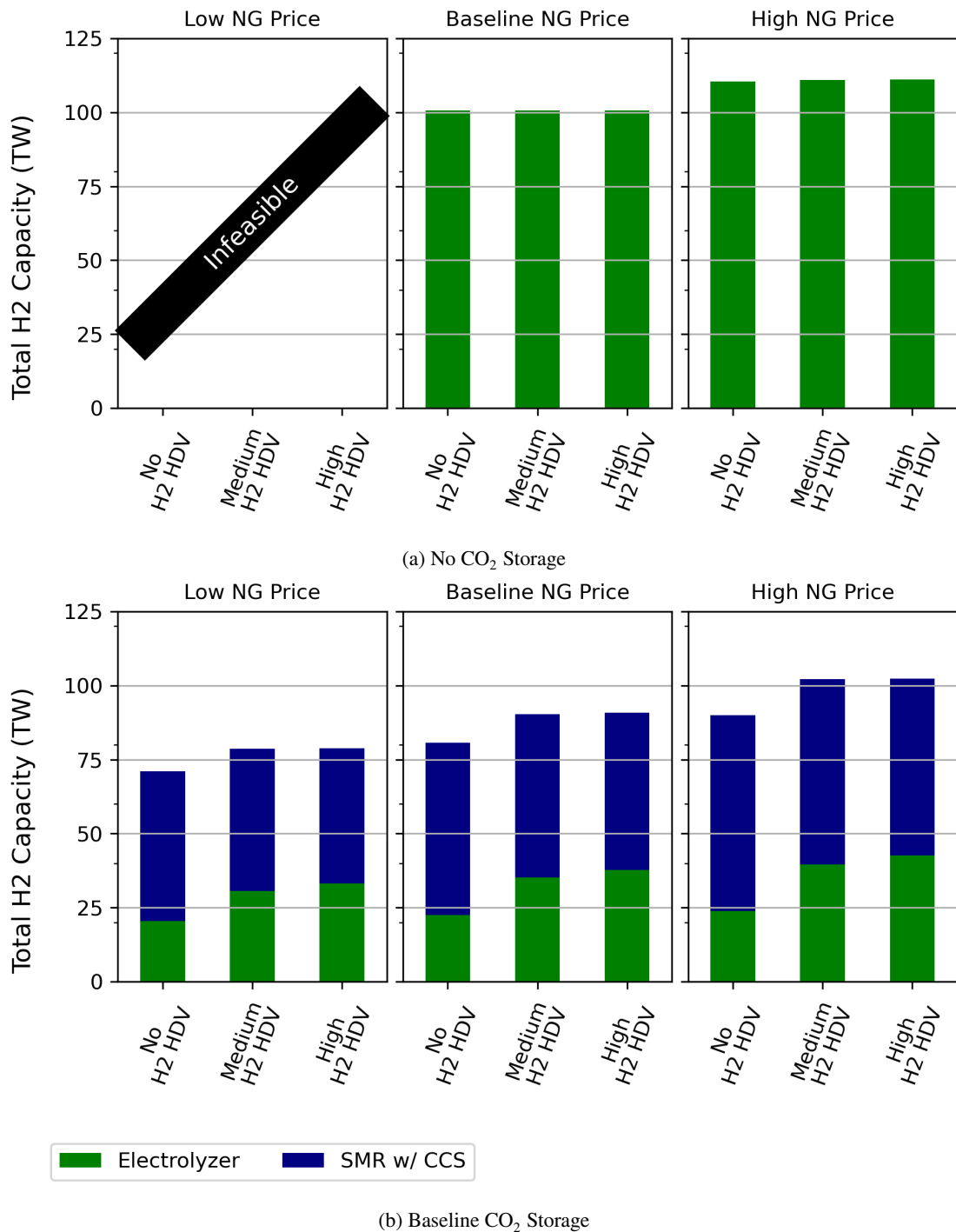


Figure A.24: H₂ capacity for no (sub-figure a) and baseline (sub-figure b) CO₂ sequestration scenarios under no synthetic fuel adoption. Within each panel, the price of natural gas increases left to right. Across panels, the amount of H₂ HDV adoption increases moving from left to right. The middle panels correspond to the core set of scenarios.

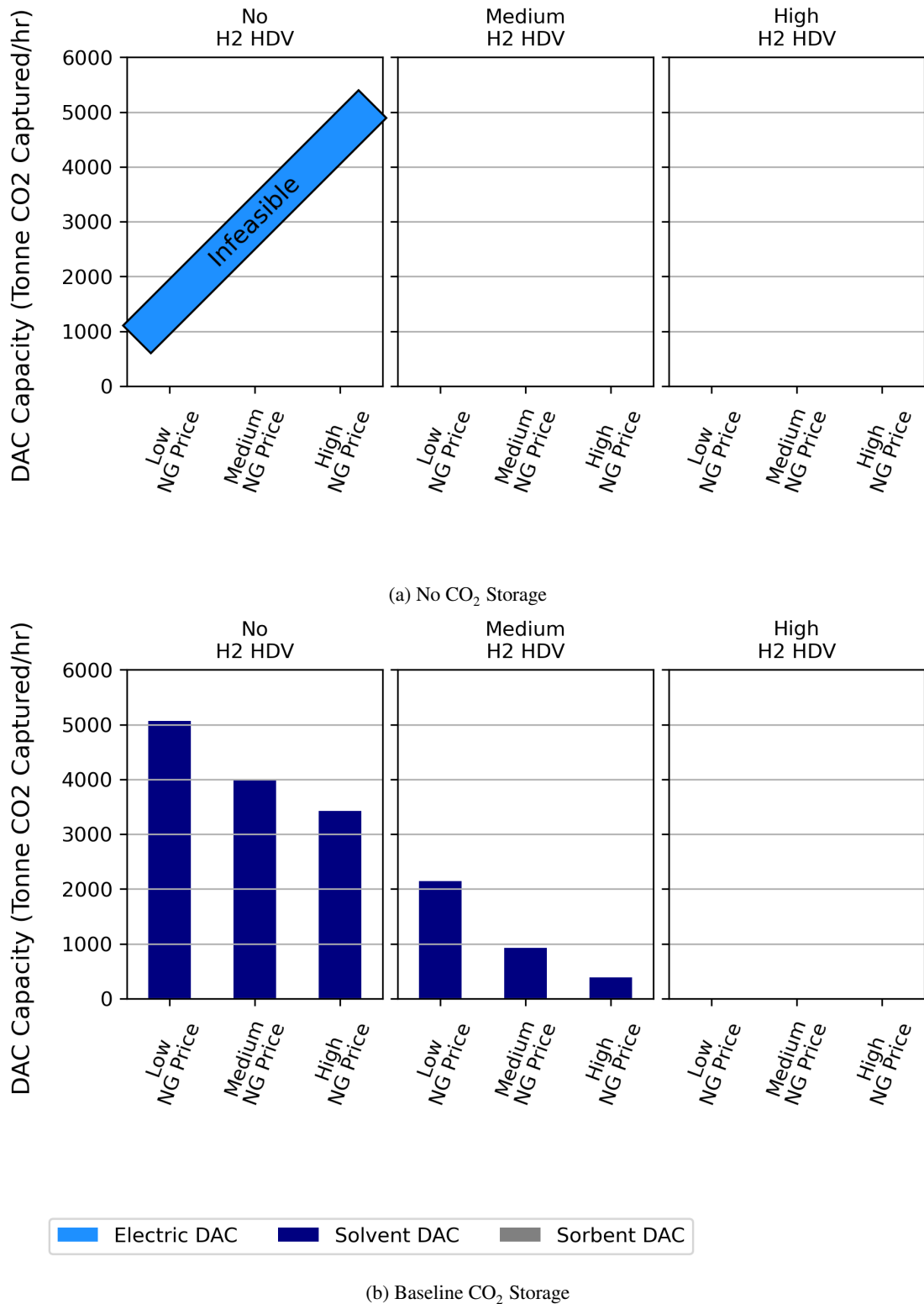


Figure A.25: Direct air capture capacity for no (sub-figure a) and baseline (sub-figure b) CO₂ sequestration scenarios under no synthetic fuel adoption. Within each panel, the price of natural gas increases left to right. Across panels, the amount of H₂ HDV adoption increases moving from left to right. The middle panels correspond to the core set of scenarios.

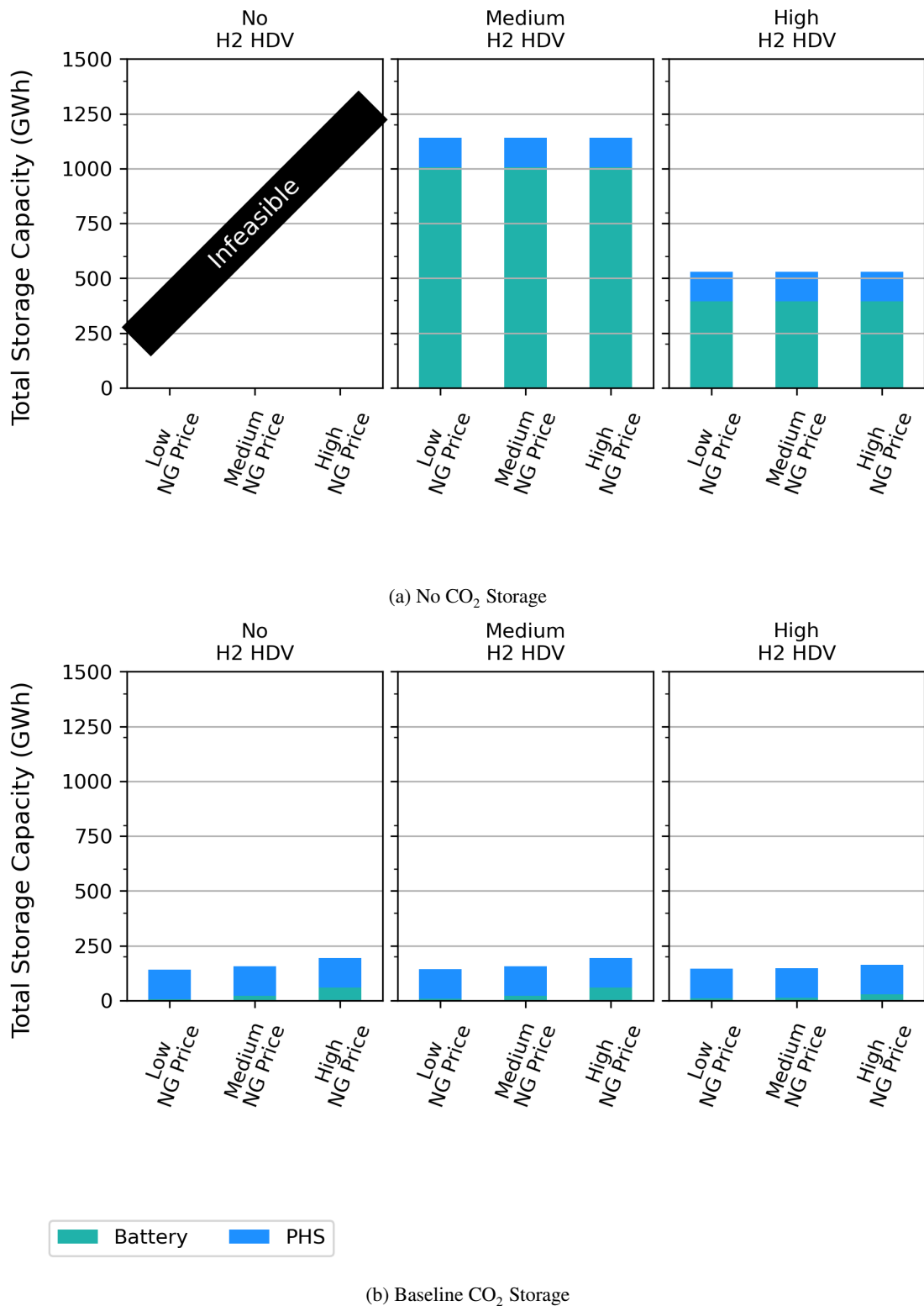


Figure A.26: Electric storage capacity for no (sub-figure a) and baseline (sub-figure b) CO₂ sequestration scenarios under no synthetic fuel adoption. Within each panel, the price of natural gas increases left to right. Across panels, the amount of H₂ HDV adoption increases moving from left to right. The middle panels correspond to the core set of scenarios.

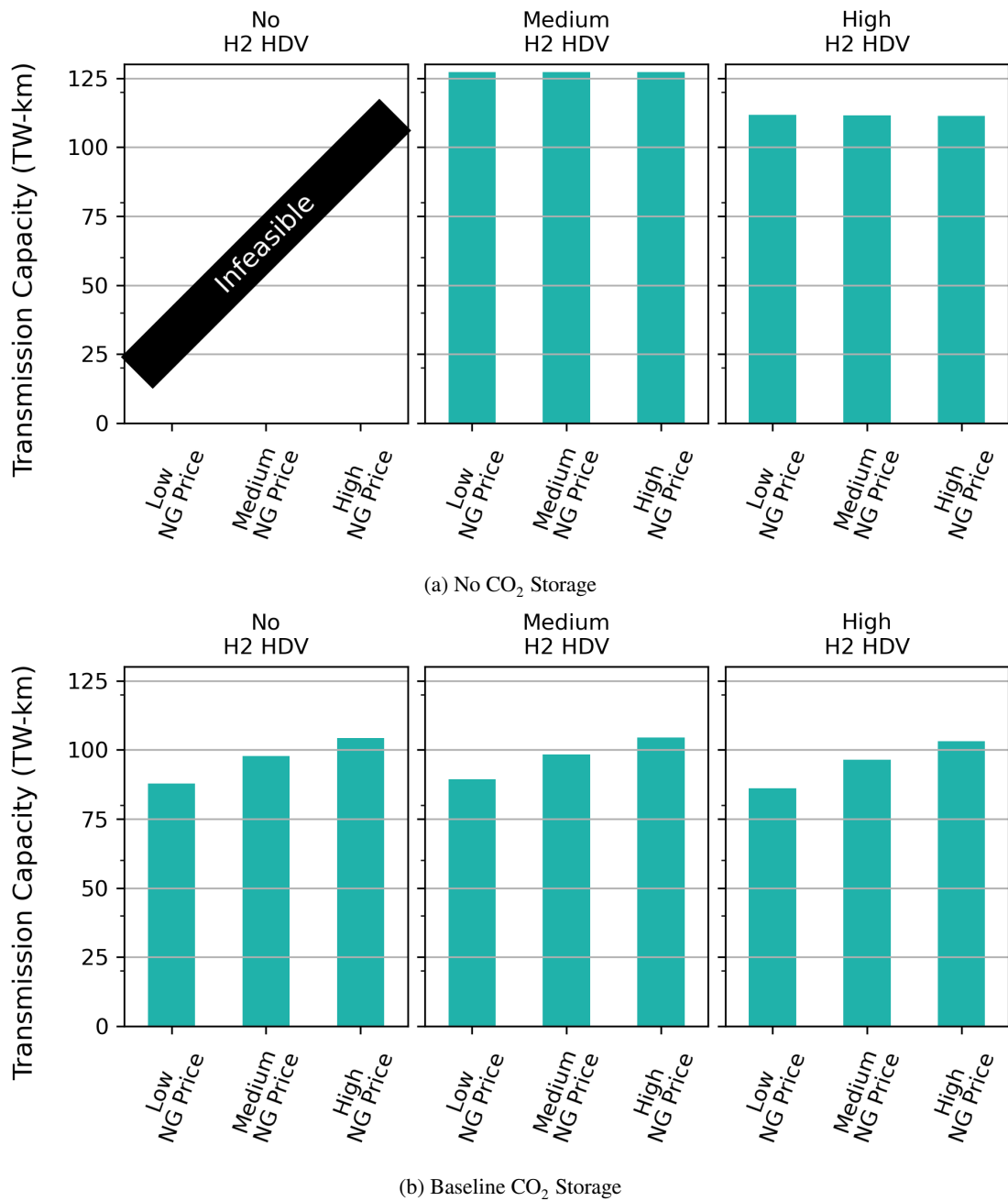


Figure A.27: Power transmission capacity for no (sub-figure a) and baseline (sub-figure b) CO₂ sequestration scenarios under no synthetic fuel adoption. Within each panel, the price of natural gas increases left to right. Across panels, the amount of H₂ HDV adoption increases moving from left to right. The middle panels correspond to the core set of scenarios.

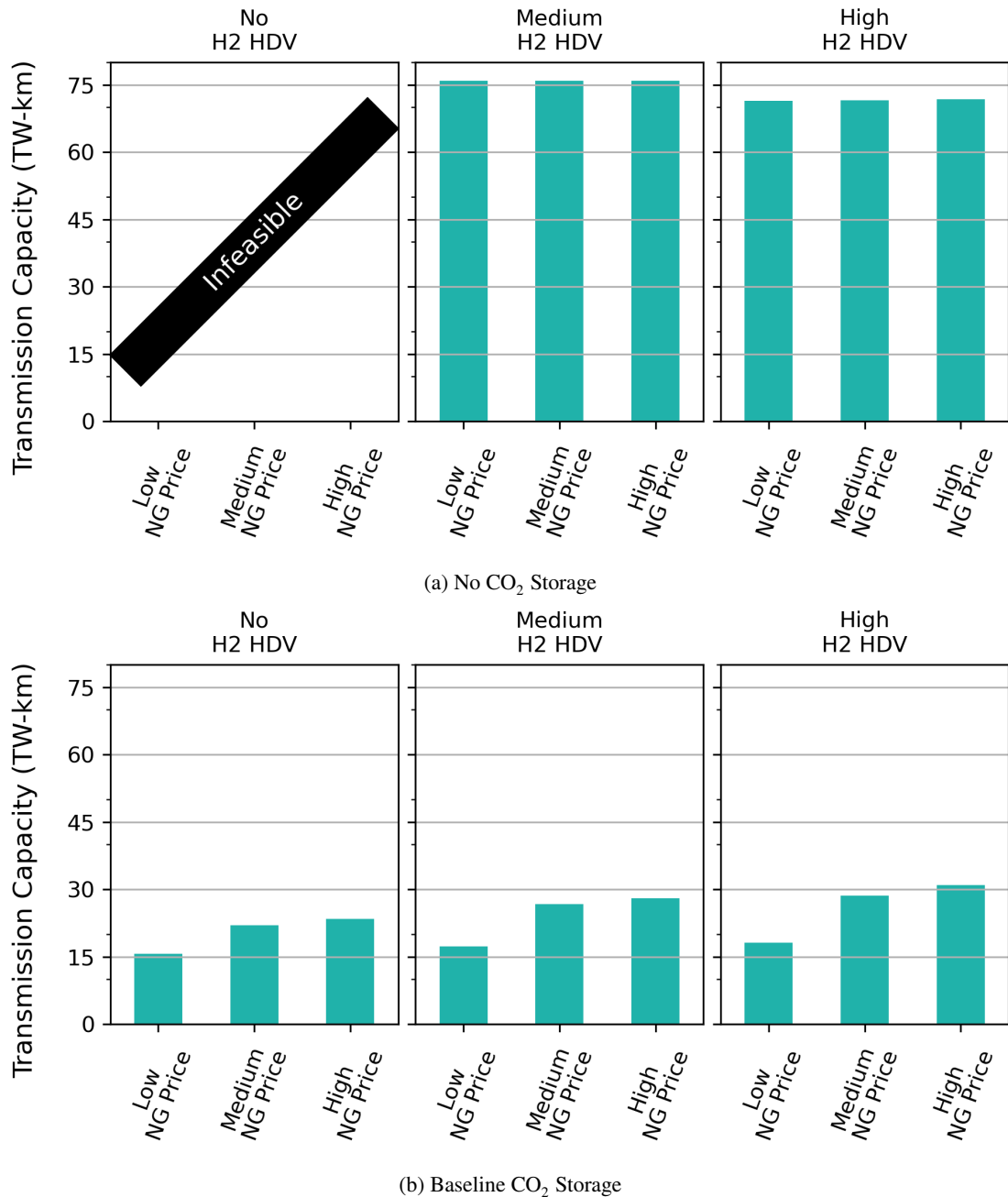


Figure A.28: H₂ transmission capacity for no (sub-figure a) and baseline (sub-figure b) CO₂ sequestration scenarios under no synthetic fuel adoption. Within each panel, the price of natural gas increases left to right. Across panels, the amount of H₂ HDV adoption increases moving from left to right. The middle panels correspond to the core set of scenarios.

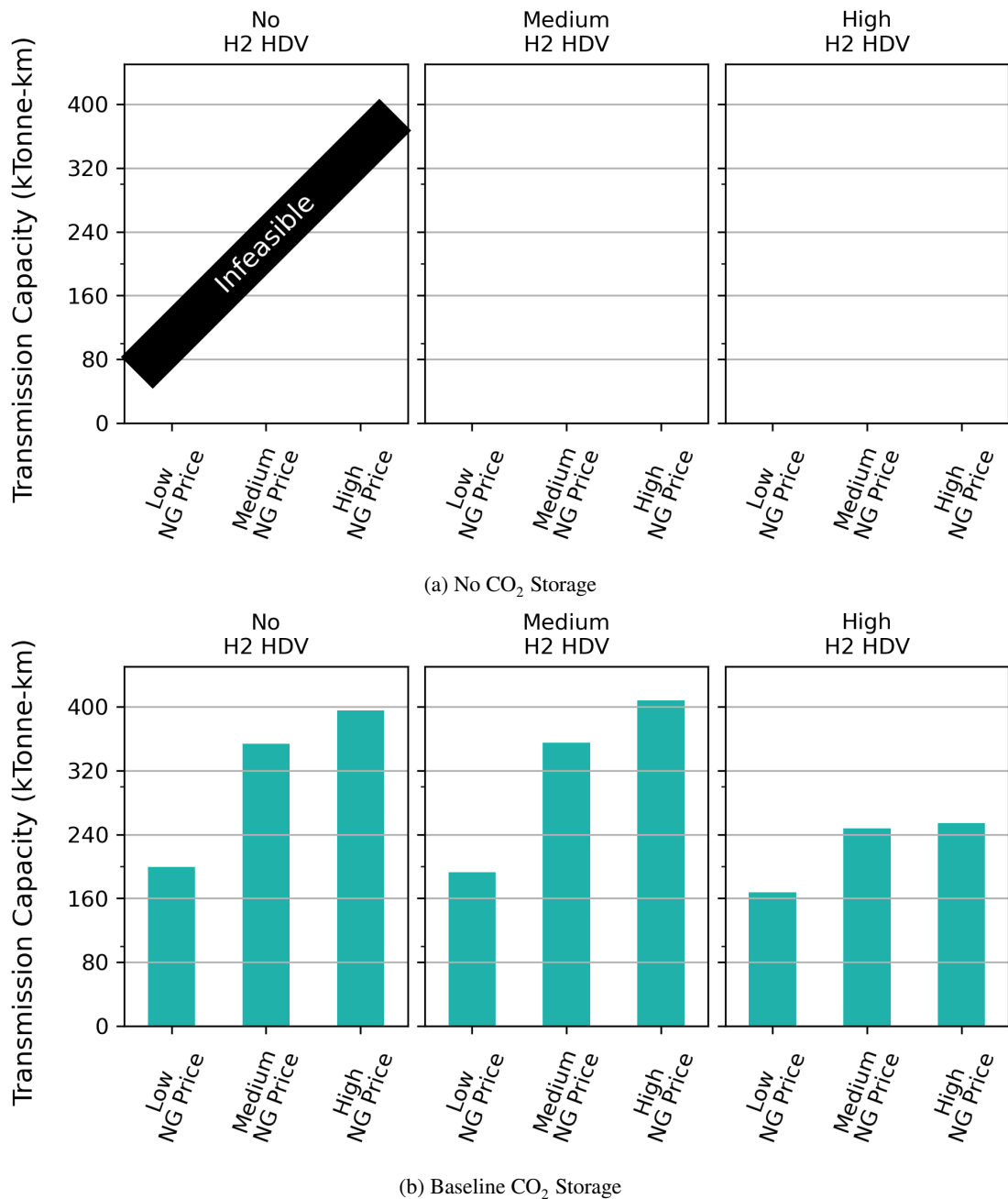


Figure A.29: CO₂ transmission capacity for no (sub-figure a) and baseline (sub-figure b) CO₂ sequestration scenarios under no synthetic fuel adoption. Within each panel, the price of natural gas increases left to right. Across panels, the amount of H₂ HDV adoption increases moving from left to right. The middle panels correspond to the core set of scenarios.

Multi-sectoral Impacts of H₂ and Synthetic Fuels Adoption for Heavy-duty Transportation Decarbonization

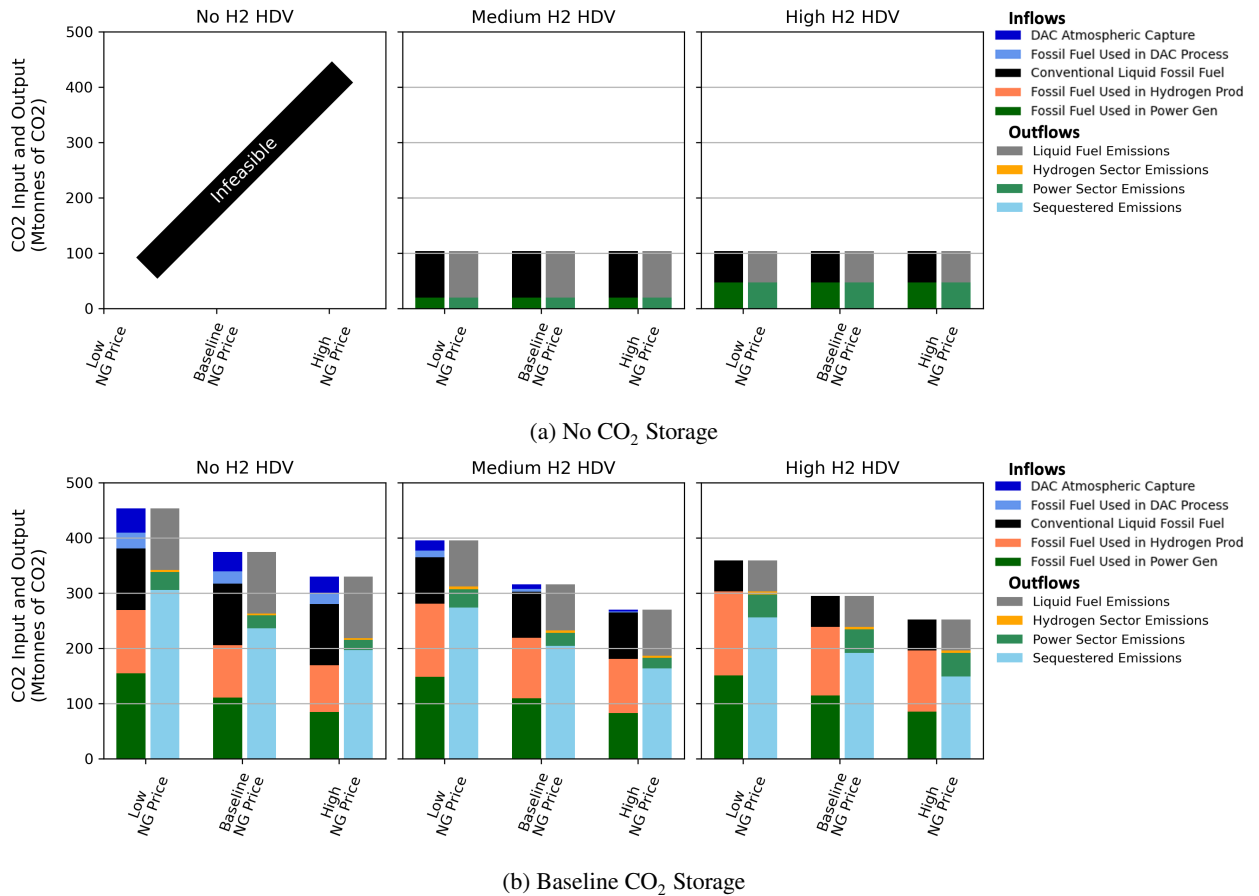


Figure A.30: System CO₂ balance under varying levels of H₂ HDV adoption and no SF adoption for no (sub-figure a) and baseline (sub-figure b) CO₂ sequestration scenarios. Within each panel, the price of natural gas increases left to right. Across panels, the amount of H₂ HDV adoption increases moving from left to right. The middle panels correspond to the core set of scenarios. The leftward column represents CO₂ input into the system, while the rightward column represents CO₂ outputted by the system. All scenarios adhere to the same emissions constraint of 103 Mtonnes. The middle panels correspond to the core set of scenarios. Emissions constraint can be calculated from the chart by subtracting sequestered emissions and DAC atmospheric capture from the emission outflows. Emissions constraint can be calculated from the chart by subtracting sequestered emissions and DAC atmospheric capture from the emission outflows.

Multi-sectoral Impacts of H₂ and Synthetic Fuels Adoption for Heavy-duty Transportation Decarbonization

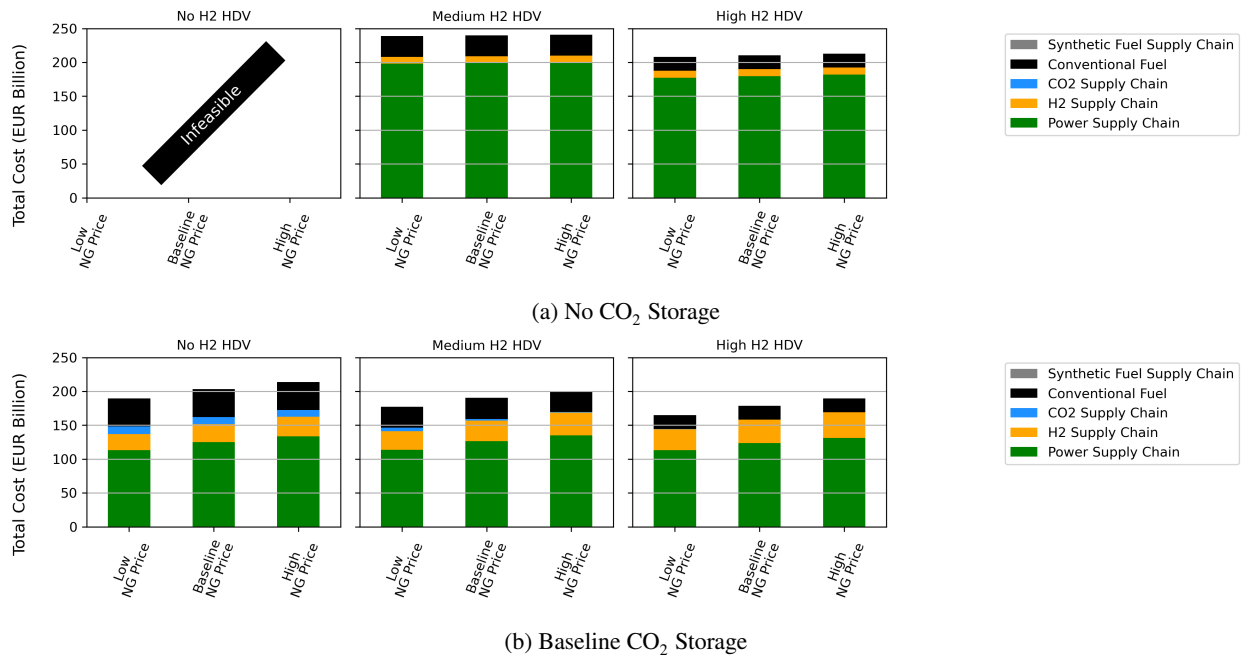


Figure A.31: Annualized bulk-system costs under varying levels of H₂ HDV adoption and no SF adoption for no (sub-figure a) and baseline (sub-figure b) CO₂ sequestration scenarios. Within each panel, the price of natural gas increases left to right. Across panels, the amount of H₂ HDV adoption increases moving from left to right. The middle panels correspond to the core set of scenarios. The costs do not include vehicle replacement or H₂ distribution costs.

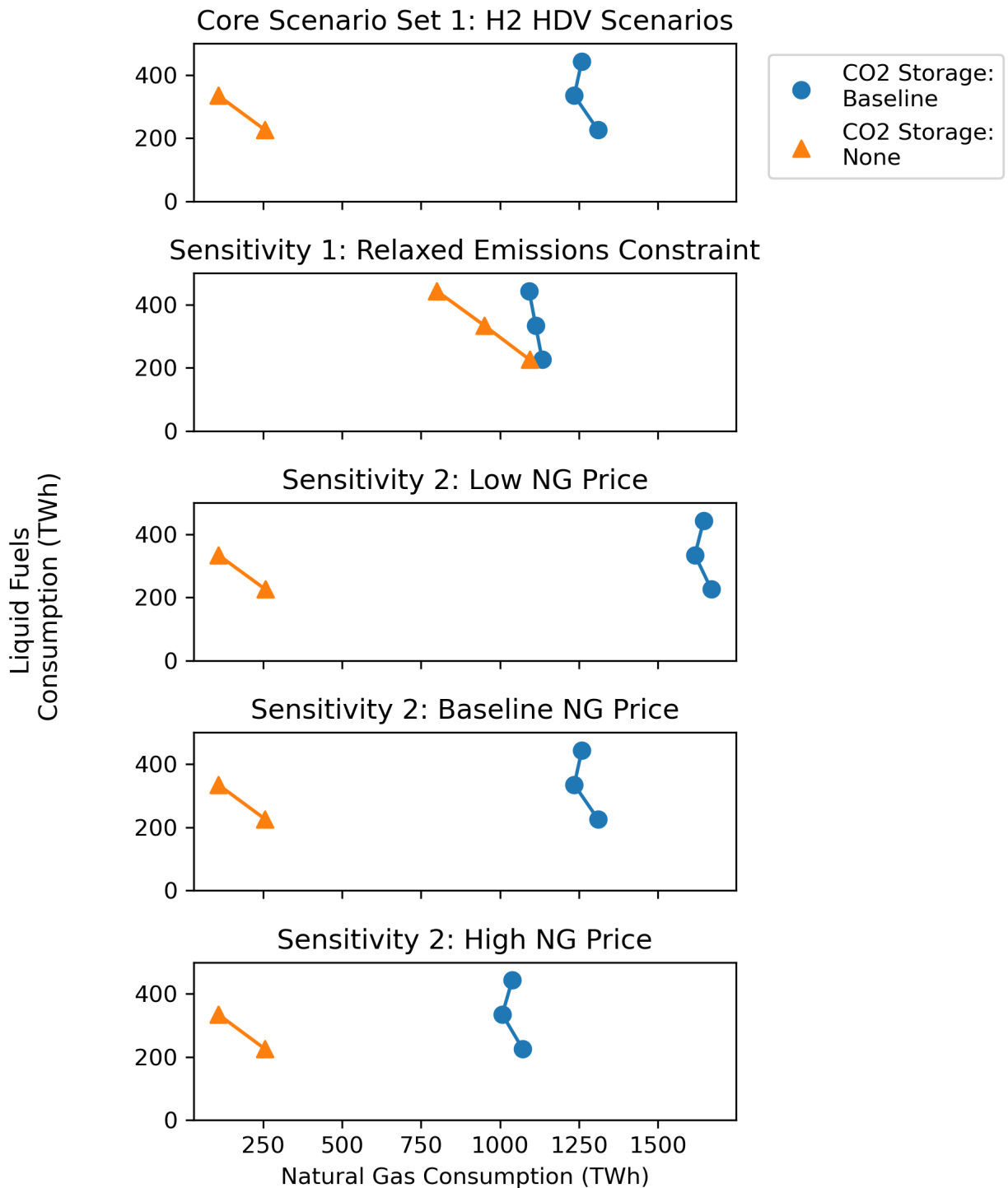


Figure A.32: Trade-off between natural gas (NG) and liquid fossil fuel utilization for scenarios where amount of H₂ HDVs is varied. The subfigure on the top shows the relationship for the H₂ HDV scenarios (i.e. scenario set 1), while the second plot shows the results for the relaxed emission sensitivity (i.e. sensitivity scenario set 1). The last 3 shows the results for the natural gas price sensitivities (i.e. sensitivity scenario set 2). Within each subplot the amount of natural gas consumption can be examined on the x-axis, while the amount of liquid fossil fuel consumption can be examined on the y-axis. The amount of H₂ and SF HDV adoption increases from top to bottom. The amount of liquid fossil fuel consumption includes diesel and gasoline, and excludes jet fuel as well as excess synthetic fuels.

Table A.4This tables shows the marginal price of abatement of CO₂ for Sensitivity Set 2

CO ₂ Storage	H ₂ HDV Level	Synthetic Fuel HDV Level	Natural Gas Price	CO ₂ Marginal Cost of Abatement
Baseline	None	None	Low	260.59
Baseline	Medium	None	Low	260.59
Baseline	High	None	Low	195.36
Baseline	None	None	Baseline	293.92
Baseline	Medium	None	Baseline	293.92
Baseline	High	None	Baseline	149.79
Baseline	None	None	High	327.27
Baseline	Medium	None	High	327.25
Baseline	High	None	High	140.91
None	Medium	None	Low	1574.14
None	High	None	Low	792.50
None	Medium	None	Baseline	1523.03
None	High	None	Baseline	746.25
None	Medium	None	High	1471.92
None	High	None	High	697.43

A.5. Sensitivity Set 3: Core Scenario Set 2 with No H₂ HDV Deployment

The results in this section represent Sensitivity Set 3 as described in Figure 3b of the main text.

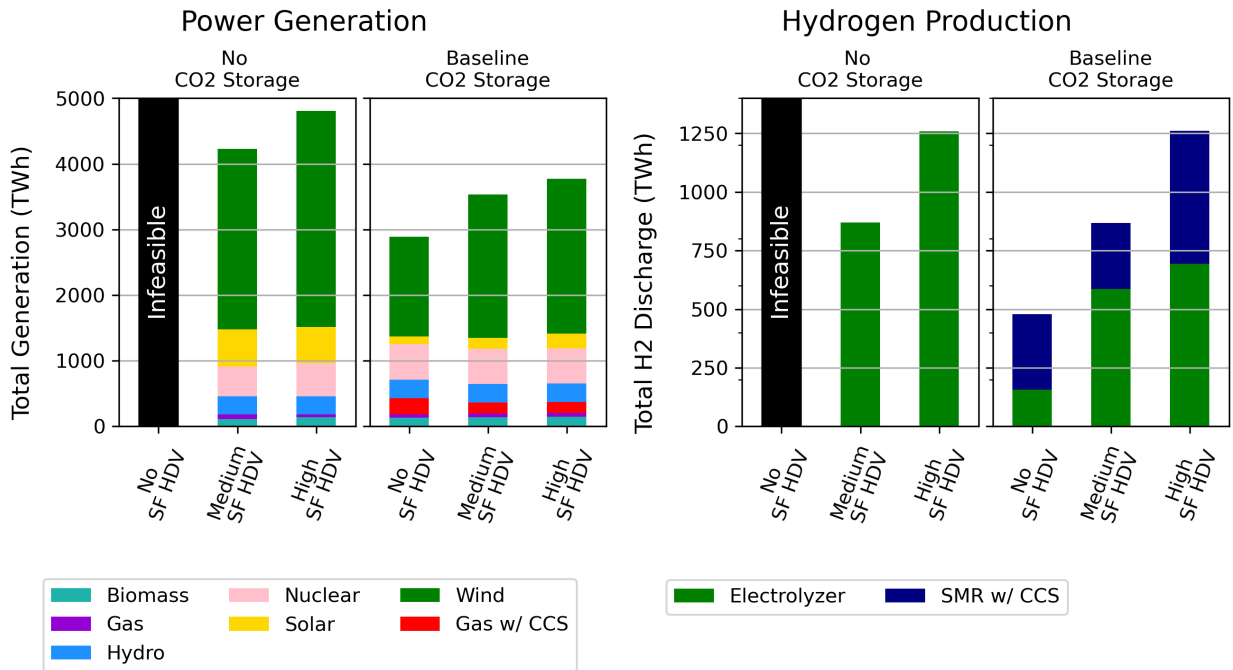


Figure A.33: Power and hydrogen generation for baseline and no CO₂ sequestration scenarios under no H₂ HDV adoption. The left set of charts shows power generation and the right set of charts shows H₂ generation. Within each panel, the amount of synthetic fuel adoption increases moving from left to right.

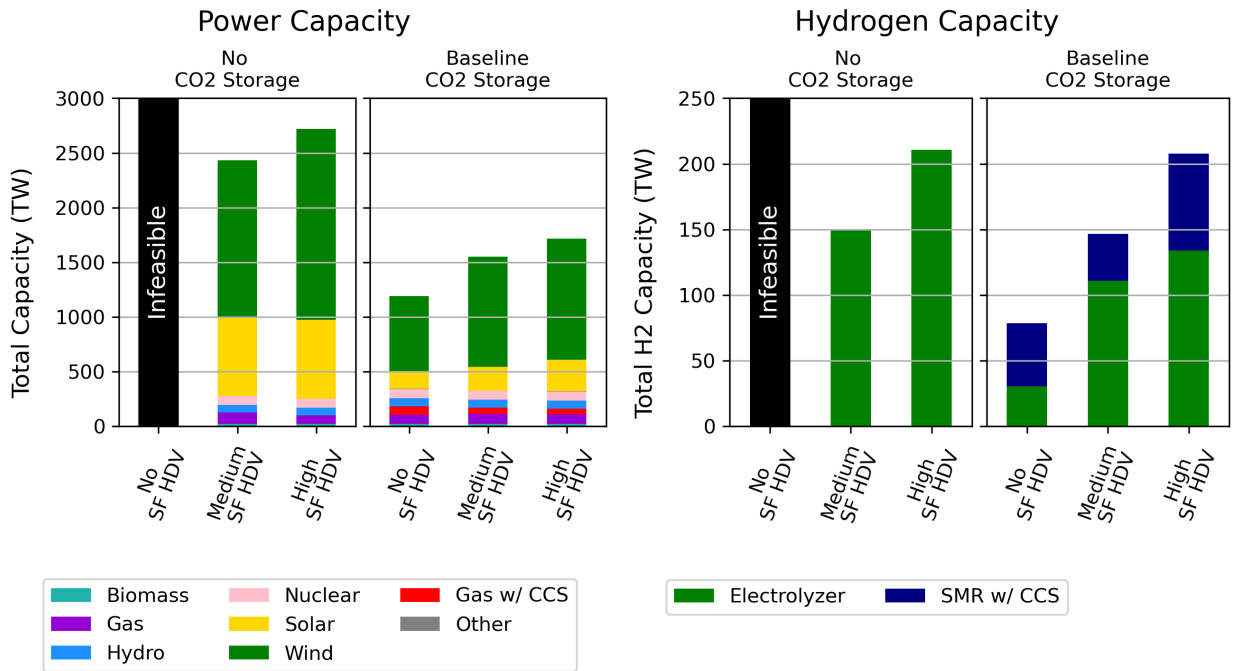


Figure A.34: Power and H₂ capacity for baseline and no CO₂ sequestration scenarios under no H₂ HDV adoption. The left set of charts shows power generation and the right set of charts shows H₂ generation. Within each panel, the amount of synthetic fuel adoption increases moving from left to right.

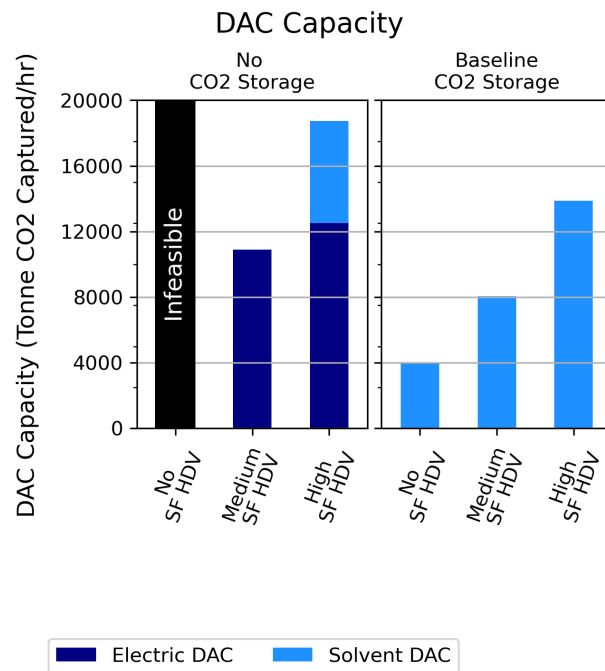


Figure A.35: Direct Air Capture capacity for baseline and no CO₂ sequestration scenarios under no H₂ HDV adoption. Within each panel, the amount of synthetic fuel adoption increases moving from left to right.

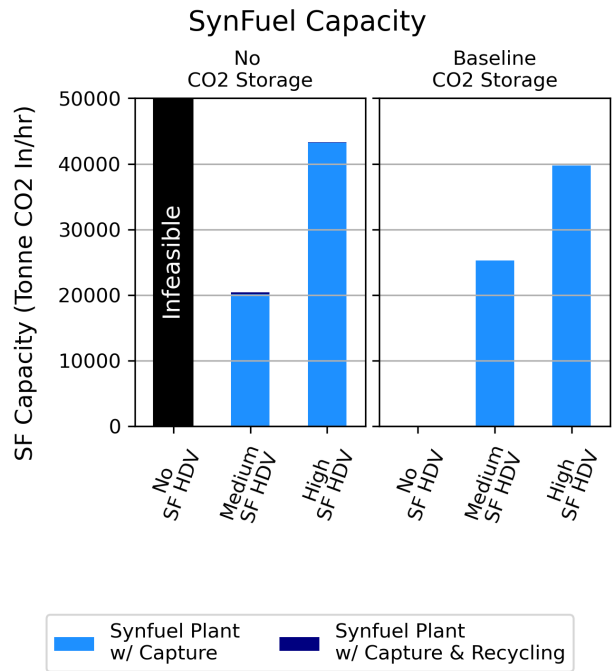


Figure A.36: Synthetic fuel capacity for baseline and no CO₂ sequestration scenarios under no H₂ HDV adoption. Within each panel, the amount of synthetic fuel adoption increases moving from left to right.

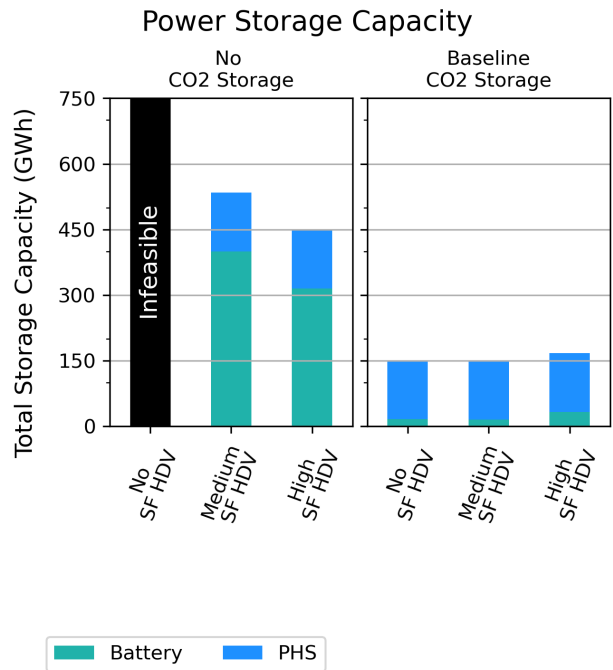


Figure A.37: Power storage capacity for baseline and no CO₂ sequestration scenarios under no H₂ HDV adoption. Within each panel, the amount of synthetic fuel adoption increases moving from left to right.

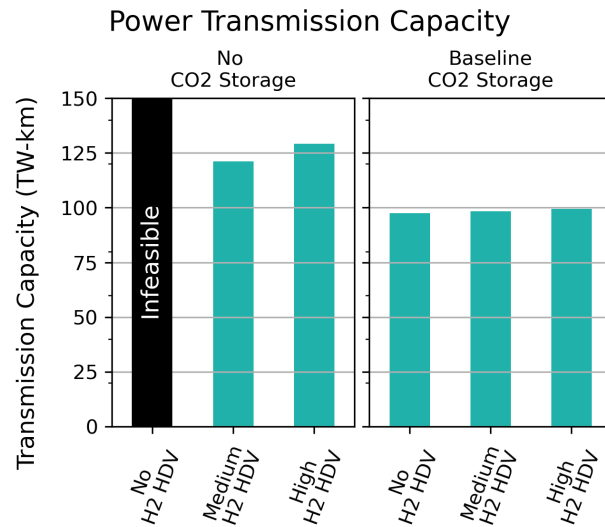


Figure A.38: Power transmission capacity for baseline and no CO₂ sequestration scenarios under no H₂ HDV adoption. Within each panel, the amount of synthetic fuel adoption increases moving from left to right.

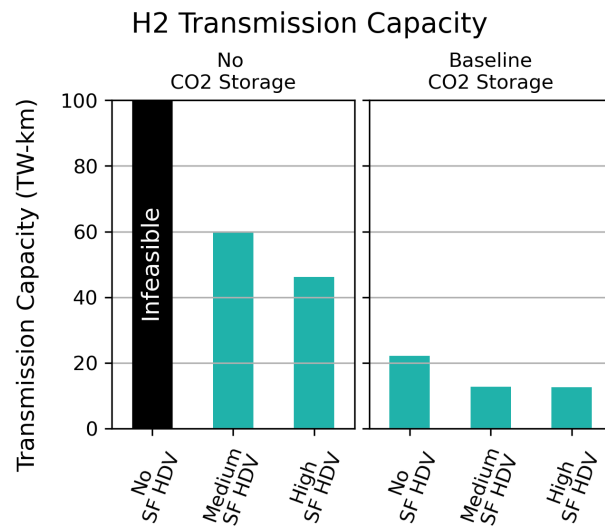


Figure A.39: H₂ transmission capacity for baseline and no CO₂ sequestration scenarios under no H₂ HDV adoption. Within each panel, the amount of synthetic fuel adoption increases moving from left to right.

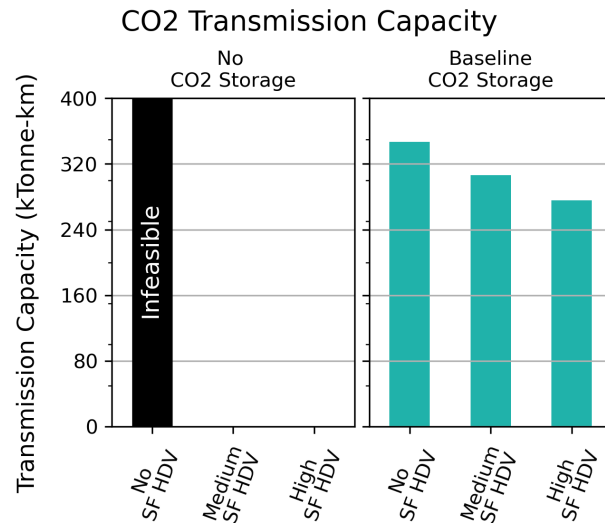


Figure A.40: CO₂ transmission capacity for baseline and no CO₂ sequestration scenarios under no H₂ HDV adoption. Within each panel, the amount of synthetic fuel adoption increases moving from left to right.

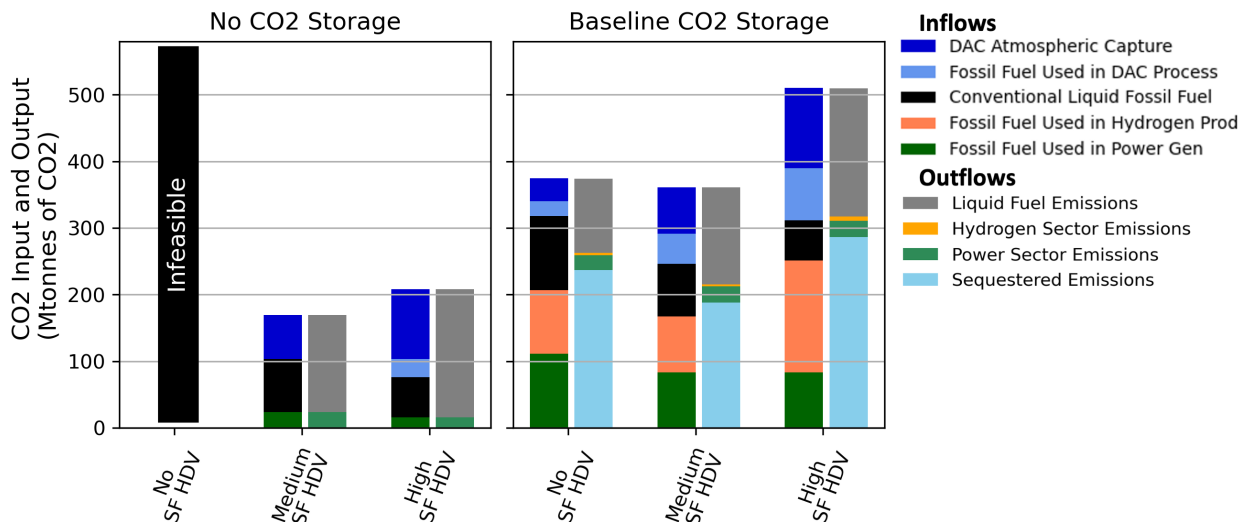


Figure A.41: System CO₂ balance under varying levels of SF adoption and no H₂ HDV adoption. The subfigure on the left shows the CO₂ balance under no CO₂ sequestration availability, while the one on the right shows the CO₂ balance under baseline CO₂ sequestration availability. Within each subplot the SF adoption level increases left to right. The leftward column represents CO₂ input into the system, while the rightward column represents CO₂ outputted by the system. Emissions constraint can be calculated from the chart by subtracting sequestered emissions and DAC atmospheric capture from the emission outflows. Emissions constraint can be calculated from the chart by subtracting sequestered emissions and DAC atmospheric capture from the emission outflows.

Table A.5

This table shows the marginal price of abatement of CO₂ for Sensitivity Scenario Set 3

CO ₂ Storage	H ₂ HDV Level	Synthetic Fuel HDV Level	CO ₂ Marginal Cost of Abatement
Baseline	None	None	293.92
Baseline	None	0.18	293.90
Baseline	None	0.35	293.91
None	None	0.18	835.18
None	None	0.35	632.72

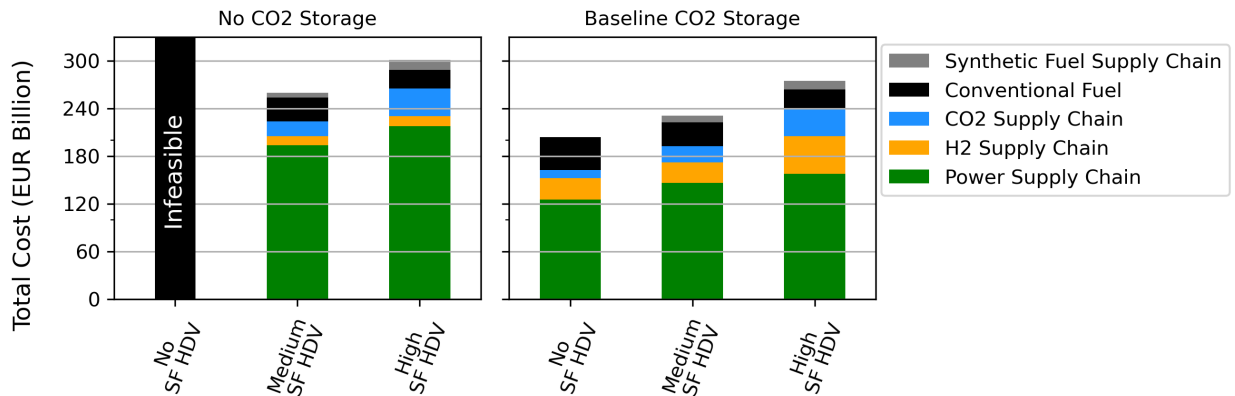


Figure A.42: Annualized bulk-system costs under varying levels of SF adoption and no H₂ HDV adoption. The subfigure on the left shows the cost breakdown under no CO₂ sequestration availability, while the one on the right shows the cost breakdown under baseline CO₂ sequestration availability. Within each subplot the H₂ HDV adoption level increases left to right. The costs do not include vehicle replacement or H₂ distribution costs.

A.6. Sensitivity Set 4: Core Scenario Set 2 with Natural Gas Price Sensitivity

The results in this section represent Sensitivity Set 4 as described in Figure 3b of the main text.

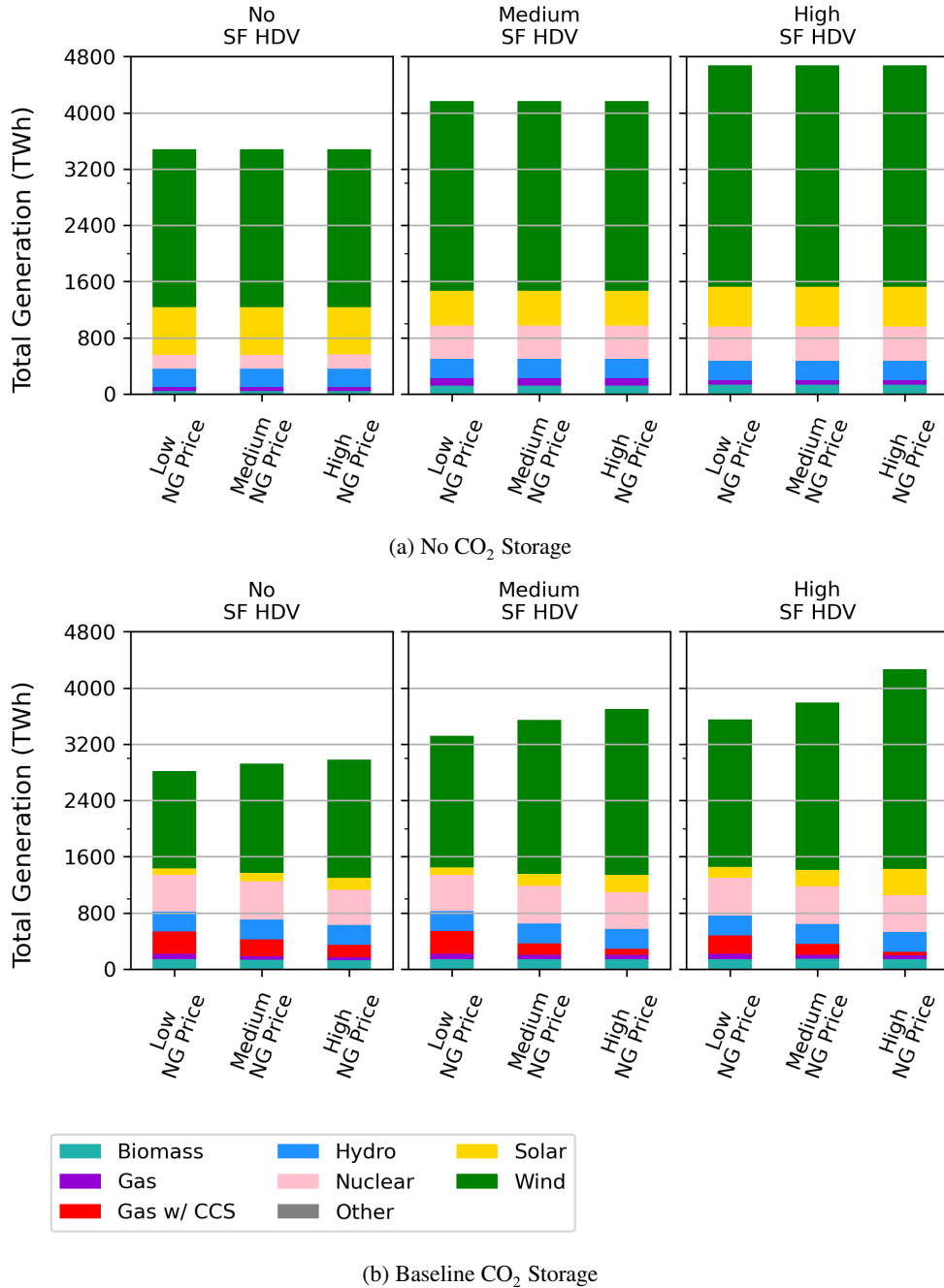


Figure A.43: Power generation for no (sub-figure a) and baseline (sub-figure b) CO₂ sequestration scenarios under medium H₂ HDV adoption and varying scenarios of synthetic fuel adoption. Within each panel, the price of natural gas increases left to right. Across panels, the amount of H₂ HDV adoption increases moving from left to right. The middle panels correspond to the core set of scenarios.

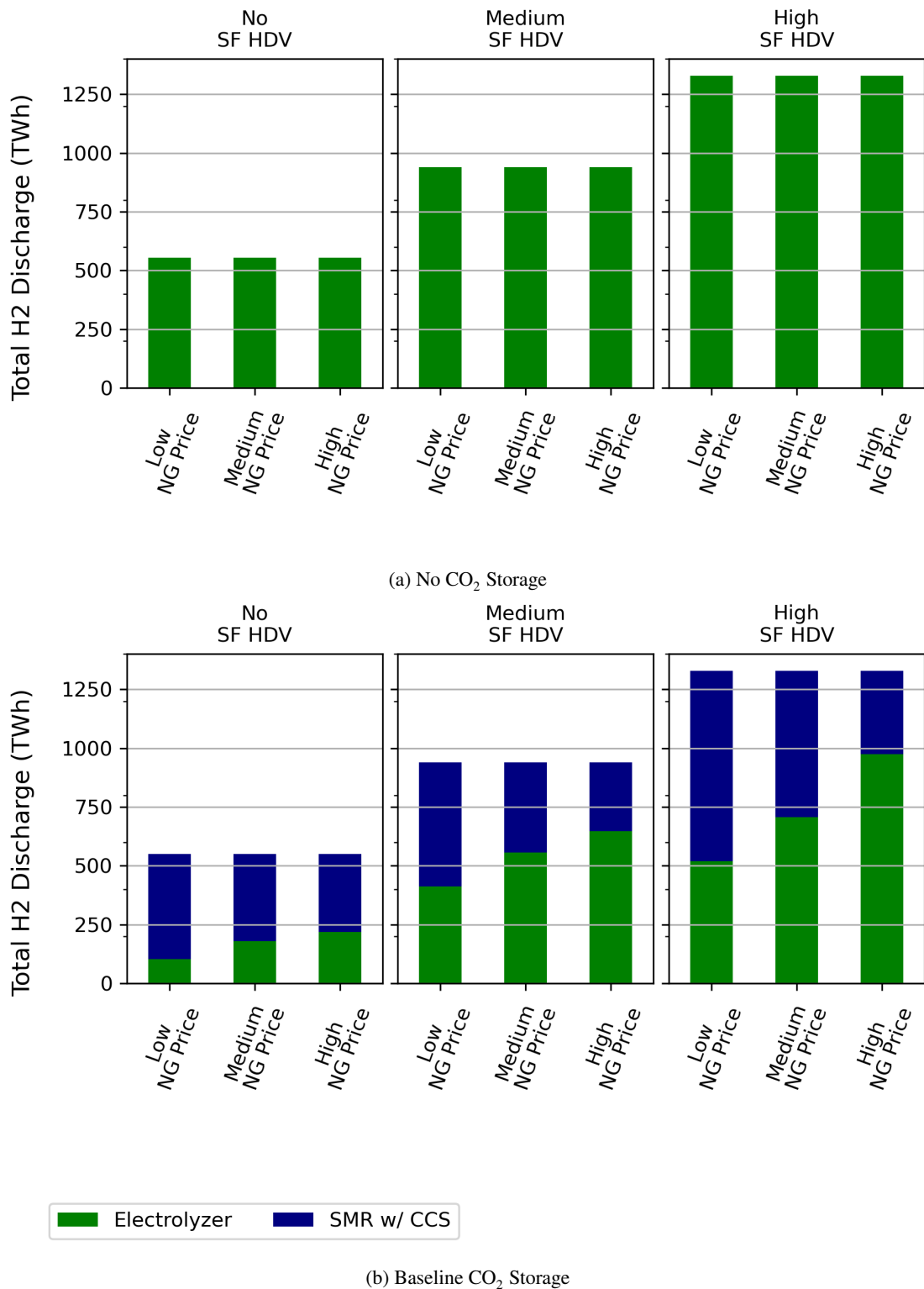


Figure A.44: H₂ generation for no (sub-figure a) and baseline (sub-figure b) CO₂ sequestration scenarios under medium H₂ HDV adoption and varying scenarios of synthetic fuel adoption. Within each panel, the price of natural gas increases left to right. Across panels, the amount of H₂ HDV adoption increases moving from left to right. The middle panels correspond to the core set of scenarios.

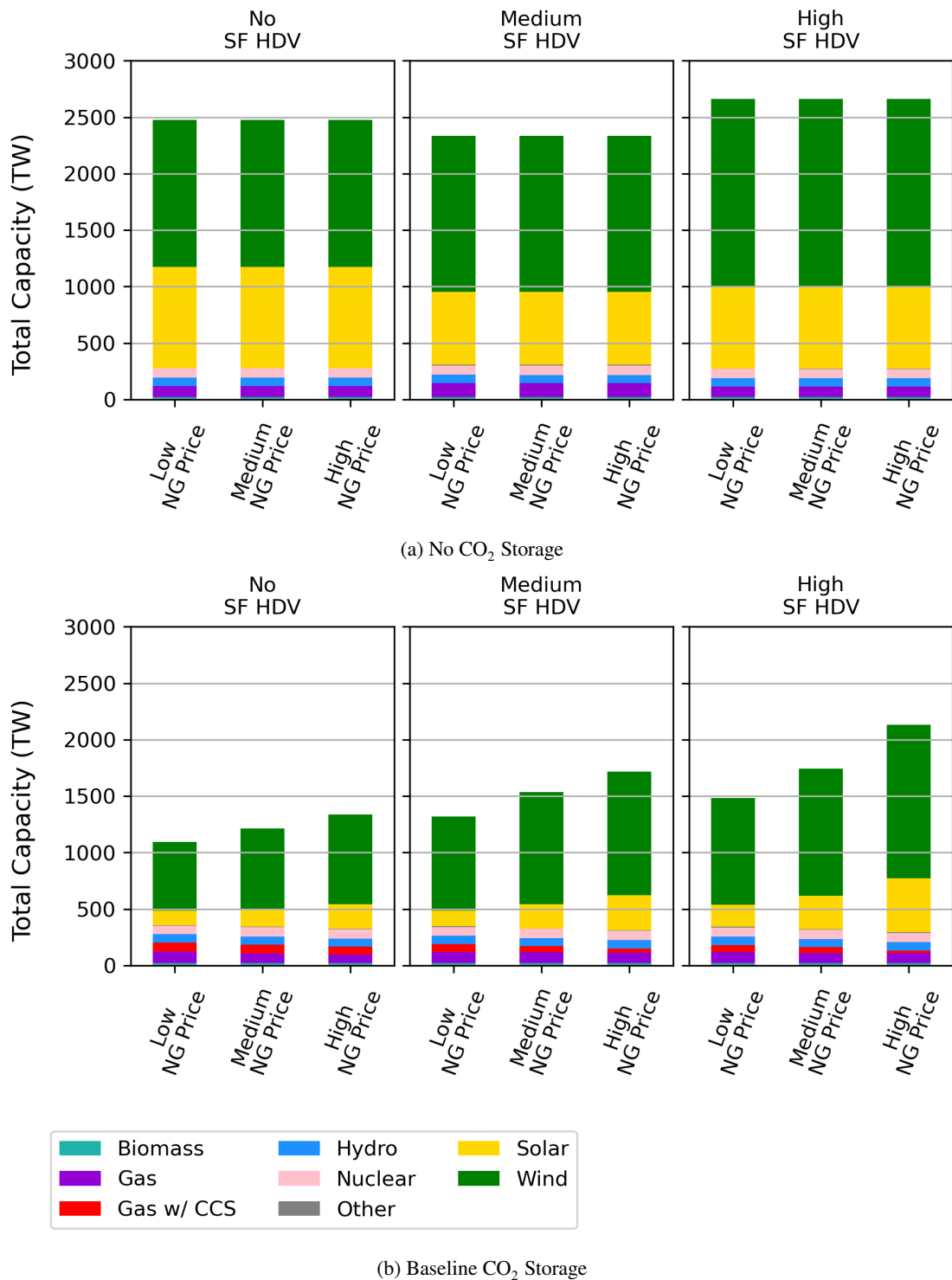


Figure A.45: Power capacity for no (sub-figure a) and baseline (sub-figure b) CO₂ sequestration scenarios under medium H₂ HDV adoption and varying scenarios of synthetic fuel adoption. Within each panel, the price of natural gas increases left to right. Across panels, the amount of H₂ HDV adoption increases moving from left to right. The middle panels correspond to the core set of scenarios.

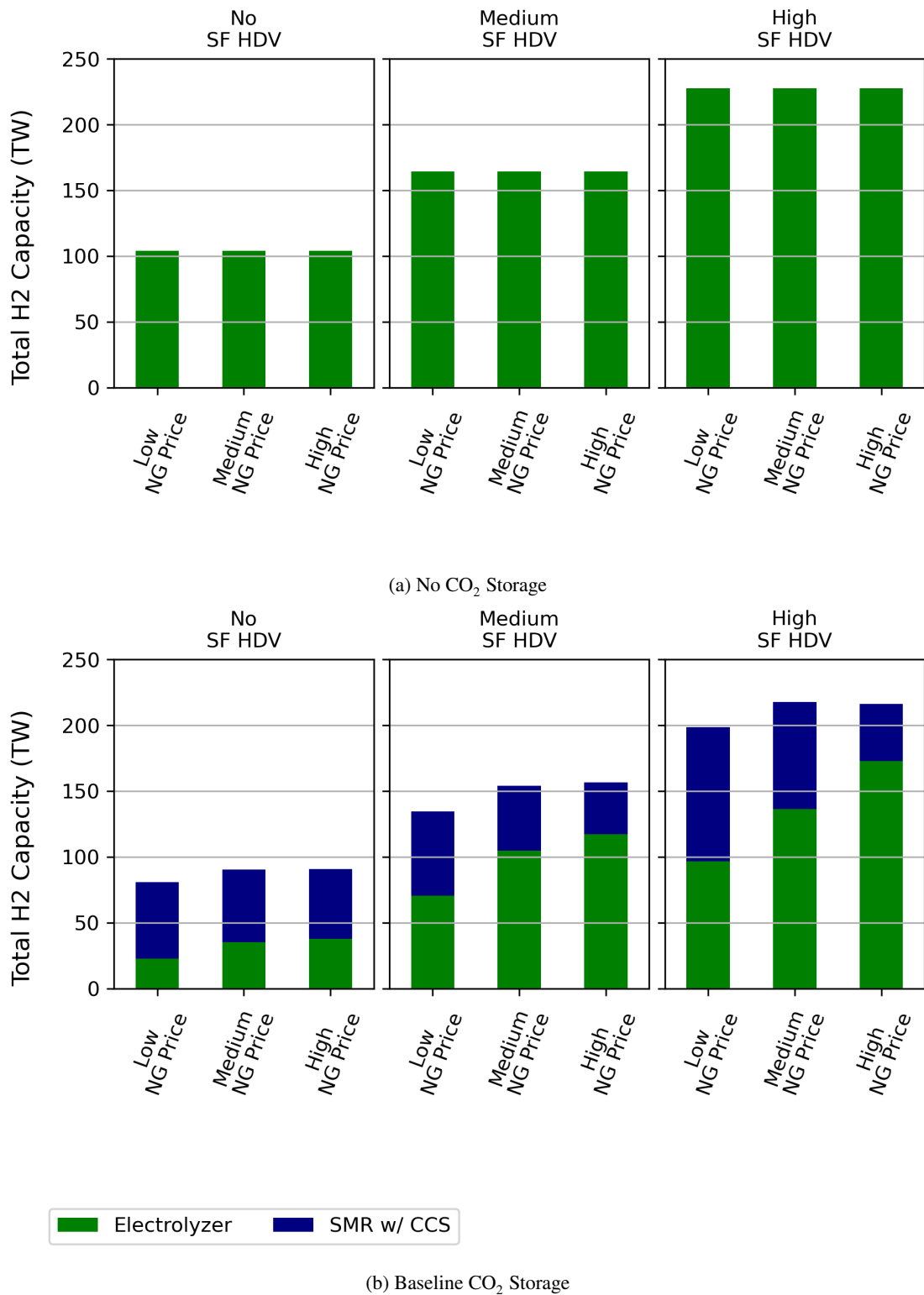


Figure A.46: H₂ capacity for no (sub-figure a) and baseline (sub-figure b) CO₂ sequestration scenarios under medium H₂ HDV adoption and varying scenarios of synthetic fuel adoption. Within each panel, the price of natural gas increases left to right. Across panels, the amount of H₂ HDV adoption increases moving from left to right. The middle panels correspond to the core set of scenarios.

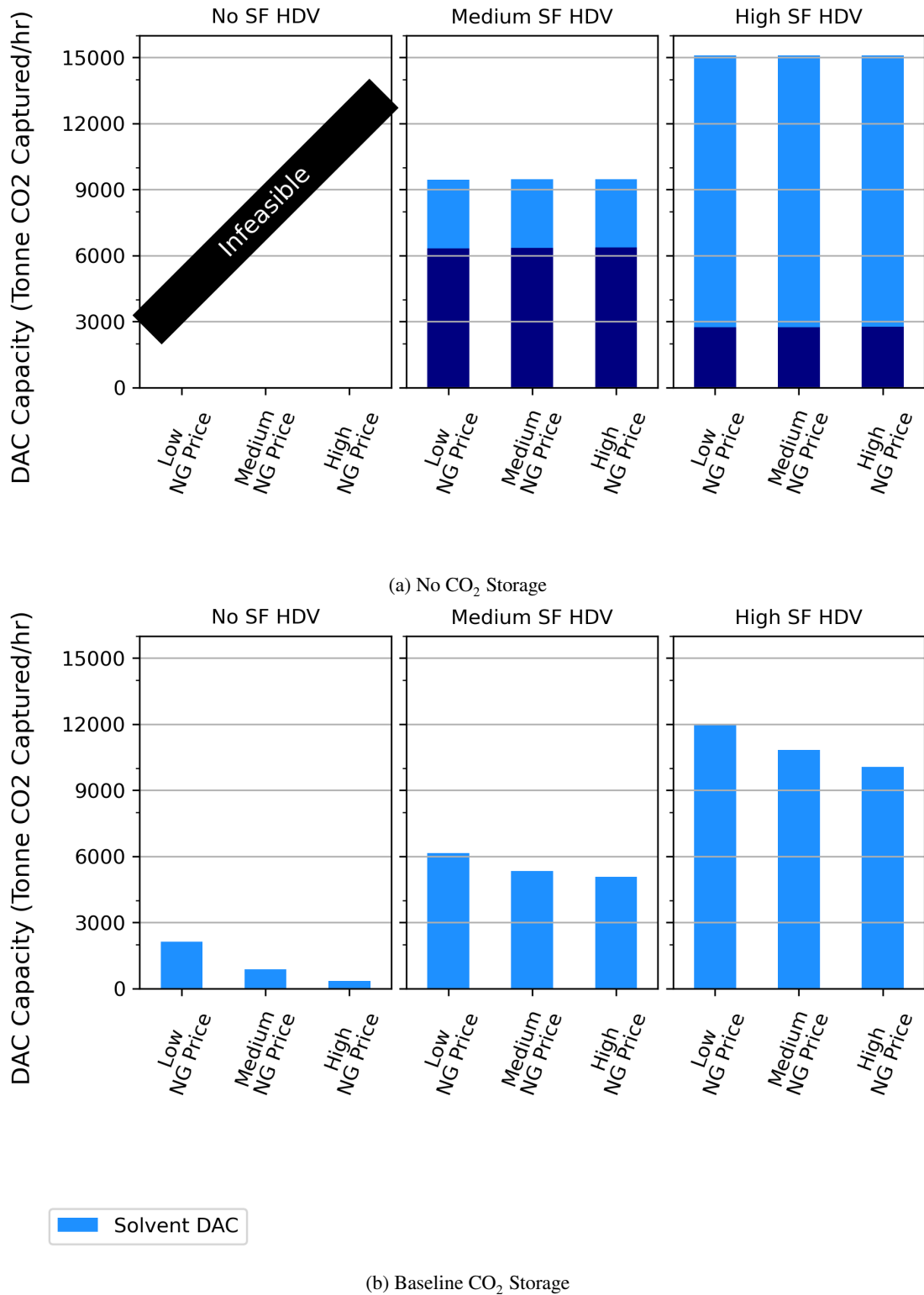


Figure A.47: Direct Air Capture capacity for no (sub-figure a) and baseline (sub-figure b) CO₂ sequestration scenarios under medium H₂ HDV adoption and varying scenarios of synthetic fuel adoption. Within each panel, the price of natural gas increases left to right. Across panels, the amount of H₂ HDV adoption increases moving from left to right. The middle panels correspond to the core set of scenarios.

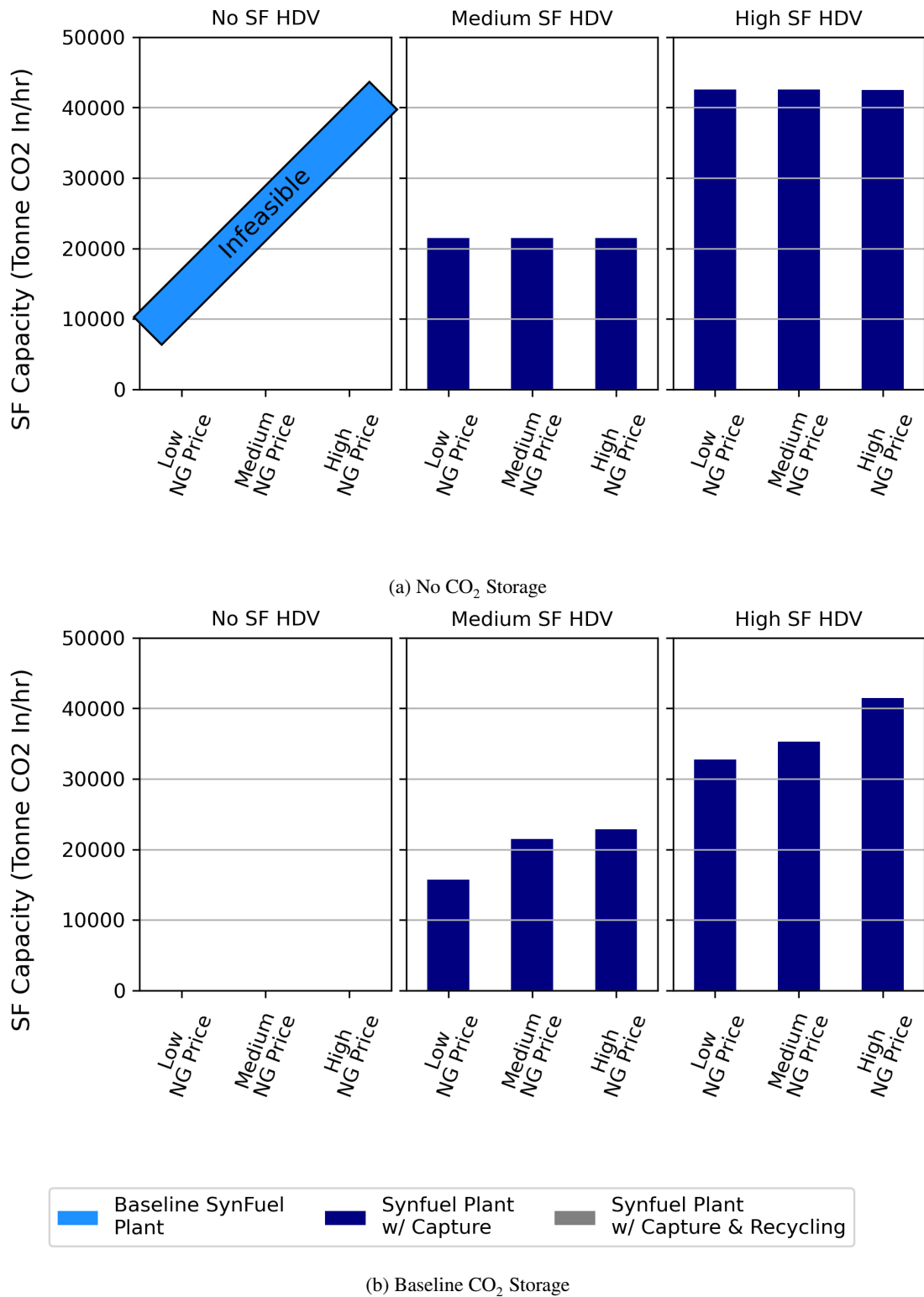


Figure A.48: Synthetic fuel plant capacity for no (sub-figure a) and baseline (sub-figure b) CO₂ sequestration scenarios under medium H₂ HDV adoption and varying scenarios of synthetic fuel adoption. Within each panel, the price of natural gas increases left to right. Across panels, the amount of H₂ HDV adoption increases moving from left to right. The middle panels correspond to the core set of scenarios.

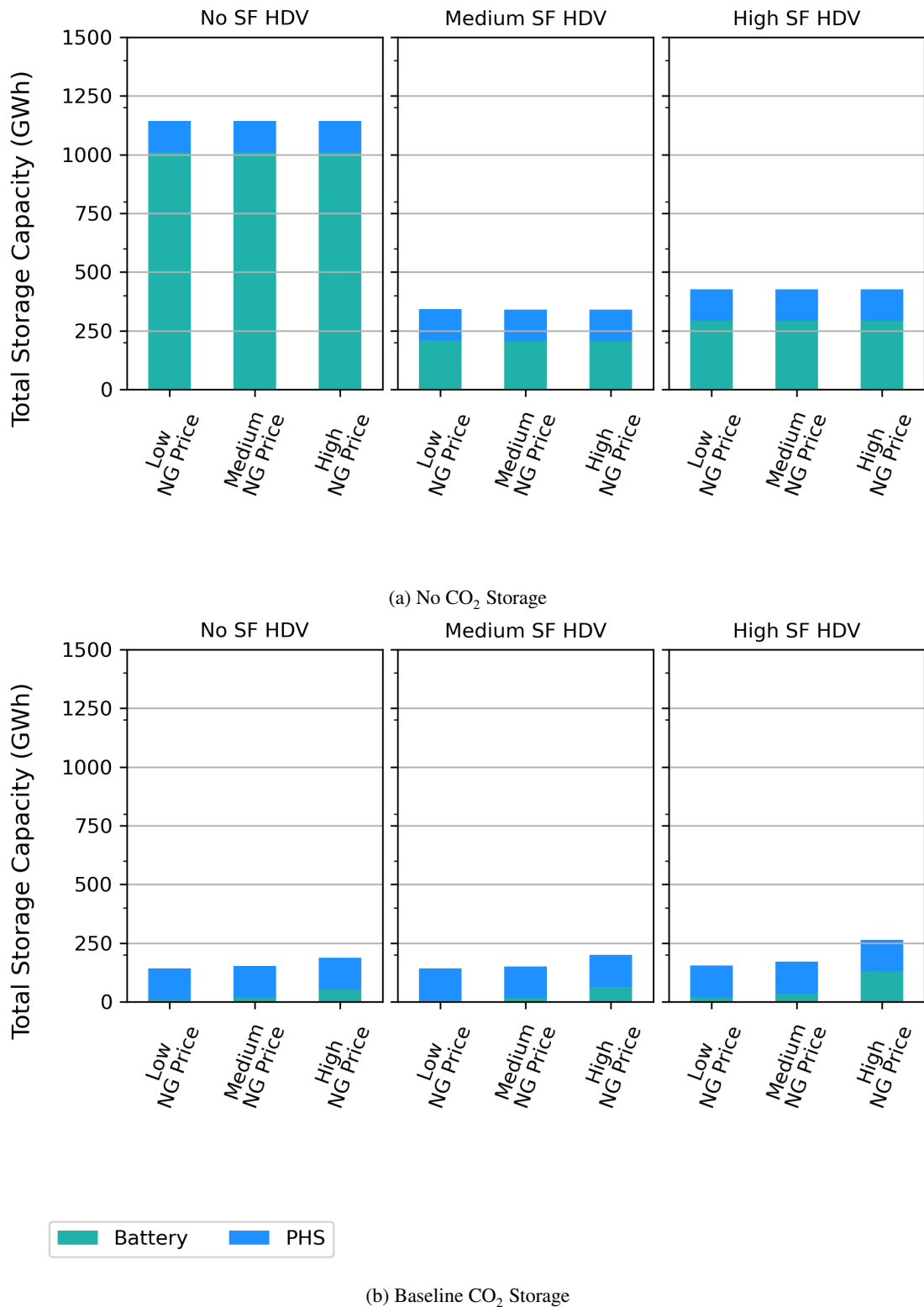


Figure A.49: Electric storage capacity for no (sub-figure a) and baseline (sub-figure b) CO₂ sequestration scenarios under medium H₂ HDV adoption and varying scenarios of synthetic fuel adoption. Within each panel, the price of natural gas increases left to right. Across panels, the amount of H₂ HDV adoption increases moving from left to right. The middle panels correspond to the core set of scenarios.

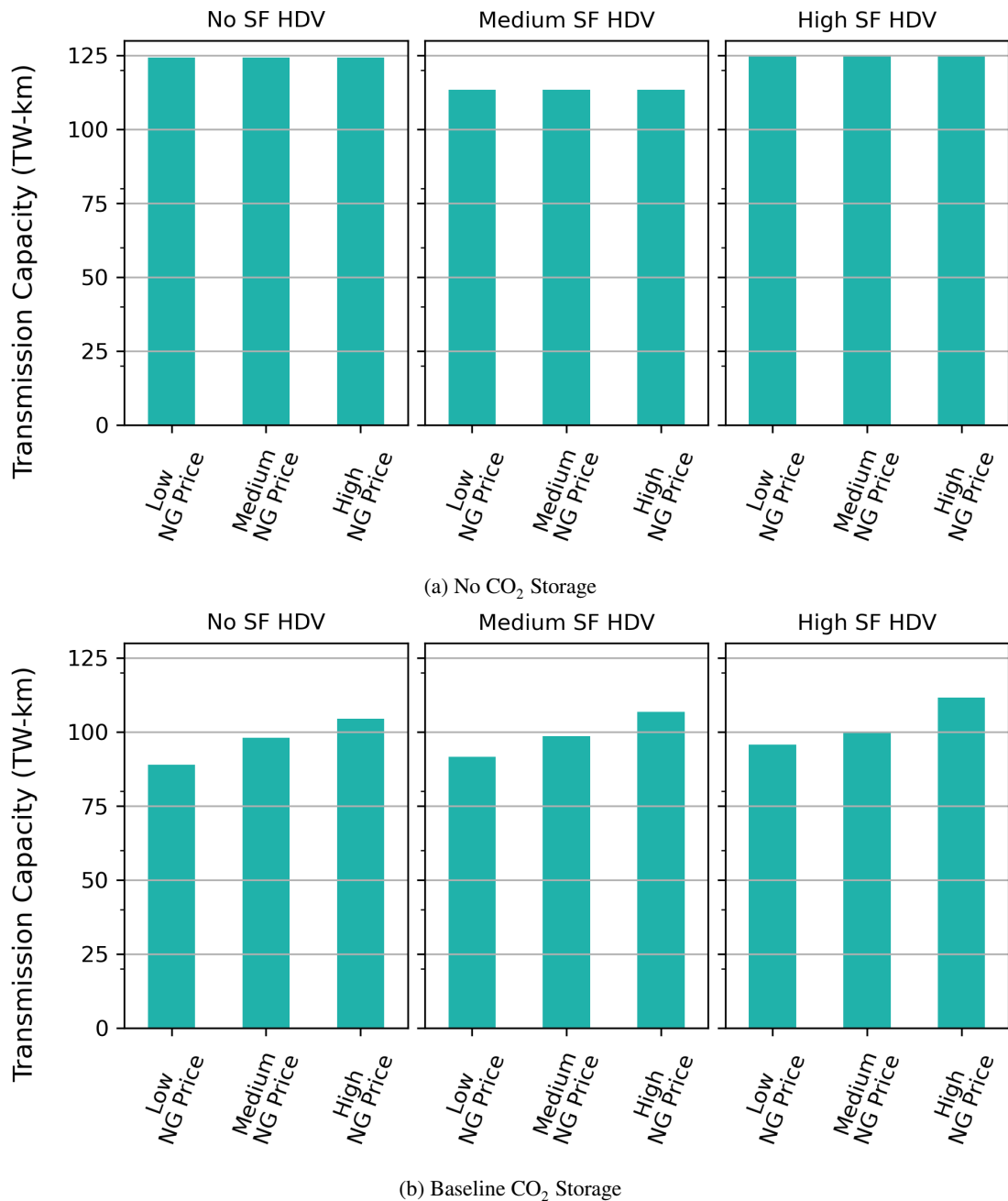


Figure A.50: Power transmission capacity for no (sub-figure a) and baseline (sub-figure b) CO₂ sequestration scenarios under medium H₂ HDV adoption and varying scenarios of synthetic fuel adoption. Within each panel, the price of natural gas increases left to right. Across panels, the amount of H₂ HDV adoption increases moving from left to right. The middle panels correspond to the core set of scenarios.

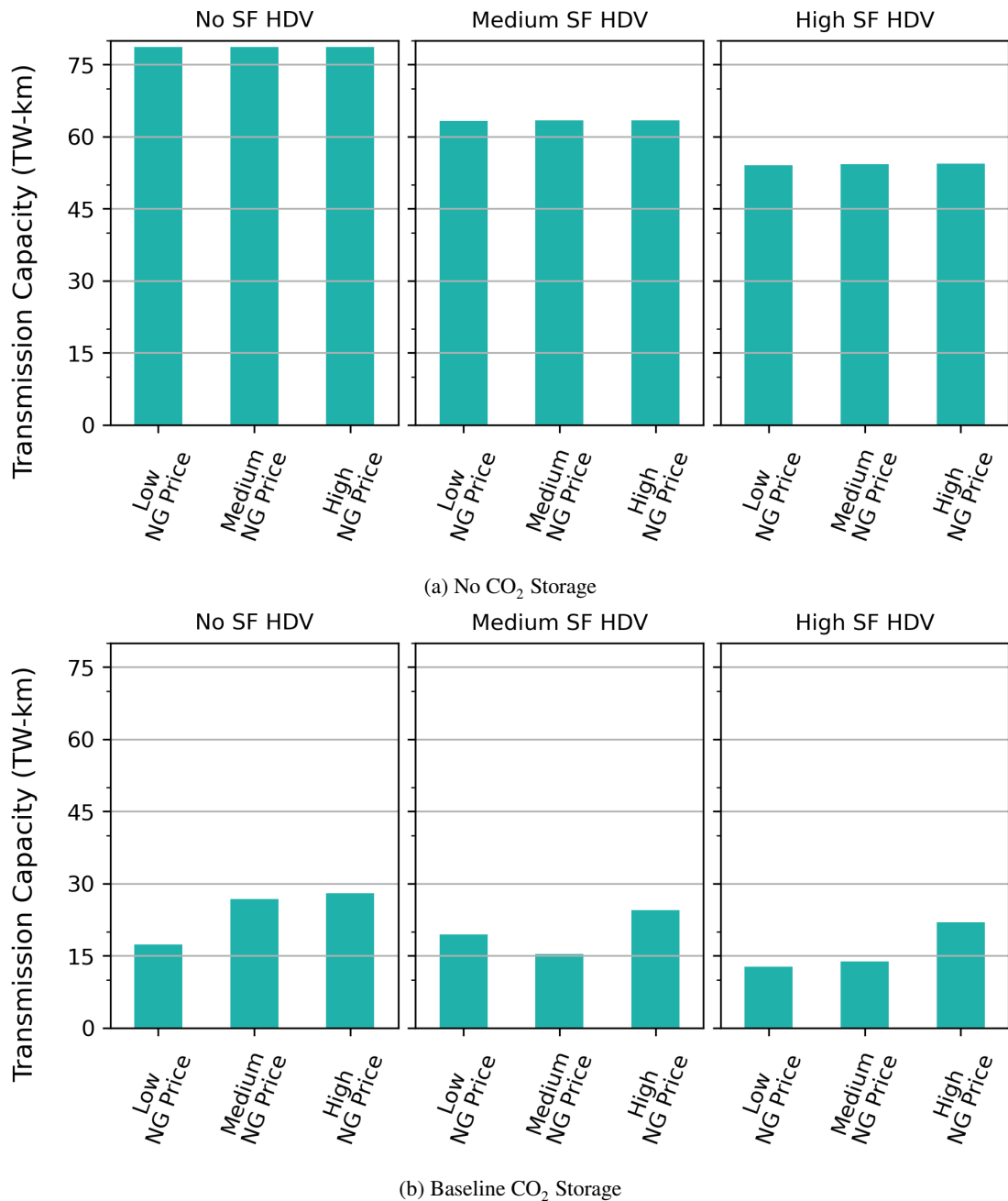


Figure A.51: H₂ transmission capacity for no (sub-figure a) and baseline (sub-figure b) CO₂ sequestration scenarios under medium H₂ HDV adoption and varying scenarios of synthetic fuel adoption. Within each panel, the price of natural gas increases left to right. Across panels, the amount of H₂ HDV adoption increases moving from left to right. The middle panels correspond to the core set of scenarios.

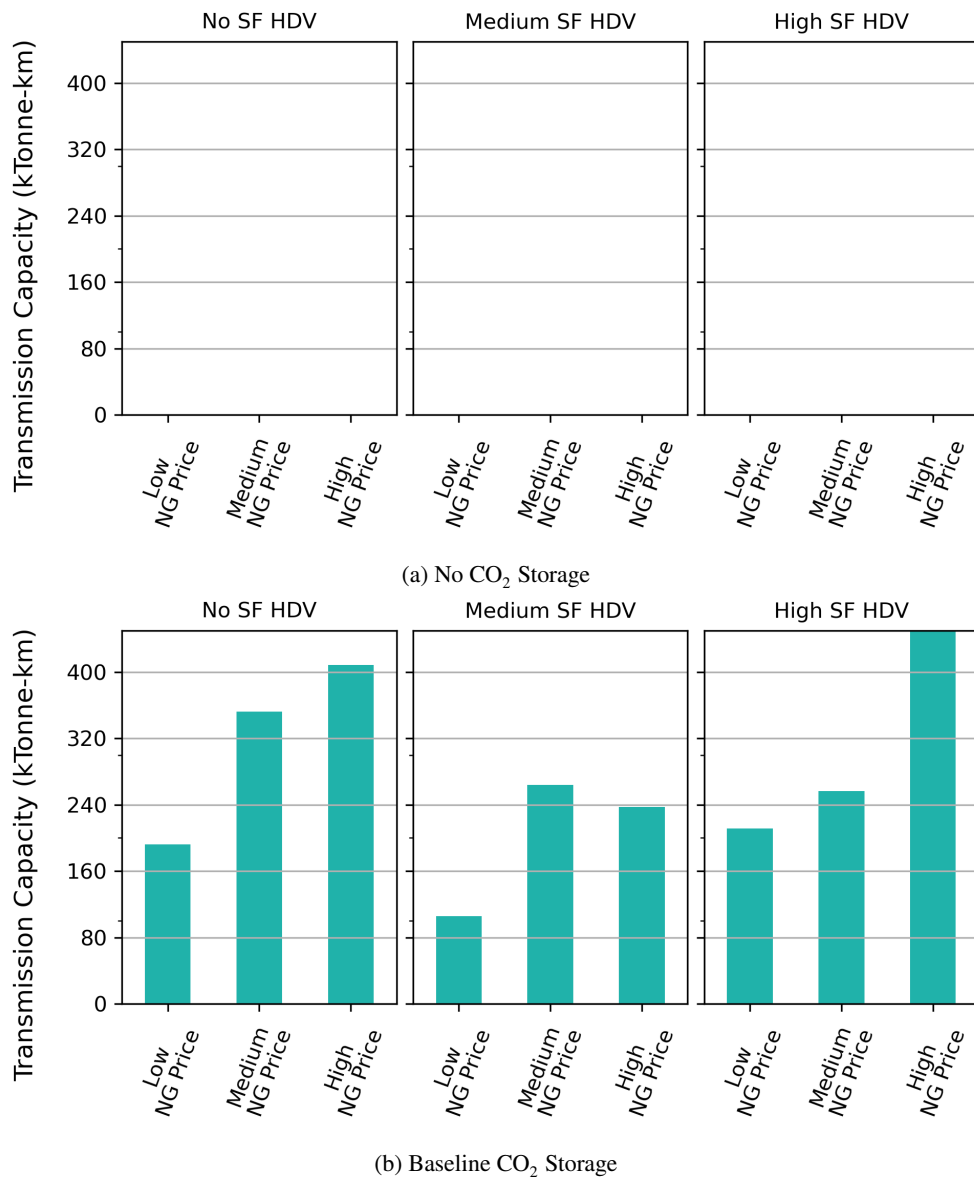


Figure A.52: CO₂ transmission capacity for no (sub-figure a) and baseline (sub-figure b) CO₂ sequestration scenarios under medium H₂ HDV adoption and varying scenarios of synthetic fuel adoption. Within each panel, the price of natural gas increases left to right. Across panels, the amount of H₂ HDV adoption increases moving from left to right. The middle panels correspond to the core set of scenarios.

Multi-sectoral Impacts of H₂ and Synthetic Fuels Adoption for Heavy-duty Transportation Decarbonization

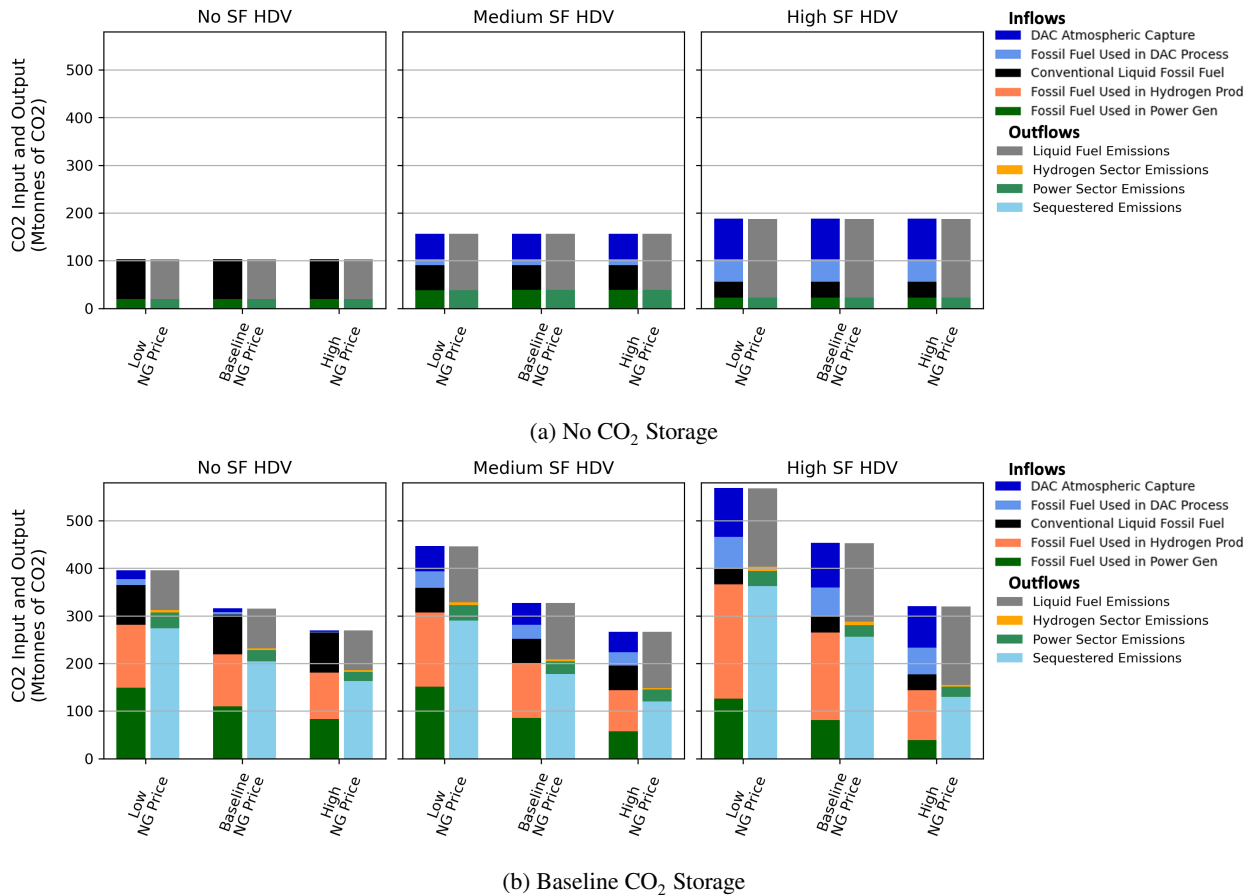


Figure A.53: System CO₂ balance under medium H₂ HDV adoption and varying scenarios of synthetic fuel adoption for no (sub-figure a) and baseline (sub-figure b) CO₂ sequestration scenarios. Within each panel, the price of natural gas increases left to right. Across panels, the amount of H₂ HDV adoption increases moving from left to right. The middle panels correspond to the core set of scenarios. The leftward column represents CO₂ input into the system, while the rightward column represents CO₂ outputted by the system. All scenarios adhere to the same emissions constraint of 103 Mtonnes. The middle panels correspond to the core set of scenarios. Emissions constraint can be calculated from the chart by subtracting sequestered emissions and DAC atmospheric capture from the emission outflows. Emissions constraint can be calculated from the chart by subtracting sequestered emissions and DAC atmospheric capture from the emission outflows.

Multi-sectoral Impacts of H₂ and Synthetic Fuels Adoption for Heavy-duty Transportation Decarbonization

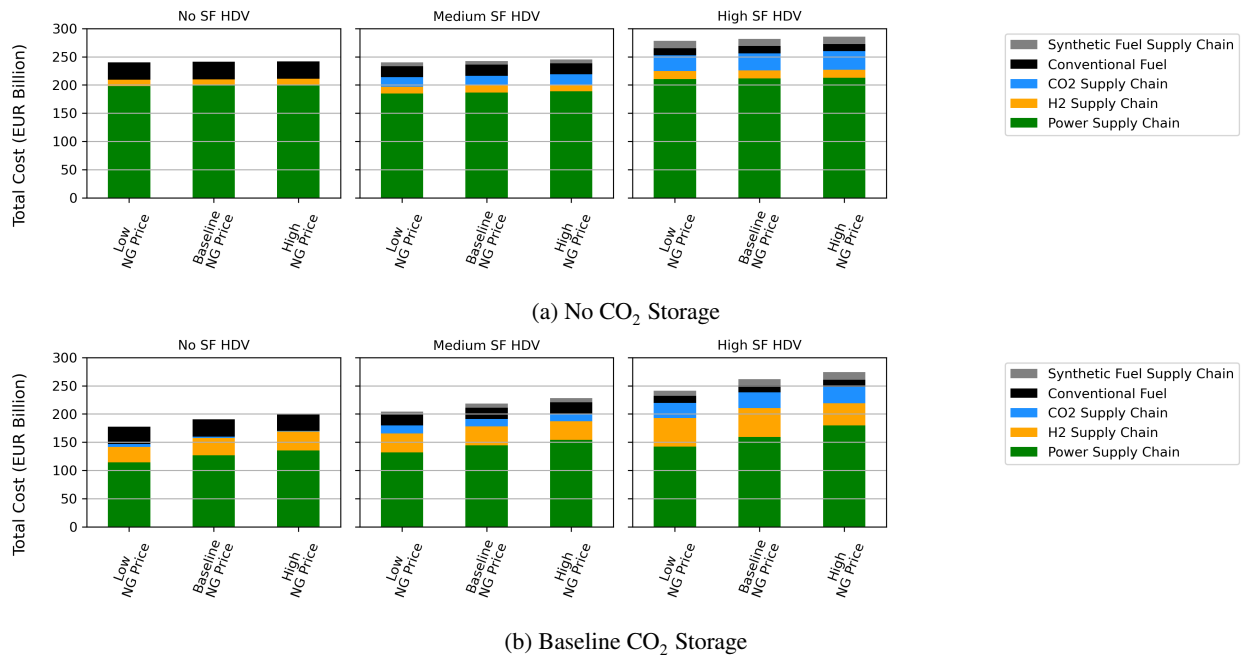


Figure A.54: Annualized bulk-system costs under medium H₂ HDV adoption and varying scenarios of synthetic fuel adoption for no (sub-figure a) and baseline (sub-figure b) CO₂ sequestration scenarios. Within each panel, the price of natural gas increases left to right. Across panels, the amount of H₂ HDV adoption increases moving from left to right. The middle panels correspond to the core set of scenarios. The costs do not include vehicle replacement or H₂ distribution costs.

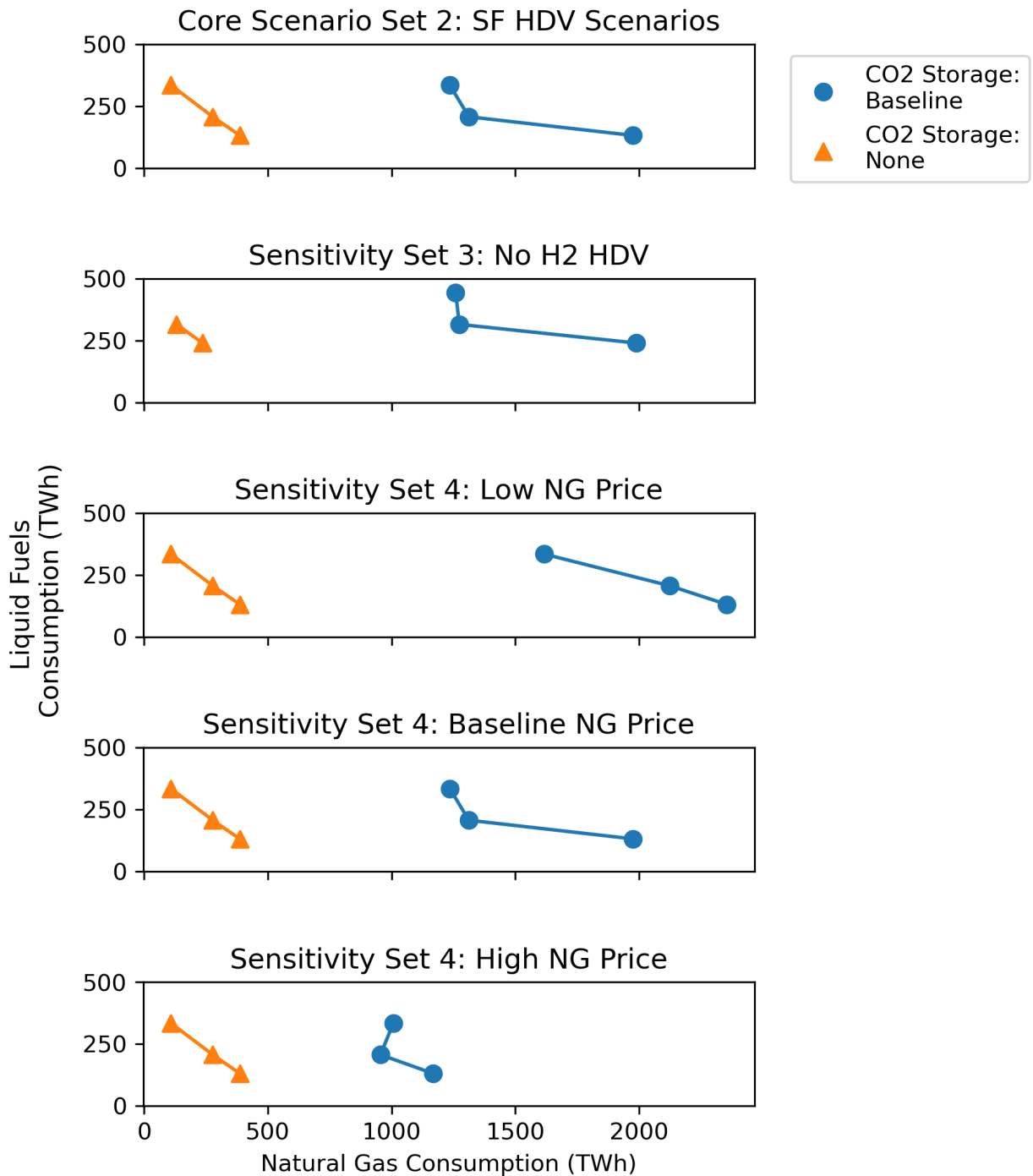


Figure A.55: Trade-off between natural gas (NG) and liquid fossil fuel utilization for scenarios where amount of SF adoption is varied. The subfigure on the top shows the relationship for the core SF HDV scenarios (i.e. scenario set 2), while the second plot shows the results for the SF scenario with no H₂ adoption (i.e. sensitivity scenario set 3). The last 3 shows the results for the natural gas price sensitivities (i.e. sensitivity scenario set 4). Within each subplot the amount of natural gas consumption can be examined on the x-axis, while the amount of liquid fossil fuel consumption can be examined on the y-axis. The amount of SF HDV adoption increases from top to bottom. The amount of liquid fossil fuel consumption includes diesel and gasoline, and excludes jet fuel as well as excess synthetic fuels.

Table A.6This tables shows the marginal price of abatement of CO₂ for Sensitivity Set 4

CO ₂ Storage	H ₂ HDV Level	Synthetic Fuel HDV Level	Natural Gas Price	CO ₂ Marginal Cost of Abatement
Baseline	Medium	None	Low	260.59
Baseline	Medium	Medium	Low	260.59
Baseline	Medium	High	Low	307.70
Baseline	Medium	None	Baseline	293.92
Baseline	Medium	Medium	Baseline	268.80
Baseline	Medium	High	Baseline	293.91
Baseline	Medium	None	High	327.25
Baseline	Medium	Medium	High	251.55
Baseline	Medium	High	High	266.02
None	Medium	None	Low	1654.20
None	Medium	Medium	Low	530.54
None	Medium	High	Low	618.74
None	Medium	None	Baseline	1603.09
None	Medium	Medium	Baseline	480.12
None	Medium	High	Baseline	567.48
None	Medium	None	High	1551.98
None	Medium	Medium	High	429.10
None	Medium	High	High	516.23

B. SI 2: Demand-side Modelling Methodology and Inputs

B.1. Demand-side Transportation Model

This section details the mathematical formulation of demand-side model for generating alternative transportation demand scenarios. In Section B.2, we detail the demand-side inputs used for this study. As shown in Figure 1, transportation demand, vehicle sub-category breakdowns, vehicle loading factors, vehicle market share, and vehicle energy consumption are combined together to create a demand profile. This model outputs the final energy consumption by fuel type (gasoline, diesel, electricity, H₂) for each timestep and country. To do so, we disaggregate transportation service demand (tonne-km (tkm) or passenger-km (pkm)) into the following categories: 1) light-duty passenger vehicles 2) buses and coaches 3) 2-wheelers, and 4) heavy-duty and light commercial vehicles. We further disaggregate into vehicle types as shown in table B.7. We also disaggregate demand by road type (urban, rural, highway). We then transform this service demand into vehicle km (vkm) demand using loading and occupancy factors. We assign service demand to a specific vehicle drivetrain type (e.g. PHEV, H₂, Diesel ICE, etc.) Using energy consumption factors for a specific fuel per vkm, we arrive at a final energy consumption by fuel (e.g. diesel, gasoline, electricity, H₂). We further subdivide into timesteps. Table B.8 shows the definitions of indices and sets used in the demand-side model. Table B.9 contains key input parameters used in this model.

Vehicle Category	Vehicle Type
HDV & LCV	HDV Light + Short Distance
	HDV Light + Long Distance
	HDV Medium + Short Distance
	HDV Medium + Long Distance
	HDV Heavy + Short Distance
	HDV Heavy + Long Distance
	HDV Super-Heavy + Short Distance
	HDV Super-Heavy + Long Distance
	HDV Ultra-Heavy + Short Distance
	HDV Ultra-Heavy + Long Distance
	LCV
Passenger Car	Small
	Medium
	Large
Buses and coaches	Buses
	Coaches
Two-wheelers	Two-wheelers

Table B.7

Service demand vehicle category and the vehicle types disaggregation categories

Indices and Sets	Definition
$r \in R$	r denotes a road type belonging to the set of road types R . Road types modeled are urban, suburban, and rural.
$v \in V$	v denotes a specific vehicle type in a set of all vehicle types V (e.g. small passenger vehicle, medium passenger vehicle, etc.).
$J \subset V$	J denotes a vehicle category (e.g., passenger cars, buses and coaches, heavy-duty, and light commercial vehicles) made up of vehicles $v \in V$. Vehicle types and categories modelled is show in Table B.7
$V_{\text{pass}} \subset V$	V_{pass} is a subset of passenger vehicles made up from vehicles $v \in V$. Vehicle types and modelled is show in Table B.7
$V_{\text{cargo}} \subset V$	V_{cargo} is a subset of cargo vehicles made up from vehicles $v \in V$.
$d \in D$	where d is a drivetrain type in a set of all drivetrain types (e.g. EV, PHEV H ₂ , Diesel ICE, etc).
$f \in F$	where f is a fuel type in a set of all fuel or drivetrain types (e.g. electricity, H ₂ , Biofuel, Diesel, Gasoline, etc).
$c \in C$	where c is a country in all countries in Western Europe.
$y \in Y$	where y is a year in possible analysis years (e.g. 2040, 2050)

Table B.8

Demand model indices and sets

Input Parameter	Definition
$p_{v,c,y}$	Passenger km demand for a given vehicle type and country in a given analysis year.
$t_{v,c,y}$	Tonne km demand for a given vehicle type and country in a given analysis year.
$o_{v,c}$	Vehicle occupancy ratio $vk m/pk m$. Only defined for $v \in V_{\text{pass}}$.
$l_{v,c}$	Loading ratio $vk m/tk m$. Only defined for $v \in V_{\text{cargo}}$.
$s_{v,c,r}$	Road type share for a given vehicle type in a given country.
$m_{v,d,y}$	Market share for a given vehicle type for a given drivetrain type in a given year.
$k_{r,v,d,f,y}$	Energy demand per vehicle km for a vehicle v on road type r , for drivetrain d , for fuel f in year y .
$e_{v,d,f,y}$	Efficiency multiplier for a given vehicle type, for a given fuel type, in a given year.
$\tau_{t,v,f}$	Load shape factor (percent consumption in a given hour).

Table B.9

Definitions of key demand model input parameters. the values of key parameters can be found in Section B.2

The following equation combines key inputs to create the energy demand loadshape at time t for each of the fuel types in a given country. To do so, we first multiply vehicle service demand by a factor (occupancy ratio for passenger vehicles, and loading factor for cargo vehicles) to calculate demand in vehicle distance (vkm). This is then multiplied by the road type share for a given vehicle type. We also subdivide the demand in vehicle distance by vehicle marketshare, which is the main lever used in this study. To convert this to energy consumption, we multiply by energy consumed per vkm for a given vehicle type, roadshare, fuel type, and year. We also have the option of multiplying by an efficiency factor, which could be used to assess the impact of efficiency measures. Finally, we multiply by a loadshape factor to calculate the energy consumption at a given timestep. The loadshape factor is the percentage of energy consumed in an hour out of total energy consumption. The first part of the equation calculates energy consumption for passenger vehicles, while the second calculates energy consumption for cargo vehicles.

$$E_{t,f,c,y} = \sum_{v \in V_{\text{pass}}} \sum_{r \in R} \sum_{d \in D} p_{v,c,y} \times o_{v,c} \times s_{v,c,r} \times m_{v,d,y} \times k_{r,v,d,f,y} \times e_{v,d,f,y} \times \tau_{t,v,f} \\ + \sum_{v \in V_{\text{cargo}}} \sum_{r \in R} \sum_{d \in D} t_{v,c,y} \times l_{v,c} \times s_{v,c,r} \times m_{v,d,y} \times k_{r,v,d,f,y} \times e_{v,d,f,y} \times \tau_{t,v,f} \quad (1)$$

The resultant loadshape is added to a given fuel type demand and is used as an input to the DOLPHYN model.

B.2. Demand-side Inputs

This section will cover key demand-side model inputs.

The following table key input parameters used in this model.

Input Parameter	Definition
$p_{v_{\text{pass}},c,y}$	Passenger km demand for a given vehicle type and country in a given analysis year.
$t_{v_{\text{cargo}},c,y}$	Tonne km demand for a given vehicle type and country in a given analysis year.
$k_{r,j,f,y}$	Energy demand per vehicle km for a vehicle v on road type r , for fuel f in year y .
$s_{j,c,r}$	Road type share for a given vehicle type in a given country.
$m_{j,f,y}$	Market share for a given vehicle type for a given fuel type in a given year.
$e_{j,f,y}$	Efficiency multiplier for a given vehicle type, for a given fuel type, in a given year.
$o_{v_{\text{pass}},c}$	Vehicle occupancy ratio vkm/pkm .
$l_{v_{\text{cargo}},c}$	Loading ratio vkm/tkm .
$\tau_{t,j,f}$	Load shape factor (percent consumption in a given hour).

Table B.10

Definitions of key demand model input parameters

To begin with, vehicle category demand is constructed based on EU Reference scenarios for the year 2040 (European Commission, 2020). The scenarios provide the service demand in pkm and tkm for 4 vehicle categories. Demand for the UK and Norway is not directly available using the EU reference scenario, and therefore utilize demand from similar countries, Germany and Sweden, respectively, adjusted by population.

We then further disaggregate the demand for these vehicle categories into vehicle types as listed in table B.7. This disaggregation is crucial as a vehicle tonnage and size affects its energy consumption. Vehicle demand is disaggregated on the basis of vehicle size for passenger vehicles and payload capacity for freight vehicles using TRACCS, a survey on transportation demand consumption (EMISIA, 2014).

To convert transportation service demand to distance demand, loading factors based on Eurostat are used. Payload factors from TRACCS energy demand inconsistent with historical data. Table B.11 shows the loading factors used for each HDV & LCV vehicle category.

Table B.11

Vehicle Payload by Category and Type

Vehicle Category	Vehicle Type	Vehicle Payload (Tonnes)
HDV & LCVs	LCV	0.40
	HDV - Light	1.36
	HDV - Medium	5.51
	HDV - Heavy	6.65
	HDV - Super Heavy	12.52
	HDV - Ultra Heavy	15.12

Additionally, the amount of vehicle distance travelled in each road type is based on (Krause et al., 2020), and is as shown in table B.12.

Table B.12

Vehicle Road Type Share by Vehicle Category and Vehicle Type Based on (Krause et al., 2020)

Vehicle Category	Vehicle Type	Road Type Share		
		Rural	Urban	Highway
Buses and Coaches	Buses	0.6	0.3	0.1
Buses and Coaches	Coaches	0.12	0.59	0.29
Passenger Cars	All	0.3	0.45	0.25
Two-wheelers	All	0.3	0.45	0.25
HDV & LCVs	HDVs	0.12	0.25	0.63
HDV & LCVs	LCVs	0.42	0.3	0.28

The baseline market shares for each vehicle drive-train type are based on (Krause et al., 2020), and are modified throughout the scenarios as outlined in Section 2.4 of the main text. For plug-in hybrid electric vehicles, it is assumed that all urban distance utilizes electricity, and the rest of the distance utilizes liquid fuel (gasoline for passenger vehicles, and diesel for the rest). Table B.13 shows the baseline market shares for each drivetrain type.

Table B.13

Vehicle Baseline Market Share by Vehicle Category and Vehicle Type. The market share is divided by drivetrain type. Based on (Krause et al., 2020).

Vehicle Category	Vehicle Type	Market Share			
		Diesel	Electric	H ₂	Hybrid Electric
Buses and Coaches	Buses		1		
Buses and Coaches	Coaches		0.4		0.6
Passenger Cars	Small		1		
Passenger Cars	Medium		1		
Passenger Cars	Large		0.5		0.5
Two-wheelers	Two-wheelers		1		
HDV & LCVs	LCV		0.6		0.4
HDV & LCVs	HDV - Light		0.6		0.4
HDV & LCVs	HDV - Medium	0.6			0.4
HDV & LCVs	HDV - Heavy	0.6			0.4
HDV & LCVs	HDV - Super Heavy	0.6			0.4
HDV & LCVs	HDV - Ultra Heavy	0.6			0.4

Finally, to convert vehicle distance demand into energy demand, we utilize energy consumption factors from the EU reference scenarios technology assumptions (Commission, 2020).

Table B.14

Vehicle Energy Consumption by Vehicle Category and Vehicle Type (MJ/km). The energy consumption depends on the mode the vehicle is operating in. Based on (Commission, 2020).

Vehicle Category	Vehicle Type	Energy Consumption (MJ/vkm)			
		Diesel	Gasoline	Electric	H ₂
Buses and Coaches	Buses			4.14	
Buses and Coaches	Coaches	9.99		4.14	
Passenger Cars	Small			0.50	
Passenger Cars	Medium			0.54	
Passenger Cars	Large SUV		2.70	0.65	
Two-wheelers	Two-wheelers			0.22	
HDV & LCVs	LCV	2.62		0.61	
HDV & LCVs	HDV - Light	4.98		2.02	
HDV & LCVs	HDV - Medium	7.18		2.66	4.32
HDV & LCVs	HDV - Heavy	10.07		4.68	6.72
HDV & LCVs	HDV - Super Heavy	13.87		5.94	9.12
HDV & LCVs	HDV - Ultra Heavy	13.87		5.94	9.12

Non-electric demand for HDV and LCV energy is assumed to be flat, while electric demand assumed a loadshape based on the ENTSOE TYDNP study (ENTSOE, 2022). For this study, no efficiency multipliers are utilized.

C. SI 3: Supply-side Modelling Methodology and Inputs

C.1. Supply-side Model Description

This section describes the modeling of the liquid fuels, including synthetic fuels within the supply-side model, DOLPHYN. DOLPHYN represents a multi-vector energy system in the form of a mixed-integer linear programming (MILP) optimization model. The full documentation of the DOLPHYN model can be found here (He et al., 2023). Figure 1 (b) shows a diagram of DOLPHYN, including all the technologies modelled. While this work has resulted in contributions to the power, H₂, and CO₂ supply chains, the liquid fuel modelling represents a novel addition to DOLPHYN, which is why we focus on detailing its formulation here. Additionally, other supply chain are documented elsewhere such as in (He et al., 2021a, 2023).

C.1.1. Liquid Fuel Model Formulation¹

This section describes the formulation of the liquid fuels supply chain. To meet a specific demand of liquid fuels, the model has a choice to utilize conventional (fossil-based) or synthetic fuels. Synthetic fuel production arises from a set of resources F . Synthetic fuel plant performance is parameterized in terms of CO₂ input into the process. The model is set-up to account for up to 3 liquid fuel products: diesel, gasoline, and jetfuel. The user can also model an unlimited number of synthetic fuel process by-products. The by-product feature is designed to account for emissions and economic value of byproducts for which there is no exogeneous demand modeled. The emissions associated with these byproducts are accounted for the emissions balances, while the revenue from the sale of by-products are accounted for in the objective function. Any of the 3 modelled liquid fuels can also be modelled as by-products, in the case they are not explicitly modelled. In the case of this study, jet fuel demand is not modelled, and therefore jet fuel is considered a by-product.

Liquid Fuel Model Notation

Notation	Description
$z \in \mathcal{Z}$	z denotes a zone, and \mathcal{Z} is the set of zones in the network
$t \in \mathcal{T}$	t denotes a time step, and \mathcal{T} is the set of time steps
$f \in \mathcal{F}$	Index and set of all synthetic fuels resources
$\mathcal{F}^z \in \mathcal{F}$	Index and set of synthetic fuels resources in zone z
$k \in \mathcal{K}$	k denotes a liquid fuel or by-products modelled in a set of all liquid fuels or by-products modelled \mathcal{K}
$L \in \mathcal{K}$	L denotes a subset containing liquid fuels modelled excluding by-products
$B \in \mathcal{K}$	L denotes a subset containing by-products modelled excluding liquid fuels
$l \in \mathcal{L}$	Index and set of all liquid fuels modelled. Currently three liquid fuels are modelled (gasoline, diesel, and jetfuel).
$b \in \mathcal{B}$	Index and set of all synthetic fuels process byproducts

Table C.15

Liquid Fuel Model Sets and Indices

Notation	Description
$x_{f,t}^{C,Syn}$	CO ₂ input into synthetic fuels resource f at time period t in tonnes of CO ₂
$x_{f,l,t}^{Syn}$	Synthetic fuel l produced by resource f at time period t in MMBTU
$x_{f,b,t}^{By,Syn}$	Byproduct b produced by synthetic fuels resource f at time period in MMBTU
$y_f^{C,Syn}$	Capacity of synthetic fuels resources in the liquid fuels supply chain in tonnes of CO ₂ /hr
$x_{z,t,l}^{Conv}$	Conventional fuel l purchased by zone z at time period t in MMBTU

Table C.16

Liquid Fuel Model Decision Variables

¹This section is adapted from documentation of the liquid fuels module in DOLPHYN (He et al., 2023). The modeling of liquid fuels was a result of a collaborative effort between Youssef Shaker and Jun Wen Law.

Notation	Description
$D_{z,t,l}$	Demand for fuel l in zone z at time t
ζ_l	Percentage of fuel l that needs to be fulfilled using synthetic fuels
$c_f^{\text{Syn,INV}}$	Investment cost per tonne CO ₂ input of synthetic fuels resource f
$c_f^{\text{Syn,FOM}}$	Fixed operation cost per tonne CO ₂ input of synthetic fuels resource f
$c_f^{\text{Syn,VOM}}$	Variable operation cost per tonne of CO ₂ input by synthetic fuels resource f
$c_f^{\text{Syn,FUEL}}$	Fuel cost per tonne of CO ₂ input by synthetic fuels resource f
$c_b^{\text{By,Syn}}$	Selling price per mmbtu of byproduct by synthetic fuels resource (if any)
c_l^{Conv}	Purchase cost per mmbtu of conventional fuel
$\bar{y}_f^{\text{C,Syn}}$	If upper bound of capacity is defined, then we impose constraints on the maximum CO ₂ input capacity of synthetic fuels resource
$\underline{y}_f^{\text{C,Syn}}$	If lower bound of capacity is defined, then we impose constraints on the minimum CO ₂ input capacity of synthetic fuels resource
$\tau_{l,f}^{\text{liquid}}$	Amount of fuel l produced per tonne of CO ₂ input at synthetic fuel resource f
$\tau_{b,f}^{\text{Byproduct}}$	Amount of by-product b produced per tonne of CO ₂ input at synthetic fuel resource f
p_f^{power}	Power MWh per tonne of CO ₂ in required for the plant f
p_f^{hydrogen}	H ₂ tonnes per tonne of CO ₂ in required for the plant f
μ_f^{emit}	Percentage of CO ₂ emitted of the CO ₂ in for a plant f
μ_f^{capture}	Percentage of CO ₂ captured of the CO ₂ in for a plant f
λ_f	Emissions of plant fuel per tonne of CO ₂ in for plant f
θ_l^{liquid}	Emissions per mmbtu for liquid fuel l
$\theta_b^{\text{Byproduct}}$	Emissions per mmbtu for by-product b
ω_t	Time-step weight for time-step t

Table C.17
Liquid Fuels Model Parameters Description

Objective function

The total cost associated with the liquid fuel infrastructure includes four main elements as shown in equation 2 : 1) the capital cost of synthetic fuel production (see equation 3) 2) the operating cost of synthetic fuel production (see equation 4) 3) production credits for any by-products that are not explicitly modelled (see equation 5), and 4) the cost of procuring liquid fossil fuels (see equation 6). These terms are added to the overall multi-sectoral model objective function, which includes cost associated with infrastructure for other vectors.

$$\min C^{\text{LF,Syn,c}} + C^{\text{LF,Syn,o}} - C^{\text{LF,Syn,r}} + C^{\text{Conv,o}} \quad (2)$$

The fixed costs associated with synthetic fuel production is defined such that:

$$C^{\text{LF,Syn,c}} = \sum_{f \in F} y_f^{\text{C,Syn}} (x c_f^{\text{Syn,INV}} + c_f^{\text{Syn,FOM}}) \quad (3)$$

The variable costs associated with synthetic fuel production is defined such that:

$$C^{\text{LF,Syn,o}} = \sum_{f \in F} \sum_{t \in T} \omega_t \times (c_f^{\text{Syn,VOM}} + c_f^{\text{Syn,FUEL}}) \times x_{f,t}^{\text{C,Syn}} \quad (4)$$

The credit associated with by-products is defined such that:

$$C^{LF, \text{Syn}, r} = \sum_{f \in F} \sum_{b \in B} \sum_{t \in T} \omega_t \times x_{f,b,t}^{\text{By}, \text{Syn}} \times c_b^{\text{By}, \text{Syn}} \quad (5)$$

The cost of conventional fuels is defined such that:

$$C^{\text{Conv}, o} = \sum_{z \in Z} \sum_{l \in L} \sum_{t \in T} \omega_t \times c_l^{\text{Conv}} \times x_{z,t,l}^{\text{Conv}} \quad (6)$$

Synthetic Fuel Production Constraints

The amount of synthetic fuels produced at a given time-step is given by:

$$x_{f,l,t}^{\text{Syn}} = x_{f,t}^{\text{C}, \text{Syn}} \times \tau_{l,f}^{\text{liquid}} \quad \forall f \in F, t \in T, l \in L \quad (7)$$

The amount of by-products produced at a given time-step is given by:

$$x_{f,b,t}^{\text{Syn}} = x_{b,t}^{\text{C}, \text{Syn}} \times \tau_{b,f}^{\text{By}} \quad \forall f \in F, t \in T, b \in B \quad (8)$$

For resources where upper bound $\overline{y_f^{\text{C}, \text{Syn}}}$ and lower bound $\underline{y_f^{\text{C}, \text{Syn}}}$ of capacity is defined, then we impose constraints on minimum and maximum synthetic fuels resource input CO₂ capacity.

$$\underline{y_f^{\text{C}, \text{Syn}}} \leq y_f^{\text{C}, \text{Syn}} \leq \overline{y_f^{\text{C}, \text{Syn}}} \quad \forall f \in F$$

The required capacity is given by the following constraint such that the amount of CO₂ flowing into the plant does not exceed the plant's capacity:

$$x_{f,t}^{\text{C}, \text{Syn}} \leq y_f^{\text{C}, \text{Syn}} \quad \forall f \in F, t \in T \quad (9)$$

Liquid Fuels Balance Constraints

For each of the liquid fuels the following constraint is implemented to ensure that a sufficient combination synthetic fuel production and conventional liquid fuel procurement occurs to meet demand:

$$\sum_{z \in Z} \sum_{t \in T} \omega_t \times x_{z,t,l}^{\text{Conv}} + \sum_{f \in F} \sum_{t \in T} \omega_t \times x_{f,t,l}^{\text{C}, \text{Syn}} \geq \sum_{z \in Z} \sum_{t \in T} D_{z,t,l} \quad \forall l \in L \quad (10)$$

Note that only one constraint is implemented across all zones and time-steps. This is to reflect the flexibility and interconnectedness of liquid fuel supply chain. The cost of transporting liquid fuels is already included in cost estimates, and is therefore not accounted for separately. Moreover, because this modeling approach presumes that the product distribution from synthetic fuel production cannot be changed without impacting the energy inputs or capital cost of the process, the amount of each fuel produced can potentially exceed the amount demanded. In this case, the fuel production is penalized from an emission perspective, without meeting any specific demand. Finally, because one constraint is implemented across all timesteps and zones, storage is not accounted for.

Additionally, to reflect possible synthetic fuel mandates, the following constraint is used to force the model to produce a specific amount of synthetic fuels as a percentage of demand, if a specific fuel mandate is specified:

$$(\zeta_l - 1) \times \sum_{f \in F} \sum_{t \in T} \omega_t \times x_{f,t,l}^{\text{C}, \text{Syn}} + \zeta_l \times \sum_{z \in Z} \sum_{t \in T} \omega_t \times x_{z,t,l}^{\text{Conv}} = 0 \quad (11)$$

This is just a reorganization version of the following formula in a way that avoids non-linearities:

$$\sum_{f \in F} \sum_{t \in T} \omega_t \times x_{f,l,t}^{C, \text{Syn}} / \left(\sum_{f \in F} \sum_{t \in T} \omega_t \times x_{f,l,t}^{C, \text{Syn}} + \sum_{z \in Z} \sum_{t \in T} \omega_t \times x_{z,t,l}^{\text{Conv}} \right) = \zeta_l \quad (12)$$

Note that only one synthetic fuel product percentage can be specified, otherwise, the model will become infeasible.

Synthetic Fuel Power Balance Term

The following expression reflects the power consumption associated with synthetic fuel production in a given zone that is added to the overall system power supply and demand balance at each time step and zone:

$$\text{BalPowerLiquidFuel}_{z,t} = \sum_{f \in F^z} \omega_t \times x_{f,t}^{C, \text{Syn}} \times p_f^{\text{power}} \quad \forall z \in Z, t \in T \quad (13)$$

This term is added to the overall power balance of the multi-sectoral model.

Synthetic Fuel H₂ Balance Term

The following expression reflects the H₂ consumption associated with synthetic fuel production in a given zone:

$$\text{BalHydrogenLiquidFuel}_{z,t} = \sum_{f \in F^z} \omega_t \times x_{f,t}^{C, \text{Syn}} \times p_f^{\text{hydrogen}} \quad \forall z \in Z, t \in T \quad (14)$$

This term is added to the overall H₂ balance of the multi-sectoral model.

Liquid Fuel Emissions Balance Terms

The following expression shows the emissions associated with the liquid fuel production and consumption process. It is made up of 4 terms: 1) the component of CO₂ input into the plant that is released into the atmosphere during the fuel production process 2) emissions from the consumption of synthetic fuels (all synthetic fuels produced are consumed even if there is no demand for them) 3) emissions from the consumption of by-products of synthetic fuels production process, and 4) emissions from the consumption of conventional liquid fuels. This term is added to the overall multi-sectoral CO₂ balance constraint.

$$\begin{aligned} \text{BalEmissionsLiquidFuel}_z = & \sum_{f \in F^z} \sum_{t \in T} \omega_t \times x_{f,t}^{C, \text{Syn}} \times \mu_f^{\text{emit}} \\ & + \sum_{f \in F^z} \sum_{t \in T} \omega_t \times x_{f,t,l}^{\text{Syn}} \times \theta_l^{\text{liquid}} \\ & + \sum_{f \in F^z} \sum_{t \in T} \omega_t \times x_{b,t,l}^{\text{Syn}} \times \theta_b^{\text{Byproduct}} \\ & + \sum_{t \in T} \omega_t \times x_{l,z,t}^{\text{Conv}} \times \theta_l^{\text{liquid}} \quad \forall z \in Z \end{aligned} \quad (15)$$

The following expression shows the emissions captured with the liquid fuel production and consumption process. It is made up of 2 terms: 1) the component of CO₂ input into the plant from all captured emissions, which is taken from the CO₂ captured in the system 2) emissions captured from the synthetic fuel plant. This term is added to the multi-sectoral CO₂ captured expression, which includes CO₂ captured from H₂ and power producing plants, as well as DAC.

$$\begin{aligned} \text{BalEmissionsCapturedLiquidFuel}_z = & - \sum_{f \in F^z} \sum_{t \in T} \omega_t \times x_{f,t}^{C, \text{Syn}} \\ & + \sum_{f \in F^z} \sum_{t \in T} \omega_t \times x_{f,t}^{C, \text{Syn}} \times \mu_f^{\text{capture}} \quad \forall z \in Z \end{aligned} \quad (16)$$

C.2. Supply-side Model Inputs

C.2.1. Power Network, Cost, and Operational Assumptions

The power system used in this study is based on a brownfield representation of the European Grid created by PYPSA-EUR (Hörsch et al., 2019). We utilize the 37-node representation of the European continent, which reduced to 10 nodes when we exclude countries outside of the region of interest. All countries are represented as one node, apart from Denmark and the UK, which are each represented using two nodes.

Transmission costs and upgrades are based on PYPSA-EUR network representations (Hörsch et al., 2019). In the model, both AC and DC transmission are treated equivalently. We assume that existing power transmission capacities can be expanded by up to 4 times. Additionally, we assume that new lines can be built between certain regions up to a capacity of 5000 MW.

The existing available generation is based on data from the ENTSOE transparency platform (ENTSOE). We assume that this capacity will be available in the year 2040.

The following table shows the key cost and operational assumptions for generation and storage technologies:

Generation Technology	Power CAPEX (Eur/kW)	Energy CAPEX (Eur/kWh)	FOM (Eur/MW/yr)	VOM (Eur/MWh)	Heat Rate (MMBTU / MWh)	Capture Rate	Round Trip Efficiency	Lifetime (Yrs)
Onshore Wind	851	-	32	0	-	-	-	30
Offshore Wind	3,751	-	69	0	-	-	-	30
Solar	680	-	13	0	-	-	-	30
Biomass	-	-	136	5.2	13.5	-	-	45
Nuclear	6,431	-	131	2.6	10.46	-	-	60
Hydro	-	-	56	0	-	-	-	100
OCGT	785	-	19	1.6	10.1	-	-	30
CCGT	937	-	25	4.6	6.5	-	-	30
CCGT w/ CCS	1,794	-	52	3.7	7.2	0.95	-	30
Coal	2,733	-	67	7.2	10.0	-	-	30
PHS	-	-	16	0.5	-	-	0.87	100
Battery	137	208	18	0	-	-	0.85	30

Table C.18

Power Technology Cost and Operational Assumptions

All costs assumptions are based on the 2022 NREL ATB for the year 2040 (NREL, 2022). For all technologies we used moderate technology assumptions, apart from the CCGT w/ CCS, battery, and floating off-shore wind. All operational assumptions (e.g. ramp up/down time, minimum run are based on Sepulveda et al. (Sepulveda et al., 2018).

The maximum available generation capacity and temporally resolved capacity factors associated with the variable renewable energy generation technologies is based on PYPSA-EUR (Hörsch et al., 2019). We assume no possible expansion in biomass plants. Additionally, we assume that only nuclear existing (without a phase-out), planned, and under-construction units will be in-operation by 2040, in line with the 2022 ENTSOE TYNDP study (ENTSOE, 2022).

C.2.2. Hydrogen Cost and Operational Assumptions

We model hydrogen generation, transmission, storage, and G2P technologies. A greenfield representation of the hydrogen system is utilized for this study.

We modelled the following H₂ production technologies: electrolyzers, SMR, SMR w/ CCS, and ATR w/ CCS technologies. We also modeled above ground hydrogen storage. Cost and operational assumptions for fossil fuel based plants (SMR, SMR w/ CCS, and ATR w/ CCS) are based on (Lewis et al., 2022). Cost and operational assumptions for electrolyzers are based on (IEA, 2019), assuming 2050 costs. Costs and operational assumptions for G2P units are based on (NREL, 2022). Storage technology cost assumptions are based on (Papadias and Ahluwalia, 2021). The following table shows key hydrogen generation technologies cost and operational assumptions:

H ₂ Production Technology	CAPEX (Eur/kTonne-H ₂ / yr)	FOM (Eur/kTonne-CO ₂ / hr/yr)	VOM (Eur/Tonne-CO ₂)	Electricity Input (MWh/Tonne-H ₂)	Natural Gas Heat Rate (GJ/Tonne H ₂)	Capture Rate	Lifetime (Yrs)
SMR	15,715	539	0.08	0.65	184.4	-	25
SMR w/ CCS	38,232	1,183	0.22	2.04	196.1	0.96	25
ATR w/ CCS	30,218	917	0.33	4.00	184.3	0.95	25
Electrolyzers	18,954	37.30	-	45.00	45.0	-	20

Table C.19
Hydrogen Production Technology Cost Assumptions

G2P Technology	CAPEX (Eur/MW)	FOM (Eur/MW/yr)	VOM (Eur/MWh)	Conversion Efficiency (MWh/ tonne-H ₂)
CCGT G2P	816,095	24,570	1.57	21.65

Table C.20
G2P Technology Cost Assumptions

Storage Technology	CAPEX (Eur/kTonne-H ₂ /hr)	CAPEX (Eur/kTonne H ₂)	FOM (Eur/kTonne H ₂ /yr)	Lifetime (Yrs)
Underground Storage	1,859	504	1.02	30

Table C.21
Hydrogen Storage Technology Costs Assumptions

C.2.3. CO₂ Sequestration Assumptions

DAC Cost and Operational Assumptions

We model solvent and sorbet direct-air capture (DAC) technologies with thermal energy provided by natural gas (NG) or electricity. The DAC utilizing NG has an additional CO₂ capture unit to capture up to 99% of the CO₂ emissions from NG combustion. The cost and operational assumptions for DAC are based on (NETL, 2022). The following are the cost and operational assumptions associated with DAC technologies:

DAC Technology	CAPEX (Eur/kTonne CO ₂ /hr)	FOM (Eur/kTonne CO ₂ /hr)	VOM (Eur/Tonne CO ₂)	Heat Rate (MMBTU/Tonne CO ₂)	Electricity Consumption (MWh / Tonne CO ₂)	NG Combustion CO ₂ Capture Rate	Lifetime (Yrs)
Solvent DAC	12,606	342	52.0	12.2	-0.13	0.99	30
Sorbent DAC	30,684	1,041	53.8	26.6	0.00	0.89	30
Electric DAC	13,772	673	19.8	NA	4.38	NA	30

Table C.22

Direct Air Capture Technology Operation and Cost Assumptions.

CO₂ Storage Assumptions

CO₂ storage costs are based on (Committee on Developing a Research Agenda for Carbon Dioxide Removal and Reliable Sequestration, Board on Atmospheric Sciences and Climate, Board on Energy and Environmental Systems, Board on Agriculture and Natural Resources, Board on Earth Sciences and Resources, Board on Chemical Sciences and Technology, Ocean Studies Board, Division on Earth and Life Studies and National Academies of Sciences, Engineering, and Medicine, 2019). The following table shows the CO₂ storage assumptions:

	CAPEX (Eur/Tonne CO ₂ /yr)	FOM (Eur/Tonne CO ₂ /yr)	Electricity Consumption (MWh / Tonne CO ₂)	Lifetime (Yrs)
CO ₂ Storage	0.46	0.09	0.007	30

Table C.23

CO₂ Storage Operation and Cost Assumptions.

Additionally, we assume that a carbon dioxide pipeline network can be built without restrictions.

Geological Sequestration Assumptions

CO₂ geological sequestration capacities are based on the EU GeoCapacity project for all countries except Sweden (Vangkilde-Pedersen, Thomas, 2009). Sweden geological storage is based on (Mortensen, 2014). We utilize the conservative assumption. In addition, we assume that only geological storage in saline aquifers is viable. Additionally, since our model captures on year, we divide the available capacity by 100 to account for the long-term need for CO₂ storage, as well as the utilization for CO₂ capture for other purposes such as industrial sequestration. In addition to DAC, we assume that CO₂ captured from the power and hydrogen sectors through PSC is combined with any CO₂ captured from DAC. This captured CO₂ is either utilized using the synthetic fuel pathway or is stored.

Table C.24 shows the modelled available capacity for geological CO₂ storage:

Country	CO ₂ Storage (Mt/yr)
Belgium	199
Germany	14,900
Denmark	2,554
France	7,922
United Kingdom	7,100
Netherlands	340
Norway	26,031
Sweden	3,400

Table C.24CO₂ Geological Sequestration Availability by Country

C.2.4. Liquid Fuels Assumptions

Synthetic Fuels Cost and Operational Assumptions

Since the focus of this study is road transportation, we focus on two liquid fuels; diesel and gasoline. We assume that liquid fuel demand can be met in one of two ways. The first is using conventional hydrocarbons and the second is through synthetic fuels. Three synthetic fuel plant configurations are modelled. The first is a baseline synthetic fuel plant based on Zang et al. (Option A) (Zang et al., 2021). Additionally, we model two modified plant configurations (Option B and Option C): Option B captures a portion of the vented CO₂ for sequestration, while Option C second captures and recycles the vented CO₂. Both were based on estimated cost and energy requirements of adding an industrial point source CO₂ unit. This was done by obtaining the energy requirement, CAPEX, FOM, and VOM costs of a Cansolv 90% CO₂ capture system used in cement plants from NETL's report of CO₂ capture from industrial point sources (Schmitt et al., 2022) as shown:

CO ₂ capture Technology	CAPEX (Eur/kTonne CO ₂ /hr)	FOM (Eur/kTonne CO ₂ /hr/y)	VOM (Eur/Tonne CO ₂)	Electricity Consumption (MWh/Tonne CO ₂)	Capture Rate	Lifetime (Yrs)
Cement Plant	2,103	67	4.21	1.04	0.90	40

Table C.25

Cement plant Cansolv 90% CO₂ capture costs and energy requirements per tonne CO₂ input into the capture system from (Schmitt et al., 2022)

These were added to the SF process by scaling the energy requirement and costs to the total CO₂ at the emission vent of the baseline SF process (Option A). It was also assumed that electricity would provide the energy requirement of the CO₂ capture units, thus adding to the total electricity input of the SF process with CO₂ capture (Option B and C). The SF process with recycling (Option C) assumes the captured CO₂ is recycled back as feed to the syngas generation unit, thus increasing the total carbon conversion and thus fuels output per raw CO₂ input feed, as well as electricity and hydrogen requirements of the process. The following parameters show the synthetic fuel processes costs and operational assumptions:

Syn Fuel Production Technology	Baseline Syn Fuel Plant (Option A)	Syn Fuel Plant w/ Capture (Option B)	Syn Fuel Plant w/ Recycling (Option C3)
CAPEX (Eur/kTonne CO ₂ In/hr)	3,635	4,744	9,028
FOM (Eur/kTonne CO ₂ In/hr/y)	193	229	435
VOM (Eur/Tonne CO ₂ In)	7.76	9.98	18.99
Lifetime (Yrs)	40	40	40
CO ₂ Utilized (%)	47.3	47.3	90.0
CO ₂ Sequestered (%)	0	47.5	0
CO ₂ Released (%)	52.7	5.2	10.0
H ₂ In (Tonnes/Tonne of CO ₂ In)	0.093	0.093	0.178
Electricity In (MWh/Tonne CO ₂ In)	0.036	0.584	1.111
Diesel Out (MMBTU/Tonne CO ₂ In)	1.791	1.791	3.408
Gasoline Out (MMBTU/Tonne CO ₂ In)	1.691	1.691	3.219
Jet Fuel Out (MMBTU/Tonne CO ₂ In)	3.057	3.057	5.817

Table C.26

Syn Fuel Production Operation and Cost Assumptions per tonne CO₂ input to the Syn Fuel plant based on (Zang et al., 2021)

Since jet fuel is a by-product on the synthetic fuel process we are modelling, but the aviation sector is not included in our model, we assume a "credit" associated with the production of jet fuels.

C.2.5. Fuel costs

Fuel	Fuel Cost (Eur/MWh)
Nuclear	1.5
Biomass	7.0
Coal	6.2
Lignite	5.8
Natural Gas	31.1
Gasoline	79.9
Diesel	96.9
Jet fuel	55.2

Table C.27
Fuel Cost Assumptions

The source for the nuclear, coal, and lignite costs is the 2022 TYNDP study (ENTSOE, 2022). The price of natural gas is based on natural gas futures viewed in June 2022 for the Dutch TTF (Barchart, 2023). The natural gas prices reflected in the TYNDP are significantly lower than natural gas futures. Given the state of current state of European natural gas supply, we believe that relying on futures estimate is more reasonable. Additionally, ENTSOE-TYNDP does not list biomass prices. The price for biomass is based from PyPSA technology database (Lisazeyen, Euronion, Millinger, Neumann, Parzen, Brown, Franken, Martavp and Lukasnacken, 2023).

The price for gasoline and diesel is based on German gasoline and diesel for 2022 excluding any carbon taxes (en2x, 2024). The price is then adjusted to 2040 based on the expected change in crude oil price between 2022 and 2040 (ENTSOE, 2022; OPEC, 2024). Jet fuel prices are calculated in a similar way; we used the global price of jet fuel for 2022, which was then adjusted to 2040 based on the expected change in the price of crude oil between 2022 and 2040 (Mundi, 2024).

C.2.6. Non-transportation demand

The baseline electricity and hydrogen demand is based on ENTSOE projected demand scenarios, excluding any road transportation demand (ENTSOE, 2022). We utilize the Distributed Energy scenario for the year 2040.

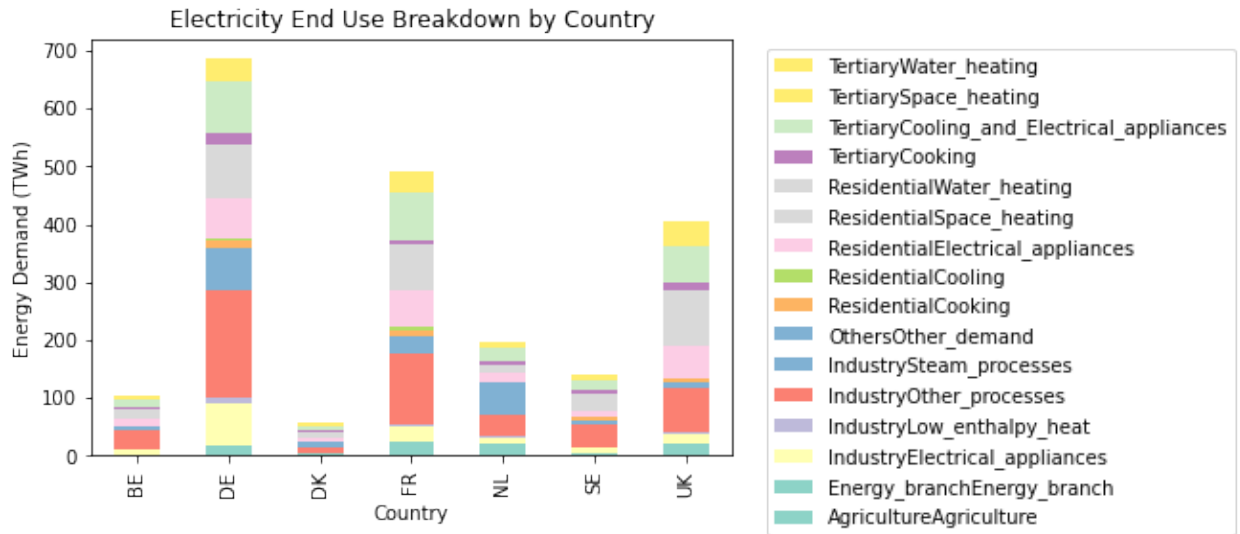


Figure C.56: Non-transportation electric demand broken down by country and end-use as reported by ENTSOE

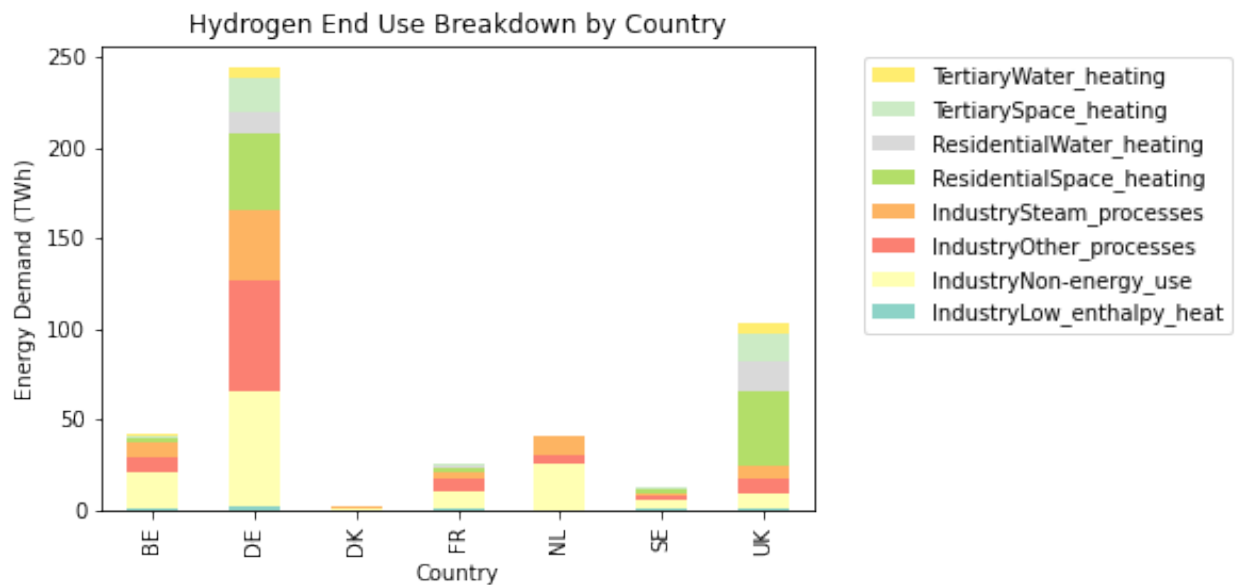


Figure C.57: Non-transportation H₂ demand broken down by country and end-use as reported by ENTSOE

C.2.7. Emissions Constraint

We establish a combined system cap on the power, hydrogen, and transportation sectors. This is reflective of a combined emission trading market. To establish a baseline, we add transportation and power sector emissions from the year 2015. We assume that by the year 2040, we will require a 90% reduction in power sector emissions and a 40% reduction in transportation emissions. It is worth noting that specific economy-wide emissions targets for the year 2040 have not been set for the EU, let alone sectoral emissions targets. As a result, we model a range of emissions sensitivities.